EUROPEAN ORGANISATION FOR NUCLEAR RESEARCH (CERN)

Submitted to: Eur. Phys. J. C

CERN-EP-2026-078
25th March 2026

Measurement and interpretation of inclusive $W\gamma$ production in proton–proton collisions at $\sqrt{s}$ = 13 TeV using the ATLAS detector

The ATLAS Collaboration

Differential cross-section measurements are presented for the production of a W boson in association with a photon. The analysis is performed using proton–proton collision data collected by the ATLAS experiment at $\sqrt{s}$ = 13 TeV, corresponding to an integrated luminosity of 140 fb^{-1}. The differential cross sections are measured in the $W\gamma \to \ell\nu\gamma$ decay channel ($\ell = e, \mu$) as a function of 16 observables. Collectively, these observables probe the kinematic properties of the $W\gamma$ system, the radiation amplitude zero effect predicted for the $W\gamma$ final state, the polarisation of the W boson, the charge conjugation and parity structure of the $WW\gamma$ triple gauge coupling, and the parton distribution functions of the proton. The data are corrected for the effects of detector inefficiency and resolution and are sufficiently precise that they can be used to distinguish between different state-of-the-art theoretical predictions provided by Sherpa, MadGraph5_aMC@NLO, and Geneva. The differential cross sections are used to search for anomalous weak-boson self-interactions induced by dimension-six operators within an effective field theory. For CP-odd operators, dedicated detector-corrected observables based on the outputs of neural networks are found to be particularly sensitive to the interference between the Standard Model and dimension-six scattering amplitudes. Constraints are placed on the Wilson coefficients of the O_W, O_{HWB}, $O_{\tilde{W}}$ and $O_{H\tilde{W}B}$ operators in the effective field theory. The sensitivity to the $O_{H\tilde{W}B}$ operator is improved by a factor of 2.5 compared to previous measurements in other final states.

Contents

1 Introduction

The production of a W boson in association with a photon in proton–proton collisions is sensitive to a diverse range of physical phenomena. The s-channel scattering amplitude contains the $WW\gamma$ triple gauge coupling as shown in Figure 1. Interference between the s-channel scattering amplitude and the t- and u- channel scattering amplitudes results in a complete cancellation at certain points in the phase space [1–5], a feature known as radiation amplitude zero. Radiation amplitude zero is an effect that occurs only at leading-order (LO) in the Standard Model (SM) and the effect is removed when either (i) higher-order quantum chromodynamic (QCD) corrections are included, or (ii) when the $WW\gamma$ coupling deviates from the SM prediction [5]. Measurements of inclusive $W\gamma$ production can therefore be used to study QCD calculations, to stress-test the gauge structure of the electroweak interaction, and to search for new physics beyond the SM (BSM physics).

Inclusive $W\gamma$ production is particularly sensitive to the dimension-six operators in effective field theory (EFT) that induce anomalous electroweak-boson self-interactions or anomalous interactions between the electroweak bosons and the Higgs boson. The anomalous interactions induce small deviations from the SM

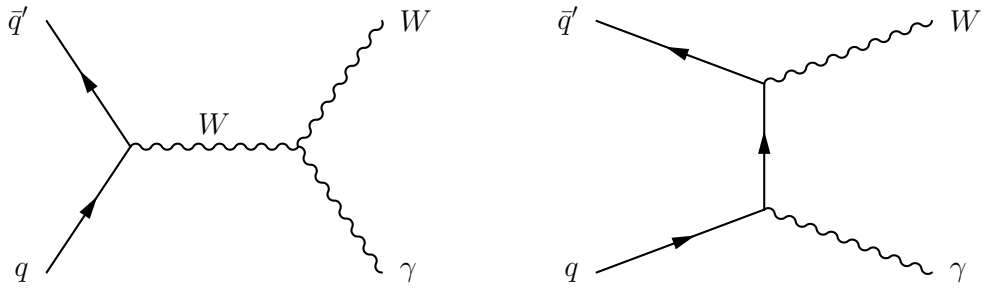

Figure 1: $W\gamma$ production in the s-channel (left) and t-channel (right). The s-channel scattering amplitude contains the $WW\gamma$ triple gauge coupling.

predictions and the largest effects should arise from the interference between the SM scattering amplitude and the BSM scattering amplitude (which contains the anomalous interaction). However, for diboson production, there exists a *no-interference theorem* [6] that states that the interference is suppressed because the dominant contributions to the SM and BSM scattering amplitudes occur for different W boson helicity. Despite this, it has been shown that interference effects can be restored by accessing the off-diagonal elements of the W boson spin density matrix via either (i) measurements of the W boson decay angles [7], or (ii) measurements of angular correlations between the W boson decay products and the photon [8, 9]. Measurements of these angular observables in the $W \to \ell\nu$ decay channel ($\ell = e, \mu$) provide competitive sensitivity to operators that conserve charge conjugation and parity (CP) [10], and have been proposed as the most sensitive observables for studying CP-violating operators [9].

Measurements of inclusive $W\gamma$ production can also be used to test the state-of-the-art predictions provided by analytical QCD calculations and Monte Carlo event generators. Analytical calculations have shown that the next-to-leading-order (NLO) inclusive $W\gamma$ cross section is a factor of three larger than the LO cross section [5, 11], with next-to-next-to-leading-order (NNLO) corrections further increasing the cross section by about 20% [12, 13]. Differential cross section measurements of the $W\gamma$ final state can test these calculations across a wide kinematic region. Alternatively, restricting the quark/gluon radiation in the final state by applying a jet veto suppresses the higher-order contributions and allows the radiation amplitude zero effect to be studied. Finally, inclusive $W\gamma$ production can also be used to probe the parton distribution functions (PDFs) of the proton. The charge of the lepton from the W boson decay determines whether the dominant contributions to the initial state arise from $u\bar{d}$ or $d\bar{u}$ at leading order. The photon preferentially couples to up-type partons and differential measurements of inclusive $W\gamma$ boost asymmetries can then help untangle the contributions of the valence quark and sea quark contributions [14].

In this paper, differential cross sections are measured for inclusive $W\gamma$ production in the $W \to \ell\nu$ decay channel using proton–proton collision data collected at a centre-of-mass energy $\sqrt{s} = 13$ TeV and with an integrated luminosity of 140 fb^{-1}. The measurements are divided into five categories:

Inclusive $W\gamma$ kinematic observables probe the basic kinematic properties of the $W\gamma$ system. Differential cross sections are measured as a function of the photon transverse momentum[1], p_{T}^{γ}, the charged-lepton

[1] ATLAS uses a right-handed coordinate system with its origin at the nominal interaction point (IP) in the centre of the detector and the z-axis along the beam pipe. The x-axis points from the IP to the centre of the LHC ring, and the y-axis points upwards. Polar coordinates (r, ϕ) are used in the transverse plane, ϕ being the azimuthal angle around the z-axis. The pseudorapidity is defined in terms of the polar angle θ as $\eta = -\ln\tan(\theta/2)$ and is equal to the rapidity $y = \frac{1}{2}\ln\left(\frac{E+p_z}{E-p_z}\right)$ in the relativistic limit. Angular distance is measured in units of $\Delta R \equiv \sqrt{(\Delta y)^2 + (\Delta\phi)^2}$.

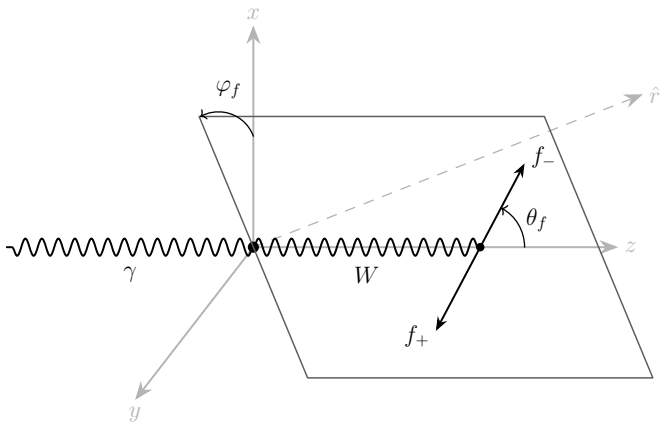

Figure 2: The reference frame used to measure the $W \to \ell\nu$ decay angles, θ_f, and ϕ_f, is constructed as follows. First, the measured missing transverse momentum is taken as a proxy for the neutrino transverse momentum; the neutrino longitudinal momentum is determined, with a two-fold ambiguity, by assuming a $W \to \ell\nu$ decay and imposing a W boson mass constraint on the $\ell\nu\gamma$ system. One of the two solutions is chosen at random. Second, the z axis is taken to be the W boson direction in the centre-of-mass frame of the $\ell\nu\gamma$ system. A vector, $\hat{\mathbf{r}}$, is defined in the centre-of-mass frame that defines the boost direction to the lab frame. The y axis is defined by $\hat{\mathbf{y}} = \hat{\mathbf{z}} \times \hat{\mathbf{r}}$ and the x axis is defined as $\hat{\mathbf{x}} = \hat{\mathbf{y}} \times \hat{\mathbf{z}}$. The azimuthal decay angle, ϕ_f, is taken to be the azimuthal angle of the negative helicity fermion (f_-) in this special frame. The polar decay angle, θ_f, is defined in the rest frame of the W boson relative to the W boost direction.

transverse momentum, p_{T}^{ℓ}, the photon pseudo-rapidity, η_γ, the invariant mass of the lepton-photon system, $m_{\ell\gamma}$, and the transverse mass of the $W\gamma$ system, $m_{\mathrm{T}}^{\ell\nu\gamma}$ [5].

Radiation amplitude zero is probed by measuring the differential cross section as a function of the difference in pseudorapidity between the charged lepton and the photon, $\Delta\eta_{\ell\gamma}$.

Polarisation-sensitive observables are constructed from the $W \to \ell\nu$ decay angles (θ_f, ϕ_f), which are defined using the negative helicity fermion from the W boson decay and measured in a special reference frame [7], which is shown in Figure 2. A double-differential cross section is measured as a function of θ_f and ϕ_f, which directly probes the W boson spin density matrix. In addition, a double differential cross section is measured as a function of ϕ_f and p_{T}^{γ}, which is sensitive to EFT interference effects that grow with energy.

CP-sensitive observables are designed to be sensitive to the interference effects caused by anomalous CP-violating $WW\gamma$ interactions [8, 9]. Two types of CP-sensitive differential cross sections are measured. The first is the differential cross section as a function of the pseudorapidity-ordered azimuthal angle between the lepton and the photon, $\Delta\phi_{\ell\gamma} = \phi_i - \phi_j$ (with $\eta_i > \eta_j$). The second is the differential cross section as a function of an optimised observable, O_{NN}, which is constructed from the outputs of a multi-class neural network [9]. $\Delta\phi_{\ell\gamma}$ is intrinsically CP-sensitive as a parity-odd observable, whereas O_{NN} is trained to optimally separate the constructive- and destructive- interference contributions for a given operator in the effective field theory. The construction of O_{NN} is discussed further in Section 6.

PDF-sensitive observables: The boost asymmetry is defined as

$$A_{\mathrm{boost}}^{W\gamma} = \frac{\sigma_{\gamma}^{\mathrm{fwd}} - \sigma_{\gamma}^{\mathrm{cent}}}{\sigma_{\gamma}^{\mathrm{fwd}} + \sigma_{\gamma}^{\mathrm{cent}}},$$

where $\sigma_{\gamma}^{\text{fwd}}$ is the cross section for events with $|\eta_{\gamma}| > |\eta_{\ell}|$ and $\sigma_{\gamma}^{\text{cent}}$ is the cross section for events with $|\eta_{\gamma}| < |\eta_{\ell}|$. The boost asymmetry is measured separately for events containing leptons and antileptons and as a function of the photon pseudorapidity and the (anti)lepton pseudorapidity.

Previous measurements of inclusive $W\gamma$ production have been carried out at the D0 and CDF experiments in proton–antiproton collisions at $\sqrt{s} = 1.96$ TeV [15–17]. At the LHC, the ATLAS and CMS experiments have measured inclusive $W\gamma$ production in proton–proton collisions at $\sqrt{s} = 7$ TeV [18, 19] . More recently, the CMS experiment has measured the inclusive $W\gamma$ fiducial and differential cross sections at $\sqrt{s} = 13$ TeV, providing the most precise measurements to date and setting tight constraints on anomalous CP-conserving $WW\gamma$ interactions [10, 20]. The measurements presented in this paper go beyond those studies in three ways, by providing (i) new sensitivity to the W-boson spin density matrix via the double differential cross sections as a function of θ_f and ϕ_f, (ii) new sensitivity to CP-violation via the differential cross sections as a function of $\Delta\phi_{\ell\gamma}$ and O_{NN}, (iii) new sensitivity to PDFs via the boost asymmetry. In addition, the differential cross section measurements as a function of the various kinematic observables has comparable precision to that achieved previously.

2 ATLAS detector

The ATLAS detector [21] at the LHC covers nearly the entire solid angle around the collision point. It consists of an inner tracking detector surrounded by a thin superconducting solenoid, electromagnetic and hadronic calorimeters, and a muon spectrometer incorporating three large superconducting air-core toroidal magnets.

The inner-detector system (ID) is immersed in a 2 T axial magnetic field and provides charged-particle tracking in the range $|\eta| < 2.5$. The high-granularity silicon pixel detector covers the vertex region and typically provides four measurements per track, the first hit generally being in the insertable B-layer (IBL) installed before Run 2 [22, 23]. It is followed by the SemiConductor Tracker (SCT), which usually provides eight measurements per track. These silicon detectors are complemented by the transition radiation tracker (TRT), which enables radially extended track reconstruction up to $|\eta| = 2.0$. The TRT also provides electron identification information based on the fraction of hits (typically 30 in total) above a higher energy-deposit threshold corresponding to transition radiation.

The calorimeter system covers the pseudorapidity range $|\eta| < 4.9$. Within the region $|\eta| < 3.2$, electromagnetic calorimetry is provided by barrel and endcap high-granularity lead/liquid-argon (LAr) calorimeters, with an additional thin LAr presampler covering $|\eta| < 1.8$ to correct for energy loss in material upstream of the calorimeters. Hadronic calorimetry is provided by the steel/scintillator-tile calorimeter, segmented into three barrel structures within $|\eta| < 1.7$, and two copper/LAr hadronic endcap calorimeters. The solid angle coverage is completed with forward copper/LAr and tungsten/LAr calorimeter modules optimised for electromagnetic and hadronic energy measurements, respectively.

The muon spectrometer (MS) comprises separate trigger and high-precision tracking chambers measuring the deflection of muons in a magnetic field generated by the superconducting air-core toroidal magnets. The field integral of the toroids ranges between 2.0 and 6.0 T m across most of the detector. Three layers of precision chambers, each consisting of layers of monitored drift tubes, cover the region $|\eta| < 2.7$, complemented by cathode-strip chambers in the forward region, where the background is highest. The muon trigger system covers the range $|\eta| < 2.4$ with resistive-plate chambers in the barrel, and thin-gap chambers in the endcap regions.

The luminosity is measured mainly by the LUCID–2 [24] detector that records Cherenkov light produced in the quartz windows of photomultipliers located close to the beampipe.

Events were selected by the first-level trigger system implemented in custom hardware, followed by selections made by algorithms implemented in software in the high-level trigger [25, 26]. The first-level trigger accepted events from the 40 MHz bunch crossings at a rate close to 100 kHz, which the high-level trigger further reduced in order to record complete events to disk at about 1.25 kHz.

A software suite [27] is used in data simulation, in the reconstruction and analysis of real and simulated data, in detector operations, and in the trigger and data acquisition systems of the experiment.

3 Monte Carlo simulation

The inclusive $W\gamma \to \ell\nu\gamma$ ($\ell = e, \mu$) signal is modelled using two different Monte Carlo (MC) event generators, Sherpa and MadGraph5_aMC@NLO. The first sample is generated using Sherpa 2.2.11 [28] with matrix elements at NLO accuracy in perturbative QCD for up to one additional parton in the final state and at LO accuracy for up to four additional partons. The matrix element calculations were matched and merged with the Sherpa parton shower based on Catani–Seymour dipole factorisation [29, 30] using the MEPS@NLO prescription [31–34]. The virtual QCD corrections were provided by the OpenLoops library [35–37]. The NNPDF3.0nnlo [38] set of parton distribution functions were used, along with the dedicated set of tuned parton-shower parameters developed by the Sherpa authors. The second inclusive $W\gamma$ sample is generated using MadGraph5_aMC@NLO [39–42]. This sample uses matrix elements at NLO accuracy in perturbative QCD for up to one additional parton in the final state. The PDF set used in the calculation is NNPDF3.0nlo. The matrix elements are matched to the Pythia8 parton shower [43] using the FxFx scheme [42]. Pythia8 is also used to model the hadronisation and underlying event, with the A14 set of tuned parameters [44]. This sample is referred to as MG5+Py8. In both the Sherpa and MG5+Py8 samples, the Frixione isolation parameters for fragmentation photons [45] are set to $\delta_0 = 0.1$, $\epsilon = 0.1$ and $n = 2$.

The electroweak production of dijets in association with the $W\gamma$ system constitutes approximately 1% of the signal process and is not included in the samples discussed above. A sample of these EW $W\gamma jj$ events is produced with Sherpa 2.2.12 and added to the signal predictions. The sample is generated using matrix elements with up to one additional parton at LO in perturbative QCD. The PDF set used in the calculation is NNPDF3.0nnlo. The matrix elements are matched to the Sherpa parton shower using the MEPS@NLO prescription. The Frixione isolation parameters are $\delta_0 = 0.1$, $\epsilon = 0.1$ and $n = 2$.

The production of $W\gamma$ with the W boson decaying first to a τ-lepton and then subsequently to an electron or muon is treated as a background in this measurement. Samples of these events are produced using Sherpa and MG5+Py8 in the same way as for the signal process (including the EW $W\gamma jj$ contribution). $Z\gamma$ events also act as a source of background when one of the leptons from the Z boson decay is not reconstructed by the detector. An inclusive $Z\gamma$ sample is generated using Sherpa 2.2.11 using the same settings as for inclusive $W\gamma$ production. The $Z\gamma$ sample is scaled by a factor of 1.08 to match the signal strength reported in recent ATLAS measurements [46]. A sample of EW $Z\gamma jj$ events is produced with Sherpa 2.2.12 and added to the prompt background, using the same event generator settings as for EW $W\gamma jj$ events.

The production of $t\bar{t}\gamma$, $tW\gamma$ and $tq\gamma$ is another source of prompt background. These events are modelled using the MadGraph5 event generator at LO accuracy in QCD, with the NNPDF2.3lo [47] PDF sets. The events were interfaced with Pythia8 to model the parton shower, hadronisation, and underlying

event, using the A14 set of tuned parameters [44]. For all backgrounds with prompt photons, the Frixione isolation parameters are defined in the same way as for the signal samples. The $t\bar{t}\gamma$ sample is scaled by a factor of 1.44 to match the signal strength reported in recent ATLAS measurements [46, 48].

Diphoton production acts as background when one of the photons is misidentified as an electron. Samples of these events are produced using Sherpa 2.2.4 with matrix elements accurate to NLO in QCD for zero or one partons in the final state and LO in QCD for up to three additional partons. The NNPDF3.0nnlo PDF set was used and the matrix elements were matched to the Sherpa parton shower using the MEPS@NLO prescription.

Background processes that do not contain prompt leptons or prompt photons are estimated using data-driven techniques as outlined in Section 5. The data-driven method to determine the background from $Z \to e^+e^-$ events in which one electron is reconstructed as a photon (referred to as $e \to \gamma$) applies scale factors to correct MC simulations. A Z + jets sample is produced using Sherpa 2.2.11 at NLO accuracy in QCD for up to two additional partons in the final state and at LO accuracy for up to 5 additional partons in the final state. NNPDF3.0nnlo set of parton distributions are used and the MEPS@NLO prescription is used to match the matrix elements to the parton shower. The data-driven estimate to determine the background from events in which a jet is misidentified as a lepton ($j \to \ell$) makes use of a dijet control region to estimate the $j \to \ell$ efficiency. Backgrounds in this control region arise from W + jets, Z + jets and γ + jets production and are subtracted from the data. The W + jets sample is produced using the same settings as for Z + jets production. The γ + jets sample is produced using Sherpa 2.2.2 with matrix elements accurate to NLO in QCD for up to one parton in the final state and to LO in QCD for up to four additional partons. NNPDF3.0nnlo set of parton distributions are used and the MEPS@NLO prescription is used to match the matrix elements to the parton shower.

EFT studies are facilitated using dedicated samples produced using the MadGraph5 event generator at LO accuracy in QCD for up to one additional parton in the final state. The NNPDF2.3lo PDFs are used in the calculation. Pythia8 is used for parton showering, hadronisation and underlying event with the A14 set of tuned parameters. The matrix elements are matched to the Pythia8 parton shower using the CKKW-L procedure [49, 50]. The anomalous coupling effects predicted by EFT operators in the Warsaw basis are implemented in SMEFTSim 3.0 [51, 52]. Samples are produced for the $O_{\tilde{W}}$, $O_{H\tilde{W}B}$, O_W and O_{HWB} operators. The M_W scheme is chosen for the EW sector in the SMEFTSim configuration and a $U(2)^3$ symmetry is adopted for light quark transformations. The masses and Yukawa couplings of all fermions except top and bottom quark are set to zero and the CKM matrix is set to the identity matrix.

All MC samples are passed through a detailed simulation of the ATLAS detector [53] based on Geant4 [54]. The effect of multiple proton–proton interactions (pile-up) in each bunch crossing is accounted for using simulations of inelastic pp collisions produced with Pythia8 [55]. These inelastic pp interactions are added to the signal and background simulations and weighted to ensure that the distribution of the average number of pile-up interactions matches that observed in the data. Residual differences between lepton trigger, identification and isolation efficiencies are corrected on an event-by-event basis using p_{T} and η dependent scale factors. A similar approach is adopted to account for residual differences in the photon identification and isolation efficiencies.

4 Event and object selection

The measurements are performed using proton–proton collision data collected at a centre-of-mass energy of $\sqrt{s} = 13$ TeV, with an integrated luminosity of 140 fb^{-1} [56]. The events are required to pass unprescaled single-lepton triggers [57, 58]. The minimum transverse momentum thresholds applied to leptons in the trigger depend on the lepton flavour, lepton isolation criteria, and data-taking period, and vary between 20 – 26 GeV. Events are required to satisfy stringent data quality criteria, which ensure that the ATLAS detector was fully operational during stable beam conditions [59]. Events are also required to have at least one reconstructed interaction vertex [60], where each candidate vertex has at least two charged-particle tracks with $p_{\mathrm{T}} > 500$ MeV. The primary vertex is defined as the vertex with the highest scalar sum of track p_{T}^2.

Muons are reconstructed by matching tracks in the inner detector to tracks in the muon spectrometer and have $p_{\mathrm{T}} > 7$ GeV and $|\eta| < 2.5$. Muons are required to pass the Loose identification working point and the PflowLoose_VarRad isolation working point [61]. In addition, muons must originate from the primary vertex by requiring $|d_0/\sigma_{d_0}| < 3$ and $|z_0 \sin\theta| < 0.5$ mm, where d_0 is the distance of closest approach to the primary vertex in the transverse plane, σ_{d_0} is the corresponding uncertainty, and z_0 is the longitudinal distance between the primary vertex and the point at which d_0 is defined.

Electrons are reconstructed from clusters of energy deposits in the electromagnetic calorimeter matched to tracks reconstructed in the inner detector and have $p_{\mathrm{T}} > 7$ GeV and $|\eta| < 2.47$ (but excluding a calorimeter crack region $1.37 < |\eta| < 1.52$). Electrons are required to satisfy the Loose identification working point [62], the Loose_VarRad isolation working point [63], $|d_0/\sigma_{d_0}| < 5$, and $|z_0 \sin\theta| < 0.5$ mm.

Photons are also reconstructed from clusters of energy deposits in the electromagnetic calorimeter and are subsequently defined as converted or unconverted. Converted photons are clusters that are matched to one or two inner detector tracks commensurate with a $\gamma \to e^+e^-$ conversion vertex, whereas unconverted photons are required to be unmatched to both inner detector tracks and photon conversion vertices. Photons are required to have $p_{\mathrm{T}} > 12$ GeV and $|\eta| < 2.37$, excluding the crack region $1.37 < |\eta| < 1.52$. In addition, photons are required to satisfy the Loose identification working point and the Loose isolation working point [62].

Jets are reconstructed using the anti-k_t algorithm [64, 65] with a distance parameter of $R = 0.4$. The inputs to the jet algorithm are calorimeter topoclusters and inner detector tracks, which are combined using particle-flow algorithms [66]. The jet energy scale and resolutions are calibrated using p_{T}- and $|\eta|$- dependent correction factors determined from MC simulations and data-driven methods [67]. Jets are required to have $p_{\mathrm{T}} > 20$ GeV and $|\eta| < 4.4$. Jets are also required to pass the tight working point of the jet vertex tagging algorithm [68], which ensures that the jets originate from the primary vertex. Jets containing a b-hadron are identified with the DL1r tagger [69] with an average efficiency of 70% for true b-jets, as estimated in ttbar events.

The magnitude of the missing transverse momentum, $p_{\mathrm{T}}^{\mathrm{miss}}$, and the associated azimuthal direction, are calculated from the negative vector sum of the transverse momenta of the muons, electrons, photons, jets, and a track-based soft term [70]. The soft term is calculated from all inner-detector tracks that are not matched to any of the reconstructed muons, electrons, photons or jets.

An object overlap removal procedure is applied to remove ambiguities in the object reconstruction. Electrons are removed if they share an ID track with a muon. Jets are removed if they have $\Delta R < 0.2$ with respect to an electron or $\Delta R < 0.4$ with respect to a photon. Jets are also removed if they have less than three tracks

and have $\Delta R < 0.2$ with respect to a muon. Photons are rejected if they have $\Delta R < 0.4$ with respect to an electron or a muon. Electrons and muons are then removed if they have $\Delta R < 0.4$ with respect to a jet.

Following the overlap removal, events are required to contain exactly one lepton, at least one photon, and have $p_{\mathrm{T}}^{\mathrm{miss}} > 40$ GeV. The leading photon and the lepton are required to have $p_{\mathrm{T}}^{\gamma} > 30$ GeV and $p_{\mathrm{T}}^{\ell} > 30$ GeV, respectively. The photon is then required to pass the Tight identification working point and the TightCaloOnly isolation working point [62]. The identification and isolation criteria for the lepton are also tightened; the Tight identification working point and Tight_VarRad isolation working point are required for electrons, whereas the Tight identification working point and the PflowTight_VarRad isolation working point are required for muons. Events are rejected if they contain any b-jets with $p_{\mathrm{T}} > 20$ GeV and $|\eta| < 2.5$, to reject backgrounds containing one or more top quarks. Similarly, events are rejected if the invariant mass of the lepton-photon system is in the range $81 < m_{\ell\gamma} < 101$ GeV, to reject backgrounds arising from $Z \to e^+e^-$ with one of the electrons reconstructed as a photon. Finally, the separation of the lepton and the photon is required to satisfy $\Delta R > 0.8$. The majority of the differential distributions are measured in this *baseline* region. The exceptions are the differential cross sections as a function of $\Delta\phi_{\ell\gamma}$ and $\Delta\eta_{\ell\gamma}$, which are measured in a *jet veto* region in which events are required to have no jets with $p_{\mathrm{T}} > 30$ GeV, in addition to the selections that define the *baseline* region. The double differential cross section as a function of ϕ_f and p_{T}^{γ} is measured in both the *baseline* and *jet veto* regions.

Figure 3 shows the number of events measured as a function of p_{T}^{γ}, η_{γ}, $m_{\ell\gamma}$ and $\Delta\eta_{\ell\gamma}$. The data are compared to a combined prediction containing the signal and all background processes. The signal and prompt backgrounds are modelled using the MC simulations discussed in Sec. 3. The other backgrounds are determined using the data-driven methods discussed in Sec. 5. The data are in reasonable agreement with the combined predictions for the p_{T}^{γ}, η_{γ} and $m_{\ell\gamma}$ distributions, which are measured in the *baseline* region. The combined prediction is below the data for the $\Delta\eta_{\ell\gamma}$ distribution, which is measured in the *jet veto* region. The theoretical uncertainties on the signal and prompt backgrounds are much smaller in the *jet veto* region and it is possible that they are underestimated due to the application of a jet veto [71].

The number of events selected in the data is 264094, with background processes accounting for 38% of the yield. The dominant source of background is $j \to \gamma$ background (40% of total background), followed by prompt backgrounds (27%), the $\ell \to \gamma$ background (18%), the $j \to \ell$ background (8%), and the pile-up γ background (7%). The agreement between data and combined prediction has also been checked separately in the electron and muon channels, with good agreement and similar signal strengths observed in each channel.

5 Background estimation

The backgrounds relevant to this analysis can be grouped into three categories. The first category comprises prompt backgrounds that arise from processes that produce genuine photons and leptons in the final state, such as $W(\to \tau\nu)\gamma$, $Z\gamma$, $t\bar{t}\gamma$, $tW\gamma$, and $tq\gamma$. These contributions are estimated from Monte Carlo simulation as discussed in Section 3. The theoretical and experimental uncertainties on these backgrounds are discussed in Section 8.

The second category consists of non-prompt or fake backgrounds, where a reconstructed object is misidentified as a photon or a lepton. These contributions are not reliably modelled in simulation and are therefore determined with data-driven techniques based on template fits, control regions, and sideband methods, with associated systematic uncertainties derived from these procedures.

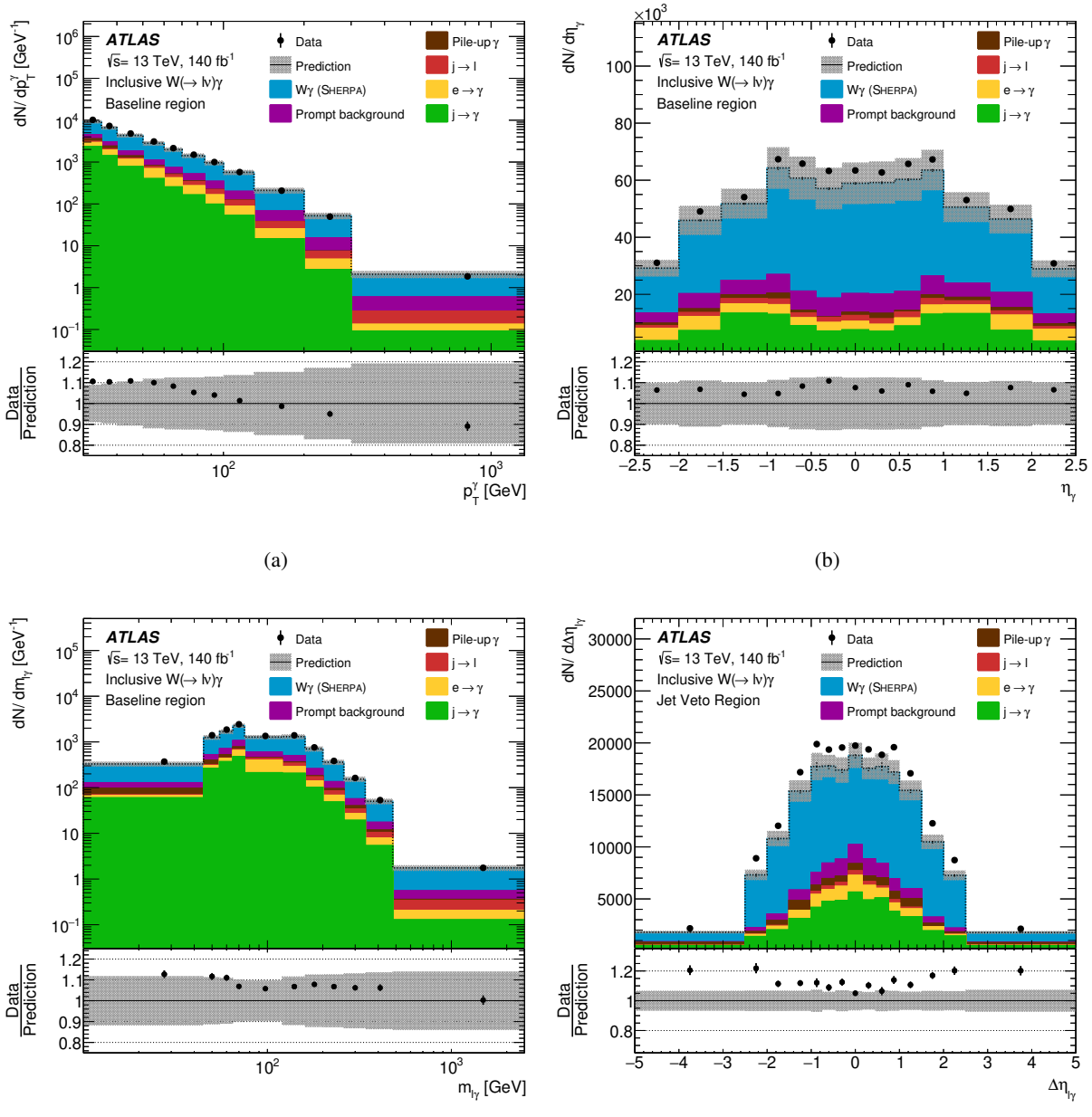

Figure 3: Predicted and observed yields as a function of (a) p_{T}^{γ}, (b) η_{γ}, (c) $m_{\ell\gamma}$ and (d) $\Delta\eta_{\ell\gamma}$. The data are represented as black points and the associated error bars represent the statistical uncertainty. Background processes with prompt leptons and photons, such as $Z\gamma$ production and the fully leptonic decays of $t\bar{t}\gamma$ production, are estimated by using simulations and labelled as 'Prompt.' Backgrounds arising from non-prompt leptons ($j \to \ell$), non-prompt photons ($j \to \gamma$), electrons-faking-photons ($e \to \gamma$) and pile-up photons are estimated using data-driven techniques as outlined in Section 5. The total uncertainty on the combined signal and background prediction is shown as a grey band (the calculation of these uncertainties is outlined in Section 8).

Finally, the pile-up background arises when a genuine photon from an additional proton–proton interaction in the same bunch crossing is combined with a lepton from the hard-scatter W boson decay. Although the photon is real, the combination fakes the $W\gamma$ signal. This background is estimated separately using data-driven techniques that exploit the separation between the photon and the primary vertex along the beam axis.

The remainder of this section describes the estimation of the non-prompt and pile-up backgrounds, which together constitute the dominant reducible contributions to the background of the analysis.

5.1 Jets faking photons

The dominant background for this analysis is due to W+jets events where either a jet is misidentified as a photon or a real photon produced within a hadronic jet passes the photon selection criteria. These contributions, referred to as $j \to \gamma$, are estimated using a data-driven method. It is based on template fits to the photon isolation distribution, and validated using an independent sideband (ABCD) method [72]. The measurement of the boost asymmetry uses an independent estimation of this background that follows the same template-fit strategy.

Photon candidates in the analysis are required to pass tight identification and isolation criteria. The calorimeter isolation variable, defined from the transverse energy within a cone of size $\Delta R = 0.4$ around the photon axis, is effective at separating real photons from jets. Prompt photons produce a narrow peak near zero isolation, while jets give rise to a broad tail at higher isolation values. This separation is exploited by constructing isolation templates for signal and background.

The signal template is obtained from simulated $W\gamma$ events containing a Tight photon. The background template is derived from data using events in which the photon passes a Loose identification working point but fails the Tight requirement, thereby enriching the sample in jet-induced photons. A small signal leakage into this control sample is estimated using simulation and corrected for in the template construction. A binned fit to the isolation distribution then determines the relative contributions of real photons and jet-induced photons. The $j \to \gamma$ background yield is obtained by integrating the fitted jet-induced photon template within the isolation range used in the analysis. This procedure is performed bin-by-bin for each observable relevant to the differential cross section measurements.

An independent cross-check is performed using an ABCD method, in which photon identification and isolation are treated as approximately uncorrelated variables. Four regions are defined: the signal region (tight ID, isolated), and three control regions corresponding to either looser identification or inverted isolation. The number of jet-induced photons in the signal region is then predicted from the control regions after correcting for signal leakage and prompt-photon contamination. The method provides good statistical precision and a conceptually simple validation of the template fit. Some discrepancies are observed in the highest p_{T} and most forward bins in η, where correlations between the two variables are significant, and the ABCD method is expected to become less reliable.

The dominant sources of systematic uncertainty in the $j \to \gamma$ estimate are associated with the construction of the background template and with the modelling of the prompt photon template. For the systematic uncertainty associated with the background template, alternative loose identification working points are used to construct the background templates. The spread of the $j \to \gamma$ predictions obtained from fitting the isolation distribution with different background templates is taken as the systematic uncertainty, which is typically around 12% . For the systematic associated with the modelling of the prompt photon template,

different event generators (SHERPA and MG5+PY8) are used in the fit to the isolation distribution and the observed differences of around 4% are propagated as uncertainties.

5.2 Jets faking leptons

Events in which a jet is misidentified as a lepton, or where a non-prompt lepton is produced inside a hadronic shower and satisfies the analysis selection, constitute another source of background for this analysis. In the electron channel, such contributions originate mainly from Dalitz decays or misidentified hadrons, while in the muon channel, they arise predominantly from semileptonic decays of heavy-flavour hadrons. Since the modelling of these processes is affected by large uncertainties in hadronisation and the detector response, a fully data-driven strategy is adopted for each lepton channel.

Two complementary approaches are considered: the matrix method, extended with a Poisson likelihood fit, and the fake factor method [73]. Both rely on defining two nested lepton selections. "Baseline" leptons satisfy looser identification and isolation criteria, chosen to enhance the contribution of fakes, while "tight" leptons correspond to the signal definition used in the analysis. By construction, every tight lepton is also a baseline lepton. The probability for a baseline lepton to pass the tight requirements is measured separately in samples enriched in prompt leptons, providing the *real efficiency* ϵ_r, and in samples enriched in fake leptons, giving the *fake efficiency* ϵ_f.

The real efficiency is measured using $Z \to \ell\ell$ events. Events with exactly two oppositely charged, same-flavour leptons with invariant mass within 10 GeV of the Z boson mass are selected. To reduce diboson and top-quark backgrounds, requirements on missing transverse energy and a b-jet veto are applied. The leading lepton is required to pass the tight selection and to match the trigger, while the subleading lepton is used as a probe. The fraction of probe leptons passing the tight criteria defines ϵ_r as a function of p_{T} and η. This region is very pure in Z boson events, and comparisons of data and simulation show excellent agreement.

The fake efficiency is measured in a dijet sample selected with one baseline lepton and at least one jet with $p_T \geq 35$ GeV. Requirements on the azimuthal separation between the lepton and the jet ($|\Delta\phi(\ell, j)| > 2.8$), as well as low missing transverse momentum ($p_{\mathrm{T}}^{\mathrm{miss}} < 25$ GeV), suppress contributions from W+jets and Z+jets events with prompt leptons. Residual prompt contributions are subtracted using simulation, and systematic uncertainties are assigned to this subtraction. To obtain stable estimates in bins of lepton p_{T} and η, a bootstrap resampling technique [74] is employed to determine both the central value and statistical uncertainty of ϵ_f.

The efficiencies are applied in an "application region" defined by the baseline lepton selection. The matrix method relates the observed numbers of tight and non-tight leptons to the underlying real and fake components via ϵ_r and ϵ_f. In the fake factor method, the prompt contribution in the application region is subtracted before applying the fake factor. The resulting $j \to \ell$ yields are computed separately in the electron and muon channels and for each observable used in the measurement.

The matrix method is taken as the nominal estimate, with the difference to the fake factor method assigned as an uncertainty that is typically about 4%. Additional systematic uncertainties are considered, including the statistical precision of the control region measurements, the subtraction of prompt leptons in the dijet region, and differences in fake composition between control and signal regions. Validation regions, defined with inverted missing transverse momentum requirements, provide further cross-checks. In all cases, the data are well described by the background model within the assigned uncertainties.

5.3 Electrons faking photons

In the electromagnetic calorimeter, electrons and photons both produce narrow, localised energy deposits, making it possible for prompt electrons to be misidentified as photons. This background, denoted $e \to \gamma$, is expected to contribute at the ~10% level to the selected data sample. This background contribution is estimated using a data-driven fake factor method, which corrects the simulation with scale factors measured in control regions.

The basic observable is the '$e \to \gamma$ fake rate',

$$F_{e\to\gamma} = \frac{N_{e\gamma}}{N_{ee}},$$

defined as the ratio of reconstructed $Z \to e\gamma$ candidates, where one electron candidate is misidentified as a photon, to reconstructed $Z \to ee$ events, where both electron candidates are identified as electrons. The $e \to \gamma$ fake rate can be measured both in data and in the simulation, using $Z \to ee$ events. The ratio of the two defines a scale factor

$$\mathrm{SF} = \frac{F^{\mathrm{data}}_{e\to\gamma}}{F^{\mathrm{MC}}_{e\to\gamma}},$$

which quantifies the mismodelling of the mis-identification rate in simulation. The method is applied by reweighting simulated events that contain an electron reconstructed as a photon with the scale factor evaluated as a function of the transverse momentum and pseudorapidity of the misidentified photon candidate.

The event yields in the $e \to \gamma$ fake rate are measured using a tag-and-probe method in control regions enriched in $Z \to ee$ events. The leading electron candidate is required to satisfy Tight identification and isolation criteria, while the second candidate electron is treated as the probe. When the probe electron candidate is reconstructed as an electron, the event is selected for the ee control region, and when it is reconstructed as a photon, it is selected for the $e\gamma$ control region. Fits to the invariant mass of the ee or $e\gamma$ system in the range $70 < m_{\ell\ell} < 110$ GeV are used to extract the yields of true Z boson events, separating them from background contributions. The scale factors obtained from the extracted yields are in agreement with those obtained in earlier ATLAS measurements [75]. The dominant systematic uncertainties arise from electron and photon identification efficiencies, energy resolution, and pile-up modelling. The $m_{\ell\ell}$ range used in the fit to extract the Z-boson yields is also varied. These uncertainties typically result in 5% variations in the $e \to \gamma$ background estimate, corresponding to a 0.5% effect on the total event yield.

5.4 Pile-up backgrounds

In proton–proton collisions at the LHC, multiple interactions typically occur within the same bunch crossing. As the position of the photon production vertex is not well measured in the absence of an ID track, a selected photon can originate from an interaction that is different from the one producing the lepton from the $W \to \ell\nu$ decay. Such mis-associations produce a background that mimics the $W\gamma$ signal. Although small in absolute size, this pile-up background contribution is non-negligible.

The method to estimate the pile-up background relies on the longitudinal separation along the beam axis between the reconstructed photon position, extrapolated to the beam line (z_γ), and the primary vertex associated with the lepton (z_{PV}). The distribution of

$$\Delta z = z_\gamma - z_{\mathrm{PV}}$$

is used to distinguish genuine $W\gamma$ events from pile-up. For signal and background events where the reconstructed photon and lepton originate from the same vertex, Δz is sharply peaked at zero, with a width determined by the detector resolution. In contrast, for pile-up events the two quantities are uncorrelated, giving a broader Gaussian distribution with width ~50 mm, consistent with the longitudinal spread of two independent proton–proton collisions.

The determination of z_γ depends on the photon type. For converted photons, z_γ is obtained from tracks associated with the conversion vertex, providing sub-millimetre precision when the conversion occurs inside the silicon detectors. For unconverted photons, z_γ is estimated by calorimeter pointing, using the shower profile of the photon in the first two calorimeter layers [76]. Since the resolution of converted photons is significantly better, the analysis uses this category to obtain a more precise estimate.

The fraction of pile-up events is extracted by comparing the observed Δz distribution in data to the expectation from simulated $W\gamma$ events. The signal component is normalised to the data in the central region around $\Delta z \approx 0$, while the tails at $|\Delta z| > 50$ mm, which are dominated by pile-up, are used to measure that contribution. This approach yields an overall pile-up fraction of $f_{\text{PU}} = (4.8 \pm 0.3)\%$. To avoid double-counting with the jet-induced photon background, which is treated separately, a photon purity correction is applied [77]. The resulting estimate for the pile-up photon background is $f_{\text{PU}} = (2.6 \pm 0.4)\%$. For the kinematic measurements presented in this paper, the estimate is performed independently for each measured bin.

6 Construction of CP-sensitive observables using neural networks

Anomalous interactions are typically described using EFT, in which the SM Lagrangian is augmented with dimension-six operators, i.e.,

$$\mathcal{L} = \mathcal{L}_{\text{SM}} + \sum_i \frac{c_i}{\Lambda^2} O_i \tag{1}$$

where $\mathcal{L}_{\text{SM}}$ is the SM Lagrangian, the O_i are a set of the dimension-six operators, and the c_i/Λ^2 are Wilson coefficients that specify the strength of the anomalous interactions. The dimension-six operators can be CP-even or CP-odd. The squared scattering amplitude for the effective field theory prediction can be written as

$$|\mathcal{M}|^2 = |\mathcal{M}_{\text{SM}}|^2 + 2\,\text{Re}(\mathcal{M}_{\text{SM}}{}^* \mathcal{M}_{\text{d6}}) + |\mathcal{M}_{\text{d6}}|^2, \tag{2}$$

where $\mathcal{M}_{\text{SM}}$ is the SM scattering amplitude and $\mathcal{M}_{\text{d6}}$ is a 'dimension-six' scattering amplitude that contains the anomalous interaction. The cross-section therefore contains three contributions: the SM contribution, the interference between the SM amplitude and the dimension-six amplitude, and a pure dimension-six contribution. The SM contribution and the pure dimension-six contributions are always CP-even, regardless of the nature of the operator. However, the interference contribution will be CP-even for CP-even operators and CP-odd for CP-odd operators. For CP-odd operators an equal amount of constructive interference and destructive interference occurs, meaning that the interference term integrates to zero for CP-even observables. The presence of CP-odd anomalous interactions can therefore only be probed using appropriately constructed CP-odd observables, such as $\Delta\phi_{\ell\gamma}$.

The EFT samples described in Section 3 are produced using a decomposition scheme, whereby the SM, interference and pure-dimension-six contributions are produced separately. Following the approach outlined in Refs. [9, 78], an optimised CP-sensitive observable is constructed using a neural network (NN).

The NN is trained to distinguish between constructive interference, destructive interference, and the SM. The outputs of the neural network are then used to construct a new observable,

$$O_{\mathrm{NN}} = P_{+} - P_{-}, \tag{3}$$

where P_{+} is the probability of the event to be constructive interference and P_{-} is the probability of the event to be destructive interference. The sum of probabilities is $P_{+} + P_{-} + P_{SM} = 1$, where the P_{SM} is the probability of the event to be a SM contribution.

The NN used in this method is a multilayer perceptron (MLP), which is composed of multiple layers of neurons, including input layer, output layer, and multiple hidden layers. All layers are arranged in a hierarchy structure and are fully connected to the subsequent layer. A dedicated MLP is trained for each CP-odd EFT operator using SM events and the related EFT interference samples. The EFT interference sample is split according to the MC event weight into two classes: positively-weighted events and negatively-weighted events, which capture the constructive and destructive interference, respectively. The MC event weight is only used to define the classes and is not used in the MLP training. The SM events make up the third class.

The MLP is constructed using Keras [79] and TensorFlow [80]. The Sequential model is chosen with three hidden layers of 100, 50 and 20 neurons, respectively, each employing a ReLU activation function [81]. Ten variables are input to the network: the transverse momentum, pseudo-rapidity, azimuthal angle and charge of the lepton, the transverse momentum, pseudo-rapidity and azimuthal angle of the photon, the magnitude and azimuthal angle of the missing transverse momentum, and the leading jet transverse momentum. To avoid inefficient training and biased learning, the input variables are scaled: the angular variables and the lepton charge are linearly scaled to the range [0,1], whereas the momentum-based variables are first log transformed and then linearly scaled to the range [0,1]. The scaling parameters for each variable are determined using the training dataset. There are three output classifications, SM, constructive interference, and destructive interference. The output layer therefore has three neurons and uses softmax activation functions. The categorical cross-entropy [82] loss function is chosen (with one-hot encoding) alongside the Adam optimiser [83] for the network weights and biases. The batch size is chosen to be 5000 and the networks are trained for up to 200 epochs. Early stopping is implemented with a min-delta of zero and a patience of 3 or 10, for the $O_{H\tilde{W}B}$ and $O_{\tilde{W}}$ operators, respectively. The min-delta and patience choices were chosen to avoid the training being stopped too early, a situation that can arise due to the kinematic similarity between the constructive- and destructive- interference classes.

For both classifiers, the input data is split into training data (80%), validation data (10%) and test data (10%). The training data is used to train the MLPs and the validation data is used in the early stopping criteria. The test data is used to test for overtraining, with no obvious biases observed in the reconstructed O_{NN} distributions. Each MLP achieves an accuracy of around 56%, which is reasonable compared to random chance (33%). Receiver-operating characteristics are checked for each class in the model using the test data and the area-under-the-curve found to be between 0.71 and 0.81 depending on the class and model.

Figure 4 shows the number of events measured in the baseline region as a function of O_{NN} for the $O_{H\tilde{W}B}$ and $O_{\tilde{W}}$ operators. The data are in good agreement with the combined prediction containing the signal and all background processes. The signal and prompt backgrounds are modelled using the MC simulations discussed in Sec. 3. The other backgrounds are determined using the data-driven methods discussed in Sec. 5. A data augmentation approach is taken when deriving the data-driven backgrounds for O_{NN} (and $\Delta\phi_{\ell\gamma}$): the distributions are filled twice using values of O_{NN} and $O_{\mathrm{NN,CP}}$, where $O_{\mathrm{NN,CP}}$ is the

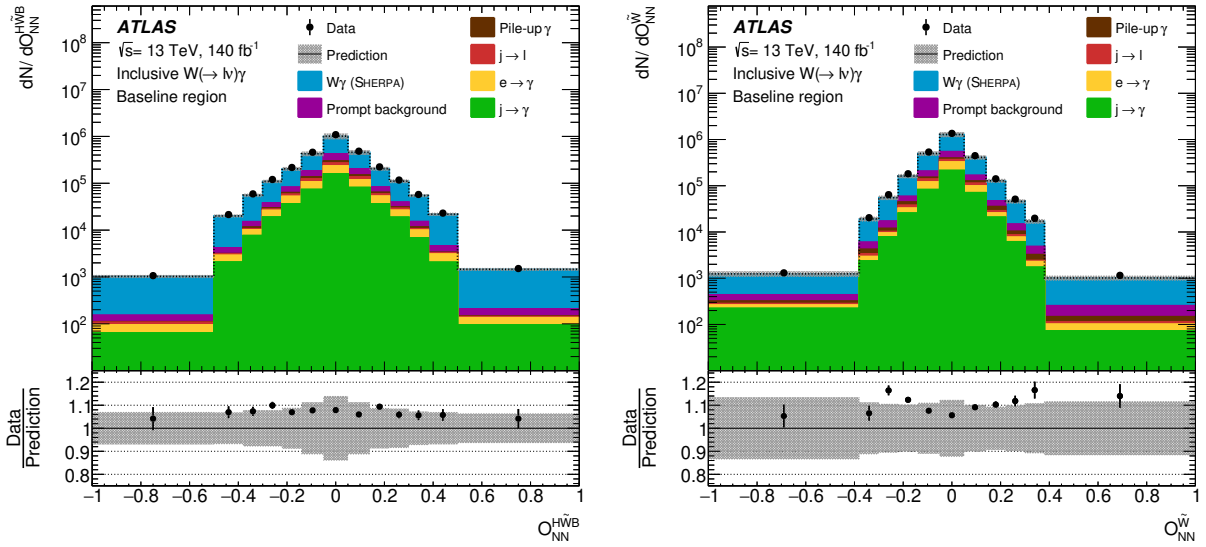

(a) (b)

Figure 4: Predicted and observed yields as a function of O_{NN} for (a) the $O_{H\tilde{W}B}$ operator and for (b) the $O_{\tilde{W}}$ operator. The data are represented as black points and the associated error bars represent the statistical uncertainty. Background processes with prompt leptons and photons are estimated by using simulations and labelled as 'Prompt'. Backgrounds arising from non-prompt leptons ($j \to \ell$), non-prompt photons ($j \to \gamma$), electrons-faking-photons ($e \to \gamma$) and pile-up photons are estimated using data-driven techniques. The total uncertainty on the combined signal and background prediction is shown as a grey band.

observable obtained after applying a CP-transform to the data. A weight of 0.5 is used for each event when filling the histograms twice to preserve the overall normalisation. The data augmentation ensures that the data-driven backgrounds are CP-even in the observable and improves the statistical accuracy of the data-driven background by a factor of $\sqrt{2}$.

7 Correction for detector effects

Differential cross sections for inclusive $W\gamma$ production are measured at the particle level, by subtracting the backgrounds from the observed event yields in each bin of each distribution and then correcting for the effects of detector inefficiency and resolution.

The particle level is defined using objects and selections that closely resemble the detector-level selections presented in Section 4. Final state particles are defined as those with $c\tau > 10$ mm. Prompt particles are defined as those that do not originate from the decay of a hadron. Charged leptons are defined by dressing prompt electrons and prompt muons with all nearby prompt photons, i.e. those within a distance $\Delta R < 0.1$. Leptons from τ decays are ignored. Dressed electrons are required to have $p_{\mathrm{T}} > 7$ GeV and $|\eta| < 2.47$, but excluding the region $1.37 < |\eta| < 1.52$. Dressed muons are required to have $p_{\mathrm{T}} > 7$ GeV and $|\eta| < 2.5$. Photons are required to be prompt and satisfy $p_{\mathrm{T}} > 12$ GeV and $|\eta| < 2.37$, but excluding the region $1.37 < |\eta| < 1.52$. Jets are defined using the anti-k_t algorithm with radius parameter of $R = 0.4$ and are required to have $p_{\mathrm{T}} > 20$ GeV and $|y| < 4.4$. The input to the jet finding algorithm are all final

state particles excluding prompt leptons. Jets are identified as b-jets if they contain a B-hadron with $p_{\mathrm{T}} > 5$ GeV within $\Delta R < 0.3$ of the jet centre. The missing transverse momentum is defined as the vector sum of all final-state non-interacting prompt particles. An overlap removal procedure is then applied to the reconstructed leptons, photons and jets to mimic the procedure applied at detector level. Jets are removed if they are within $\Delta R < 0.4$ of a photon or $\Delta R < 0.2$ of a lepton. Following this, photons and jets are removed if they are within $\Delta R < 0.4$ of a lepton.

The *baseline* fiducial region for the majority of the differential measurements is defined as containing exactly one lepton, at least one photon, zero b-jets, and $p_{\mathrm{T}}^{\mathrm{miss}} > 40$ GeV. The lepton and the leading photon are required to have $p_{\mathrm{T}} > 30$ GeV. Photons are also required to be isolated, i.e. the scalar sum of transverse momenta of all interacting particles within $\Delta R < 0.4$ of the photon is required to satisfy $p_{\mathrm{T}}^{\mathrm{iso}} < 0.026 p_{\mathrm{T}}^{\gamma} + 8.21$ GeV. The photon and lepton are required to be separated by $\Delta R > 0.8$ and have an invariant mass of $m_{\ell\gamma} < 81$ GeV or $m_{\ell\gamma} > 101$ GeV. For the differential cross sections measured as a function of $\Delta\phi_{\ell\gamma}$ and $\Delta\eta_{\ell\gamma}$, events are also required to have no jets with $p_{\mathrm{T}} > 30$ GeV; this is referred to as the *jet veto* fiducial region. The double differential cross section as a function of p_{T}^{γ} and ϕ_f is measured in both the *baseline* and *jet veto* regions. Finally, the measurements of the boost asymmetry are unfolded to a common phase space for leptons, i.e. $|\eta_\ell| < 2.5$.

Each distribution is unfolded to particle level using D'Agostini's iterative unfolding method [84]. This method uses Monte Carlo simulations to (i) remove events that are reconstructed at detector level but not in the fiducial region at particle level (fiducial fraction), (ii) reverse the migrations between bins of distributions, and (iii) correct for events that are in the fiducial region at particle level but not reconstructed at detector level (reconstruction efficiency). The Sherpa $W\gamma$ sample is used as the default simulation for unfolding, with the EW $W\gamma jj$ contribution included. The binning of each distribution is chosen such that the purity of each bin is typically greater than 60% and that the expected statistical accuracy of the background-subtracted data is around 1-2%. The number of iterations is chosen to minimise the overall uncertainty, accounting for statistical uncertainties and bias in the unfolding method. The unfolding bias is determined using a data-driven method and described in Sec. 8. Two iterations are chosen for all distributions except $O_{\mathrm{NN}}^{H\tilde{W}B}$ and $O_{\mathrm{NN}}^{\tilde{W}}$, where three iterations are needed.

The unfolding procedure introduces statistical correlations between neighbouring bins in the measured distributions. These correlations are small (1-4%) for the p_{T}^{γ}, p_{T}^{ℓ}, η_γ, $\Delta\eta_{\ell\gamma}$, $\Delta\phi_{\ell\gamma}$ and $m_{\ell\gamma}$ distributions, but rise to 10% for the $m_{\mathrm{T}}^{\ell\nu\gamma}$ distribution. The largest correlations (around 20%) are observed for some bins in the $O_{\mathrm{NN}}^{\tilde{W}}$ and $O_{\mathrm{NN}}^{H\tilde{W}B}$distributions, and for the double differential distributions involving the W boson decay angles.

8 Systematic uncertainties

Experimental systematic uncertainties arise from lepton reconstruction, photon reconstruction, jet reconstruction, b-jet identification, missing transverse momentum reconstruction, the pile-up of multiple proton–proton interactions, and the luminosity of the dataset.

The lepton trigger efficiencies and lepton and photon reconstruction, identification and isolation efficiencies in simulation are corrected on an event-by-event basis using scale factors as outlined in Sec. 3. Systematic uncertainties associated with this procedure are determined by varying the scale factors by their corresponding uncertainties [61–63, 85, 86]. Lepton and photon energy and momentum scales are also calibrated using data and the calibrations are accounted for by scaling and smearing the lepton and

photon transverse momenta accordingly. The overall impact of the muon uncertainties and the electron efficiency uncertainties on the measured differential cross sections is typically less than 1%. The impact of photon efficiency uncertainties is larger, being about 2.5% at low p_{T}^{γ} and 1.5% at high p_{T}^{γ}. The impact of electron/photon energy scale and resolution systematics rises from sub-percent at low p_{T}^{γ} to 3% at high p_{T}^{γ}. For the boost asymmetry measurements, the lepton and photon uncertainties impact the numerator and denominator of the ratio in a correlated way and largely cancel.

The jet energy scale is calibrated using p_{T}- and η- dependent correction factors as described in Sec. 4. Systematic uncertainties on these correction factors are propagated through the analysis by scaling and smearing the reconstructed jet momentum accordingly [87, 88], which accounts for residual differences between data and simulation in the jet energy scale and resolution. Uncertainties due to the inefficiency of the jet vertex tagger [68] and b-jet identification [69, 89] algorithms are evaluated by applying scale factors to the MC event weights. The impact of jet energy scale and resolution uncertainties on the measured differential cross sections are typically around 2%, except in the jet veto phase space and at low $m_{\mathrm{T}}^{\ell\nu\gamma}$, where the impact is 5% and 6%, respectively. The impact of flavour-tagging uncertainties is less than 0.5%. Again, these experimental uncertainties largely cancel for the boost asymmetry measurements.

The missing transverse momentum is evaluated using the negative vector sum of all identified electrons, muons, photons and jets, as well as a soft-term to account for low-p_{T} activity. The uncertainties in the leptons, photons and jets reconstruction and calibration are propagated directly to the missing transverse momentum calculation. An additional uncertainty associated with the energy scale and resolution of the soft term is evaluated independently [70] and found to have an impact of about 1% – 1.5% on the differential cross sections.

The uncertainty in the luminosity at ATLAS is determined to be 0.83% for the Run 2 dataset [56], using a combination of Van Der Meer beams scans and measurements taken by the LUCID-2 detector [24]. The pile-up modelling in simulation involves overlaying the simulated hard-scatter events with inelastic proton–proton collisions as described in Sec. 3. The uncertainty in the pile-up modelling is obtained by reweighting the distributions to account for residual differences between the data and simulation. The impact of this uncertainty is typically less than 1%, but as high as 1.5% at very low p_{T}^{ℓ}.

Prompt backgrounds are impacted by all of the experimental uncertainties discussed above. Theoretical uncertainties in the estimation of the prompt backgrounds are obtained by independently varying the renormalisation scale, μ_{R}, and factorisation scale, μ_{F}, by factors of 0.5 and 2.0, with the added requirement that $0.5 < \mu_{\mathrm{R}}/\mu_{\mathrm{F}} < 2.0$. This produces six possible variations, each of which changes the normalisation and shape of the background. These variations are propagated through the analysis. The final uncertainty in the differential cross section is taken to be the envelope of the results obtained from the six variations. PDF uncertainties are accounted for using the quadrature sum of the deviations induced by the 100 eigenvectors of the Hessian NNPDF set. The uncertainty in the PDFs due to the choice of α_S is estimated separately by NNPDF by varying the value of α_S by ± 0.001; this is added in quadrature with the uncertainty obtained from the eigenvectors. The combined impact of scale and PDF variations in the prompt backgrounds is found to be typically 2%. Statistical uncertainties in the prompt backgrounds are propagated through the analysis directly and found to be typically 0.2%.

The uncertainties in the data-driven background estimates for $j \to \gamma$, $j \to \ell$, $e \to \gamma$, and pile-up (PU) photons, are described in Sec. 5. These uncertainties are propagated directly through the analysis chain. The statistical uncertainties in these estimates arise from data and are included in the statistical uncertainty of the unfolded measurement. The largest systematic uncertainty is associated with the $j \to \gamma$ estimate, which is around 4% at low p_{T}^{γ} but falling to 1% at high p_{T}^{γ}. The systematic uncertainty associated with

the $j \to \ell$ estimate is typically about 1.5% but rises to 4% for low p_{T}^{ℓ}. The impacts of the systematic uncertainties in the PU photon estimate and in the $e \to \gamma$ estimate are negligible.

The unfolding procedure is outlined in Sec. 7 and uses inclusive $W\gamma$ simulations produced with Sherpa to correct the background-subtracted event yields for the effects of detector inefficiency and resolution. The signal simulations are affected by all of the experimental uncertainties discussed above. In addition, theoretical uncertainties in the signal modelling are evaluated in four ways. First, the factorisation scales and renormalisation scales in the default Sherpa simulation are varied by factors of 0.5 and 2.0, with the restriction that $0.5 < \mu_{\mathrm{R}}/\mu_{\mathrm{F}} < 2.0$. Second, the uncertainty due to PDF choice is evaluated in the same way as for the prompt backgrounds, using the 100 eigenvector variations of the NNPDF set and by varying the choice of α_S used in the PDFs. Third, a data-driven test of the bias in the unfolding is estimated by independently reweighting the response matrix such that the Sherpa simulation better matches the data for each measured distribution. Finally, the impact of the choice of event generator is determined by using the MG5+Py8 simulation of $W\gamma$ events, but after reweighting the MG5+Py8 response matrix to match the Sherpa response matrix to avoid double counting the uncertainty estimated using the data-driven bias test. The latter is the largest of the four contributions, which are treated as independent and uncorrelated estimates of the signal modelling uncertainty. The overall impact of the signal modelling uncertainties on the differential cross sections is typically 2-3%, but can rise to over 10% at high $|O_{\mathrm{NN}}|$ and at high transverse momentum in the $p_{\mathrm{T}}^{\gamma} \times \phi_f$ distributions.

The impact of each source of uncertainty on the differential cross sections is shown in Figure 5 for the p_{T}^{γ}, η_{γ}, $\Delta\eta_{\ell\gamma}$ and O_{NN} distributions. The systematics associated with the data-driven background are typically the dominant uncertainties in the measurements, with signal modelling uncertainties being important at high-p_{T}^{γ} and high-$|O_{\mathrm{NN}}|$.

9 Results

In this section, the detector-corrected measurements that probe the kinematic properties of the $W\gamma$ system are presented. This includes differential cross sections sensitive to the radiation amplitude zero effect, the polarisation of the W boson, and the CP-structure of the $WW\gamma$ triple gauge interaction, as well as boost asymmetry observables that can be used in global PDF fits.

The differential cross sections are compared to four different Standard Model particle-level predictions for inclusive $W\gamma$ production. Two of these are constructed from the Sherpa and MG5+Py8 samples presented in Section 3. Sherpa is accurate to NLO in QCD for zero and one jets in the final state and to LO for up to four additional jets. MG5+Py8 is accurate to NLO in QCD for zero and one jets in the final state. Geneva [13, 90–93] is used to provide an inclusive $W\gamma$ prediction that is accurate to NNLO in QCD. Geneva matches a resummed soft collinear effective field theory prediction to fixed order NNLO predictions and is interfaced to Pythia8 for parton showering, hadronisation and underlying event. The NNPDF3.1nnlo PDF is used and the CP5 set of tuned parameters [94]. This prediction is referred to as Geneva+Py8. A final prediction is produced by scaling the Geneva+Py8 prediction with virtual EW corrections estimated with Sherpa. This prediction is referred to as Geneva+Py8+$\mathrm{EW}_{\mathrm{virt}}$ in the subsequent discussion. Uncertainties on the Sherpa and MG5+Py8 predictions are determined by independently varying the renormalisation and factorisation scales by factors of 0.5 and 2.0 and taking the envelope of all such variations. Uncertainties on the Geneva+Py8 prediction arise from renormalisation/factorisation scale variations as well as variations in the resummation scales (beam scale, soft scale, and profile transition). The total uncertainty on Geneva+Py8 is taken to be the quadrature sum of two envelopes, one formed

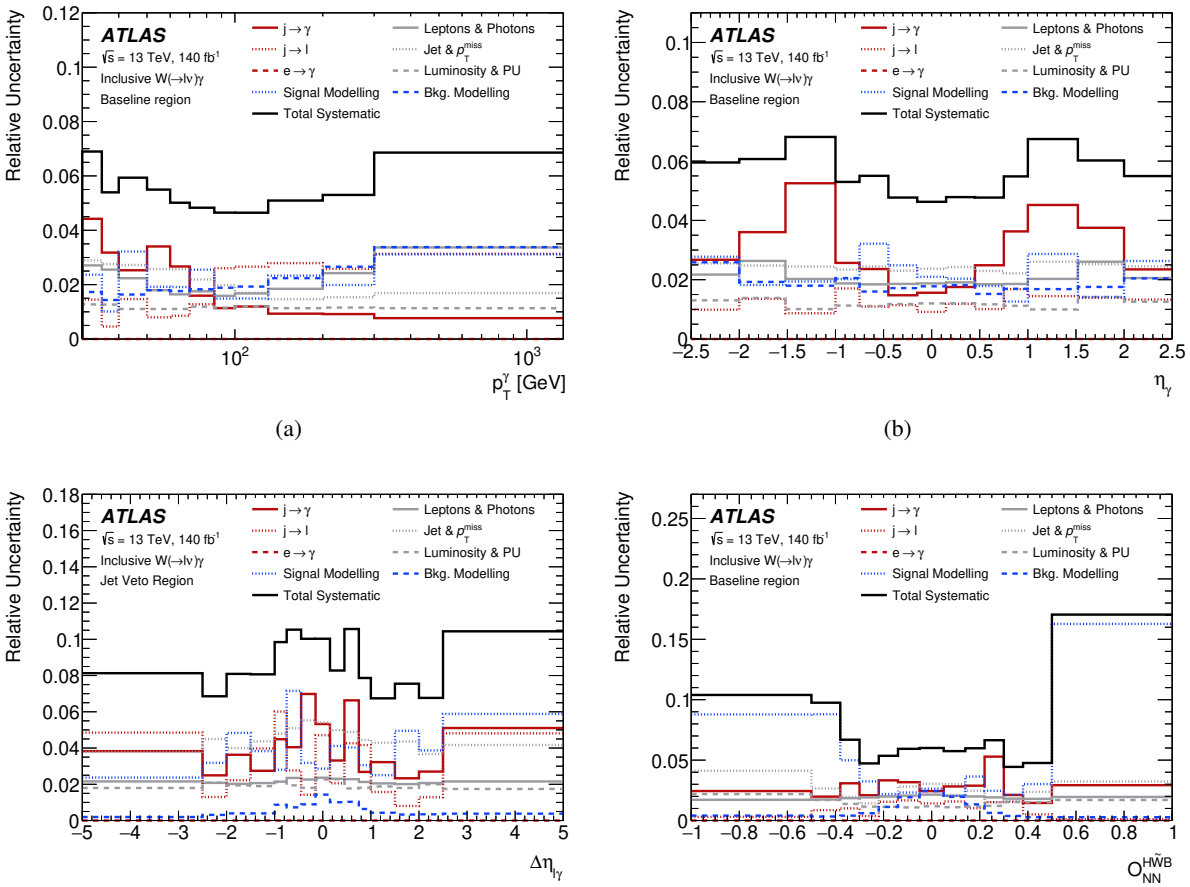

Figure 5: Relative uncertainties on the differential cross-sections as a function of (a) p_{T}^{γ}, (b) η_{γ}, (c) $\Delta\eta_{\ell\gamma}$ and (d) O_{NN}. Sources of uncertainty are grouped together for clarity. The total systematic uncertainty is shown as the quadrature sum of each source of uncertainty.

from the renormalisation and factorisation scale variations and one formed from the resummation scale variations. The uncertainty on Geneva+Py8 is propagated to the Geneva+Py8+EW$_{\mathrm{virt}}$ prediction.

Figures 6 (a)-(c) show the differential cross section measurements as a function of p_{T}^{γ}, η_{γ}, and $m_{\ell\gamma}$ in the *baseline* fiducial region. The Sherpa prediction is in agreement with the data for all three distributions but has large theoretical uncertainties. The MG5+Py8 prediction has smaller uncertainties than Sherpa and is in agreement with the data at low p_{T}^{γ} but it overestimates the cross section at high-p_{T}^{γ}. The Geneva+Py8 prediction has smaller uncertainties than both Sherpa and MG5+Py8 but also overestimates the cross section at high-p_{T}^{γ}. The Geneva+Py8+EW$_{\mathrm{virt}}$ prediction has the best agreement with the data across all kinematic regions, with the NLO EW virtual corrections playing a crucial role at high momentum scales.

Figure 6 (d) shows the differential cross section as a function of $\Delta\eta_{\ell\gamma}$ in the *jet veto* fiducial region. This variable can be used to probe the radiation amplitude zero (RAZ) effect, which is predicted at LO in QCD but is removed when higher-order QCD corrections are included in the calculation. Imposing the jet veto restricts real emissions and enhances the RAZ effect. The data and the theoretical predictions demonstrate the dip at $|\Delta\eta_{\ell\gamma}| = 0$ that is a characteristic of RAZ. Although all theoretical predictions are below the data

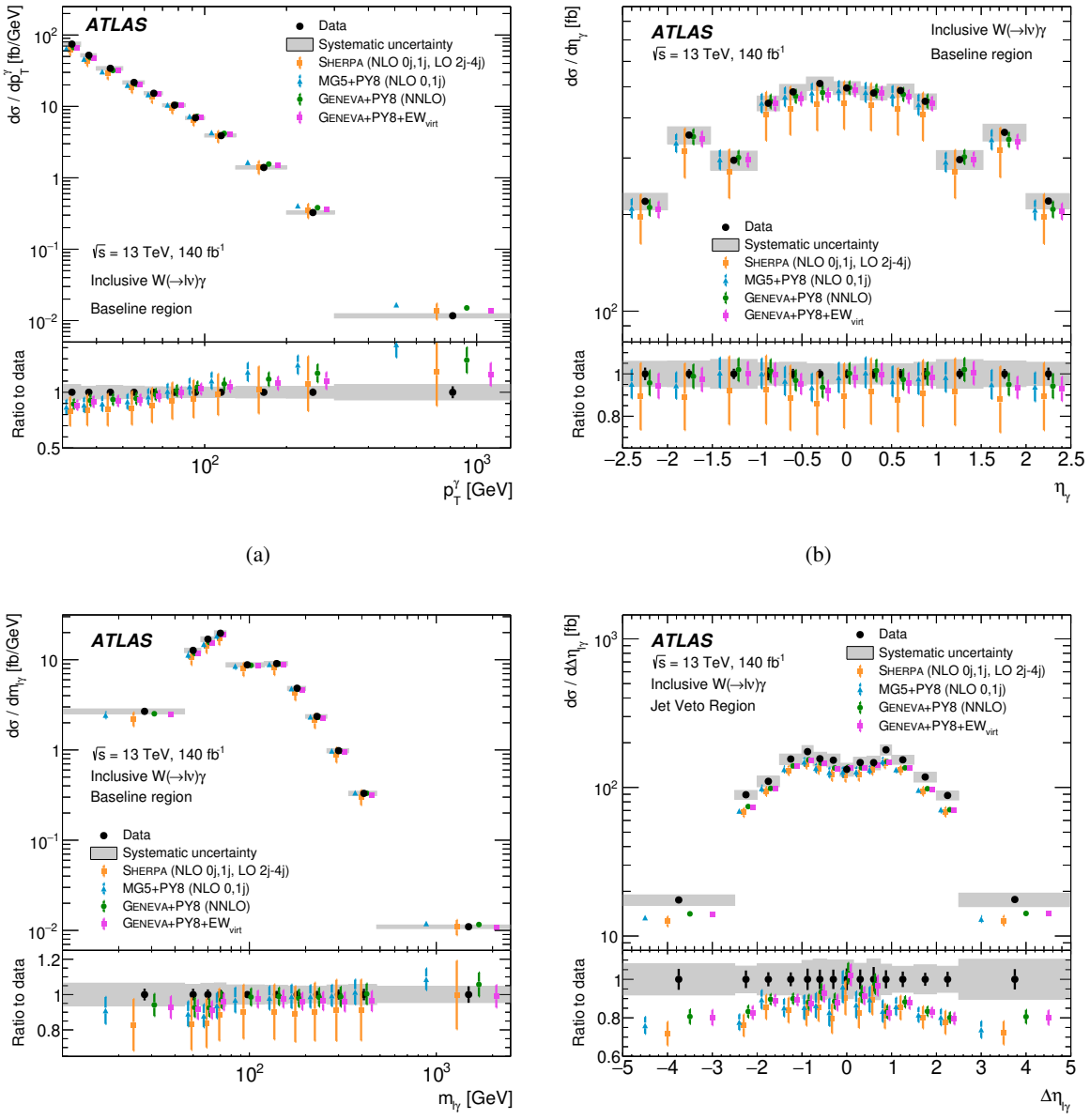

(a) (b)

(c) (d)

Figure 6: Differential cross sections measured as a function of (a) p_{T}^{γ}, (b) η_{γ}, (c) $m_{\ell\gamma}$ and (d) $\Delta\eta_{\ell\gamma}$. The unfolded data are shown as black points, with the statistical uncertainty represented by an error bar and the systematic uncertainty represented as a grey band. The data are compared with theoretical predictions produced by SHERPA (orange points), MG5+PY8 (blue points) and GENEVA+PY8 (green points). The SHERPA and MG5+PY8 predictions are accurate to NLO in QCD for zero and one jets. GENEVA+PY8 is accurate to NNLO for inclusive $W\gamma$ production. The GENEVA+PY8+EW$_{\mathrm{VIRT}}$ prediction (pink points) is accurate to NNLO in QCD and NLO for virtual EW corrections. Uncertainty bands derived from scale variations are shown for all four theoretical predictions. Each theory prediction is slightly offset from the bin centre to avoid overlap.

at high values of $|\Delta\eta_{\ell\gamma}|$, it is possible that their uncertainties are underestimated due to the application of a jet veto when measuring a process that has large higher-order corrections [71].

Figure 7 (a) shows the double differential cross section as a function of θ_f and ϕ_f, which are the polar and azimuthal angles of the negative helicity fermion from the W boson decay as reconstructed in the special reference frame defined in Section 1. This distribution is measured in the *baseline* fiducial region. These angular variables probe the polarisation state of the W boson and provide direct sensitivity to the W boson spin-density matrix. The measured angular distributions are in good agreement with the Standard Model predictions, indicating the data are consistent with the expected W boson polarisation states for inclusive $W\gamma$ production.

Figure 7 (b) shows the double differential cross sections as a function of ϕ_f and p_{T}^{γ}. The ϕ_f observable is sensitive to the interference between scattering amplitudes that contain W bosons in different polarisation states. The ϕ_f observable was proposed in Ref. [7] as a way to probe EFT interference effects for CP-even operators. Measuring the double differential distribution as a function of ϕ_f and p_{T}^{γ} then increases these interference effects because contributions from dimension-six EFT operators are typically enhanced with respect to the SM at high momentum scales. The measurement is performed in the *jet veto* fiducial region, which additionally suppresses the SM with respect to the EFT contributions due to the RAZ effect. The data are again in good agreement with the SM predictions, except at lower p_{T}^{γ} values. This discrepancy may be related to the use of a jet veto, where scale variations may not provide a reliable estimate of the theoretical uncertainty.

Figure 8 shows the differential cross section as a function of the optimised observables, O_{NN}, which are constructed from the outputs of a multiclass neural network (described in Section 6). The O_{NN} observables allow the interference effects predicted by anomalous CP-violating $WW\gamma$ interactions to be probed. The measured distributions are in good agreement with the Standard Model expectations.

Additional differential cross sections, measured as a function of p_{T}^{ℓ}, $m_{\mathrm{T}}^{\ell\nu\gamma}$ and $\Delta\phi_{\ell\gamma}$, are presented in the Appendix. The p_{T}^{ℓ} and $m_{\mathrm{T}}^{\ell\nu\gamma}$ distributions are measured in the baseline regions, whereas the $\Delta\phi_{\ell\gamma}$ measurement is performed in the *jet veto* region. In addition, a double differential cross section as a function of ϕ_f and p_{T}^{γ} in the *baseline* fiducial region is also presented. The agreement between the data and the theoretical predictions is similar to the other observables shown in this section.

PDF-sensitive observables are studied using the $W\gamma$ boost asymmetry, $A_{\mathrm{boost}}^{W\gamma}$, defined in Section 1. The detector corrected differential cross sections that are used in the boost asymmetry calculation are measured separately for events containing leptons and antileptons, and also separated by lepton flavour. They are unfolded to the modified *baseline* fiducial region discussed in Section 7 that uses a common selection for lepton/antilepton pseudorapidity. The electron and muon channel measurements are then combined to reduce the statistical uncertainty using the BLUE method [95]. The measured boost asymmetries are

$$A_{\mathrm{boost}}^{W^-\gamma} = -0.091 \pm 0.012(\mathrm{stat.}) \pm 0.017(\mathrm{sys.}) \pm 0.002(\mathrm{th.}), \tag{4}$$

$$A_{\mathrm{boost}}^{W^+\gamma} = 0.033 \pm 0.012(\mathrm{stat.}) \pm 0.009(\mathrm{sys.}) \pm 0.003(\mathrm{th.}). \tag{5}$$

These are in good agreement with the predicted values of -0.101 ± 0.003 for the $W^-\gamma$ process and 0.043 ± 0.003 for the $W^+\gamma$ process, obtained using Sherpa with the NNPDF3.0nnlo PDF set.

Differential measurements of the boost asymmetry as a function of $|\eta_{\gamma}|$ are shown in Figure 9 for both $W^+\gamma$ and $W^-\gamma$ production. The data are compared to Sherpa predictions produced with different PDF sets [96–99]. Boost asymmetries contain complementary information that can help untangle the contributions

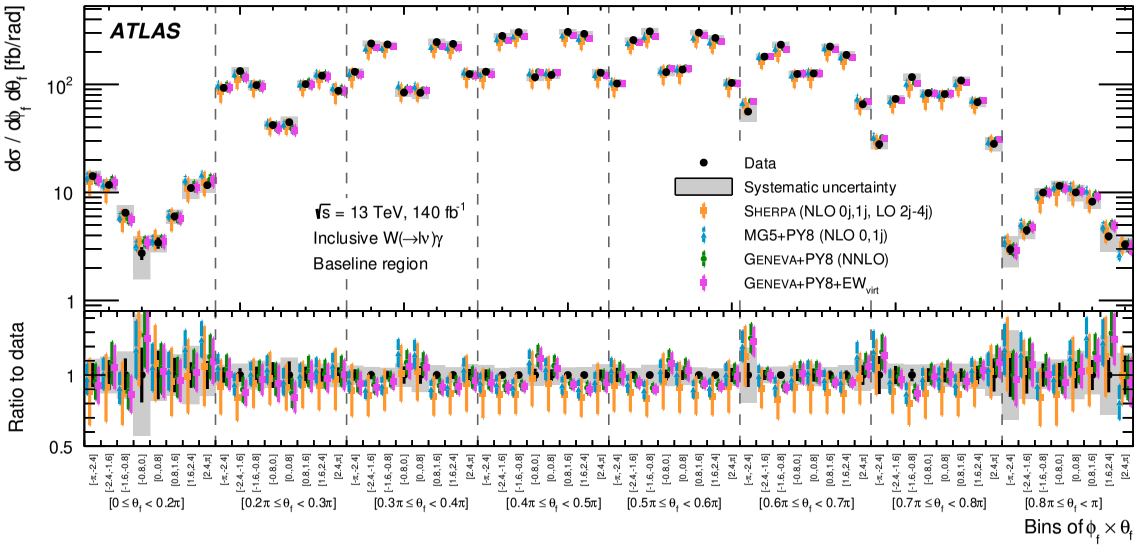

(a)

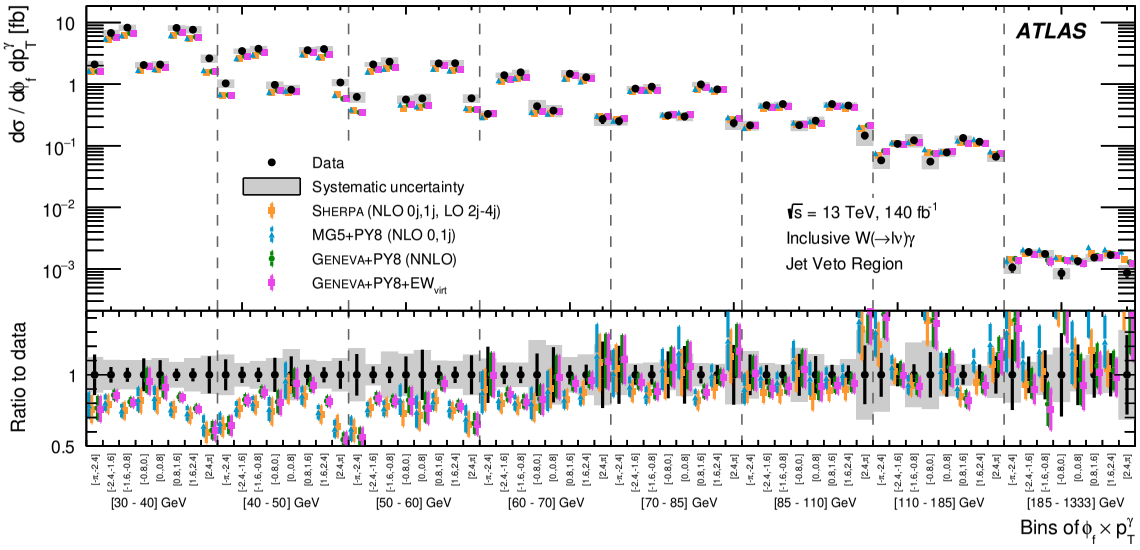

(b)

Figure 7: (a) Double differential cross section as a function of ϕ_f and θ_f. (b) Double differential cross section as a function of ϕ_f and p_{T}^{γ}. The vertical dashed lines highlight the bins of θ_f in the top figure and the bins of p_{T}^{γ} in the bottom figure. The data and theoretical predictions are presented in the same way as for Figure 6.

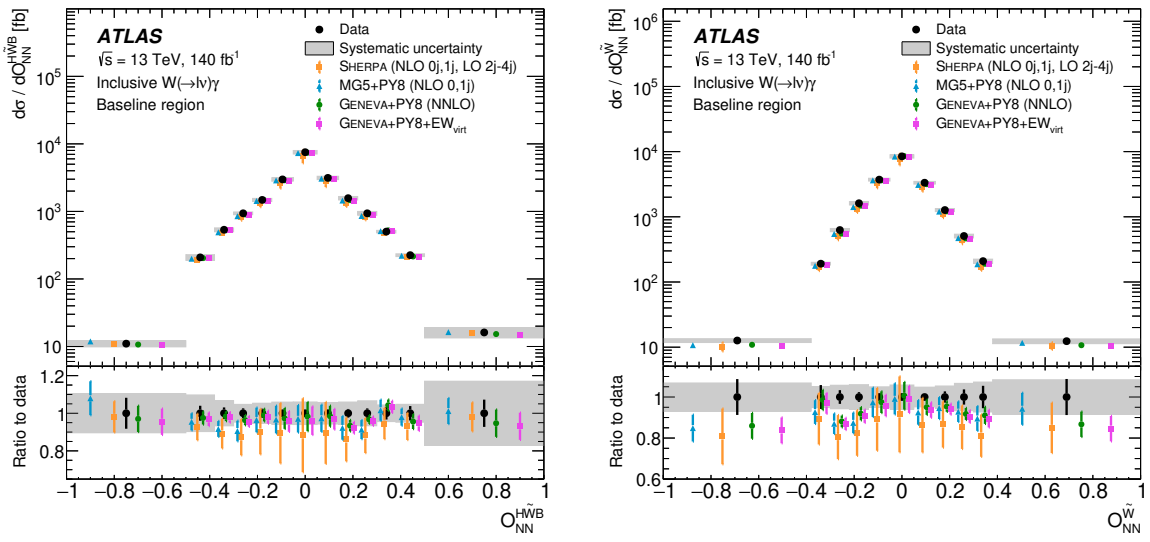

(a) (b)

Figure 8: Differential cross sections as a function of (a) $O_{\mathrm{NN}}^{H\tilde{W}B}$ and (b) $O_{\mathrm{NN}}^{\tilde{W}}$, which are CP-sensitive observables constructed from the outputs of neural networks, as discussed in Section 6. The data and theoretical predictions are presented in the same way as for Figure 6.

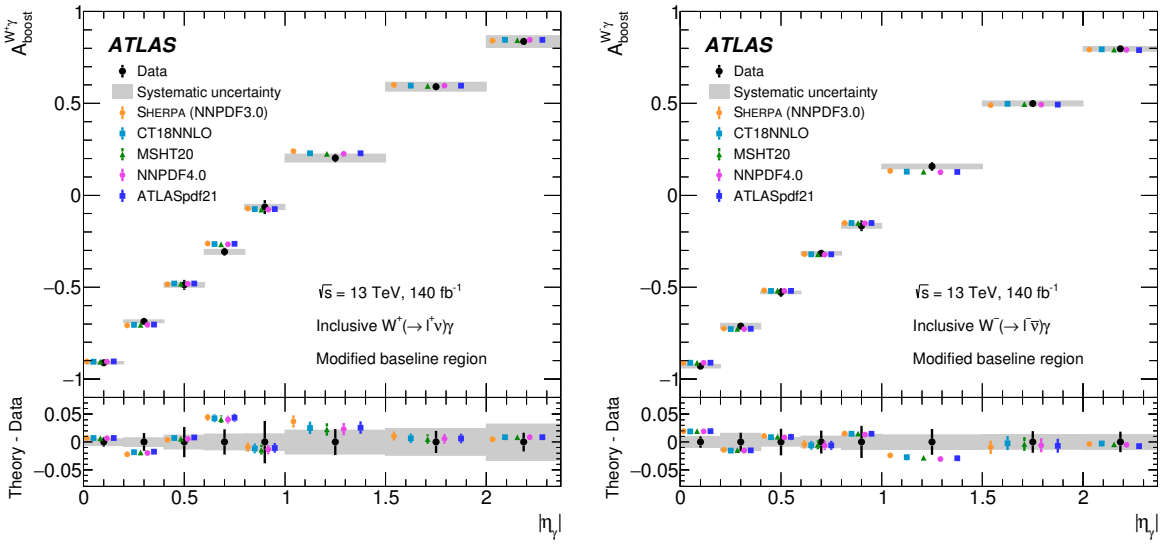

(a) (b)

Figure 9: Differential measurements of the boost asymmetry as a function of $|\eta_\gamma|$ for (a) for $W^+\gamma$ production and for (b) $W^-\gamma$ production. The data are presented in the same way as for Figure 6 and compared to theoretical predictions obtained with SHERPA but using different PDF sets. The uncertainty on the theoretical predictions include renormalisation/factorisation scale variations and PDF uncertainties.

of valence quarks and sea quarks [14]. The measurements are well described by the Standard Model predictions for all PDF sets considered. Additional differential measurements of the boost asymmetry as a function of $|\eta_\ell|$ are presented in the Appendix.

10 EFT interpretation

The differential cross section measurements for inclusive $W\gamma$ production can be interpreted in terms of physics beyond the Standard Model, using the framework of the Standard Model Effective Field Theory (SMEFT), introduced in Section 6. For $W\gamma$ production, the focus is on the operators O_{HWB}, O_W, $O_{H\tilde{W}B}$ and $O_{\tilde{W}}$, which modify the weak-boson self-interactions and the interaction between the weak bosons and the Higgs boson.

Each operator in the SMEFT (O) has an associated Wilson coefficient (c/Λ^2) that describes the strength of the anomalous interactions. The scattering amplitude squared contains three contributions: the SM contribution, an interference term proportional to c/Λ^2, and a pure dimension-six contribution proportional to c^2/Λ^4, as shown in Equation 2. The SMEFT prediction in bin i of a differential distribution is therefore parametrised as

$$\sigma_i^{\text{SMEFT}} = \sigma_i^{\text{SM}} + \frac{c}{\Lambda^2}\sigma^{\text{int}} + \frac{c^2}{\Lambda^4}\sigma^{\text{d6}} \tag{6}$$

where σ_i^{SM} is the SM cross section and σ^{int} and σ^{d6} are the interference and pure dimension-six contributions, respectively, evaluated at a Wilson coefficient of unity. The interference and pure dimension-six contributions are determined from the SMEFT simulated samples presented in Sec. 3.

Figure 10 shows the deviations from the SM prediction induced by each operator as a function of p_{T}^{γ} and ϕ_f. The deviations are presented at representative values of the Wilson coefficients and broken down into the interference contribution, the pure dimension-six contribution, and both contributions combined. The interference terms for CP-even (CP-odd) operators induce symmetric (antisymmetric) deformations relative to the SM as a function of ϕ_f. Furthermore, as expected the EFT effects typically increase with p_{T}^{γ} relative to the SM. Figure 11 shows the deviation from the SM predictions induced by the CP-odd operators as a function of $\Delta\phi_{\ell\gamma}$ and O_{NN}. The interference (pure dimension-six) contributions are asymmetric (symmetric). The interference contribution is larger, relative to the SM, for the O_{NN} distributions than for the $\Delta\phi_{\ell\gamma}$ distribution, indicating a better separation of the constructive and destructive interference.

The CP-odd operators, $O_{H\tilde{W}B}$ and $O_{\tilde{W}}$, are constrained using the differential cross section measurements as a function of the optimised observables based on neural network discriminants, $O_{\text{NN}}^{H\tilde{W}B}$ and $O_{\text{NN}}^{\tilde{W}}$, respectively. Constraints on the CP-even operators, O_{HWB} and O_W, are extracted in the *baseline* and *jet veto* regions, respectively, using the double-differential cross section measurements as a function of p_{T}^{γ} and ϕ_f. The most sensitive distribution for each operator was evaluated using Asimov data constructed from the Sherpa simulation. The O_{NN} observables improve the expected limits on the CP-odd operators by a factor of nearly two compared to the use of $\Delta\phi_{\ell\gamma}$ alone.

The SMEFT simulations are produced at LO accuracy in QCD for zero and one jets in the final state, and are therefore well below the accuracy of the SM predictions presented in this paper. k-factors can be applied to the interference and pure-dimension-six contributions to recover the higher-order QCD corrections, under the assumption that they factorise from the EFT corrections. The k-factors are determined bin-by-bin using the SM prediction, i.e. $k = \sigma^{\text{SM}}_{\text{Sherpa}}/\sigma^{c_j=0}_{\text{EFT}}$, where $\sigma^{\text{SM}}_{\text{Sherpa}}$ is the SM prediction evaluated using Sherpa

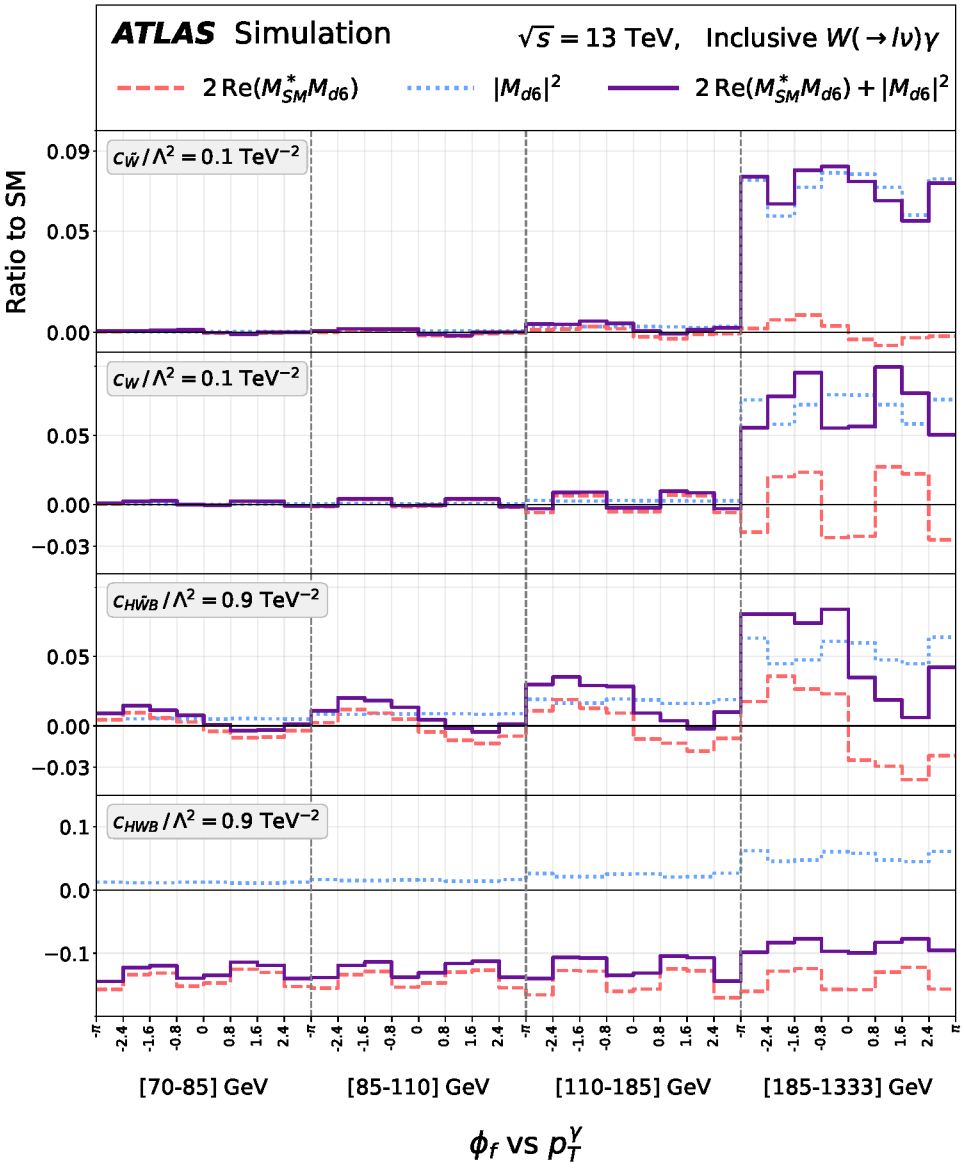

Figure 10: Impact of the O_W, O_{HWB},$O_{\tilde{W}}$ and $O_{H\tilde{W}B}$ operators on the inclusive $W\gamma$ double differential cross section measured as a function of p_{T}^{γ} and ϕ_f. The deviations are shown for a subset of the measured bins at high-p_{T}^{γ}. The expected contributions from the pure dimension-six term ($|\mathcal{M}_{\mathrm{d6}}|^2$) and from the interference between the SM and dimension-six amplitudes ($2\,\mathrm{Re}(\mathcal{M}_{\mathrm{SM}}^{*}\mathcal{M}_{\mathrm{d6}})$) are shown relative to the pure-SM prediction and represented as dotted and dashed lines, respectively. The total contribution to the $W\gamma$ cross-section is shown as a solid line.

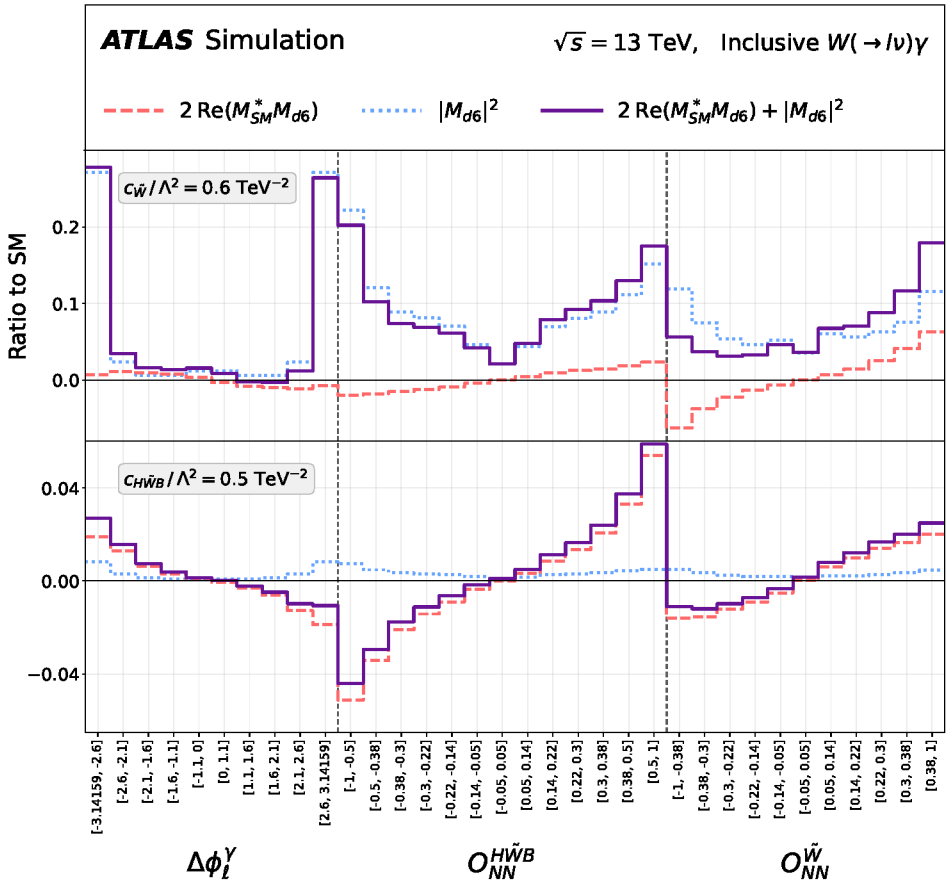

Figure 11: Impact of the O_W, O_{HWB},$O_{\tilde{W}}$ and $O_{H\tilde{W}B}$ operators on the inclusive $W\gamma$ differential cross section measured as a function of $\Delta\phi_{\ell\gamma}$, $O^{\tilde{W}}_{\mathrm{NN}}$ and $O^{H\tilde{W}B}_{\mathrm{NN}}$. The theoretical predictions are presented in the same way as for Fig. 10.

and $\sigma^{c_j=0}_{\mathrm{EFT}}$ is the prediction obtained from the SMEFT framework with all Wilson coefficients set to zero. However, in the case of $W\gamma$ production, the k-factors calculated from the SM samples are about 1.5-2. For this reason, the constraints on the Wilson coefficients are presented with and without the k factor applied. The factorisation of QCD corrections and EFT corrections has been investigated using the SMEFT@NLO model [100], which provides EFT predictions accurate to NLO in QCD, but only for CP-even operators. The NLO QCD k-factor was found to similar for both $c_W/\Lambda^2 = 0$ and $c_W/\Lambda^2 = 1$ TeV^{-2} and have similar kinematic dependences.

The unfolded differential cross sections and the EFT-dependent theoretical predictions are used to define a likelihood function. Statistical correlations between the bins of the measured distributions are evaluated during the unfolding procedure and included in the likelihood using a covariance matrix. Experimental systematic uncertainties are included as Gaussian-constrained nuisance parameters and each source is treated as fully correlated across the bins of the observable but uncorrelated to other sources. Uncertainties in the theoretical prediction due to renormalisation and factorisation scale uncertainties are also implemented as Gaussian-constrained nuisance parameters, with two nuisance parameters used to account for uncertainties in the normalisation and shape of the theoretical prediction. For observables measured in the *baseline* region, the standard envelope of the scale variations is used. For observables measured in the *jet veto*

Table 1: Expected and observed 95% confidence-level (CL) intervals on selected dimension-six Wilson coefficients derived from the $W\gamma$ differential cross-section measurements. For each coefficient, limits are obtained using the observable providing the strongest sensitivity and are shown for all combinations of inclusion of the pure dimension-six contribution ($|\mathcal{M}_{d6}|^2$) and application of a k-factor.

Wilson coefficient	Observable	Includes $\lvert\mathcal{M}_{d6}\rvert^2$	k-factor	95% CL [TeV^{-2}]	
				Expected	Observed
c_W/Λ^2	$\phi_f \times p_{\mathrm{T}}^{\gamma}$	no	no	$[-0.37, 0.38]$	$[-0.42, 0.36]$
		yes	no	$[-0.12, 0.11]$	$[-0.06, 0.06]$
		no	yes	$[-0.23, 0.25]$	$[-0.28, 0.21]$
		yes	yes	$[-0.09, 0.09]$	$[-0.05, 0.05]$
$c_{\tilde{W}}/\Lambda^2$	$O_{\mathrm{NN}}^{\tilde{W}}$	no	no	$[-0.53, 0.54]$	$[-0.74, 0.23]$
		yes	no	$[-0.61, 0.36]$	$[-0.67, 0.19]$
		no	yes	$[-0.32, 0.32]$	$[-0.45, 0.14]$
		yes	yes	$[-0.43, 0.25]$	$[-0.54, 0.11]$
c_{HWB}/Λ^2	$\phi_f \times p_{\mathrm{T}}^{\gamma}$	no	no	$[-1.21, 0.90]$	$[-0.67, 1.21]$
		yes	no	$[-0.97, 0.82]$	$[-0.47, 0.67]$
		no	yes	$[-0.84, 0.62]$	$[-1.09, 0.50]$
		yes	yes	$[-0.76, 0.60]$	$[-0.58, 0.38]$
$c_{H\tilde{W}B}/\Lambda^2$	$O_{\mathrm{NN}}^{H\tilde{W}B}$	no	no	$[-0.39, 0.39]$	$[-0.59, 0.13]$
		yes	no	$[-0.39, 0.39]$	$[-0.60, 0.13]$
		no	yes	$[-0.20, 0.21]$	$[-0.31, 0.07]$
		yes	yes	$[-0.20, 0.21]$	$[-0.31, 0.07]$

region, the theoretical uncertainties are evaluated with the Stewart-Tackmann method [71], which provides a conservative treatment of scale variations in exclusive jet bins. Confidence levels are calculated using the profile-likelihood test statistic, which is assumed to follow a χ^2 distribution with one degree of freedom [101]. This allows the 95% confidence intervals to be constructed for each Wilson coefficient.

The expected and observed 95% confidence intervals on the Wilson coefficients are reported in Table 1. The results are derived for each Wilson coefficient after setting the other Wilson coefficients to zero. Constraints are presented with and without the application of a k-factor to account for missing higher-order corrections in the EFT predictions. The constraints on the Wilson coefficients are up to a factor of two stronger with the k-factor applied, highlighting the importance of developing EFT predictions that include higher-order QCD effects for all SMEFT operators. Constraints are also derived with and without the inclusion of the pure dimension-six term as a way to assess the impact of higher-order EFT contributions. Robust EFT interpretations are typically obtained when constraints on the Wilson coefficients are driven by the interference term, which is formally the leading deformation to the SM prediction as it is $O(\Lambda^{-2})$. The constraints on the CP-odd operators are largely unaffected by the inclusion of the pure-dimension six term, with $O_{H\tilde{W}B}$ unchanged. Conversely, the constraints on the Wilson coefficient of the CP-even operator O_W tighten significantly when the pure dimension-six contribution is included in the EFT prediction. The sensitivity to the Wilson coefficients is limited by statistical uncertainties.

The constraints on $c_{H\tilde{W}B}/\Lambda^2$ represent a substantial improvement over previous measurements. The most stringent prior limits on $c_{H\tilde{W}B}/\Lambda^2$ were obtained using measurements of $H \to 4\ell$ [102] with 95%

confidence intervals of $[-0.72,\ 0.72]$ TeV^{-2} (expected) and $[-0.97,\ 0.98]$ TeV^{-2} (observed). Even without the application of a k-factor, the observed constraints on this operator are improved by a factor of 2.5 using the inclusive $W\gamma$ measurements presented in this paper. With the application of the k-factor, the observed constraints are improved by a factor of 5. The inclusion of the inclusive $W\gamma$ measurements in global fits for CP-violation in the Higgs sector [103] would therefore improve the constraints on $c_{H\tilde{W}B}/\Lambda^2$ considerably. For c_W/Λ^2, when using a k-factor to account for missing higher-order QCD corrections, the constraints are similar to both the constraints obtained by the CMS Collaboration in the $W\gamma$ final state [10] and to the constraints obtained in the ATLAS measurement of EW Zjj production [104].

11 Conclusions

Differential cross sections for inclusive $W\gamma$ production have been measured in proton–proton collisions at $\sqrt{s} = 13$ TeV using the full Run 2 ATLAS dataset of 140 fb^{-1}. The analysis is performed in the $W\gamma \to \ell\nu\gamma$ ($\ell = e, \mu$) channel and the measurements are unfolded to a particle-level fiducial phase space that closely matches the detector-level selection.

A comprehensive set of 16 observables is studied that collectively probe the kinematic properties of the $W\gamma$ system, the radiation amplitude zero effect predicted in the $W\gamma$ final state, the polarisation of the W boson, the charge conjugation and parity structure of the $WW\gamma$ triple gauge coupling, and the parton distribution functions of the proton. The measurements achieve sufficient precision to discriminate between state-of-the-art theoretical predictions including higher-order NNLO QCD and (virtual) NLO EW corrections. Novel observables based on the output of neural networks are used to construct CP-sensitive observables that are highly sensitive to anomalous CP-violating $WW\gamma$ interactions. Furthermore, double differential cross sections are measured as a function of the $W \to \ell\nu$ decay angles, providing sensitivity to the W boson spin density matrix.

Within the framework of a dimension-six effective field theory, constraints are placed on the Wilson coefficients of the O_W, $O_{\tilde{W}}$, O_{HWB} and $O_{H\tilde{W}B}$ operators using the differential cross section measurements. Constraints are placed on the Wilson coefficients of four operators: O_W, O_{HWB}, $O_{\tilde{W}}$ and $O_{H\tilde{W}B}$. The sensitivity to the $O_{H\tilde{W}B}$ operator is improved by a factor of at least 2.5 relative to previous measurements in other final states.

Acknowledgements

We thank CERN for the very successful operation of the LHC and its injectors, as well as the support staff at CERN and at our institutions worldwide without whom ATLAS could not be operated efficiently.

The crucial computing support from all WLCG partners is acknowledged gratefully, in particular from CERN, the ATLAS Tier-1 facilities at TRIUMF/SFU (Canada), NDGF (Denmark, Norway, Sweden), CC-IN2P3 (France), KIT/GridKA (Germany), INFN-CNAF (Italy), NL-T1 (Netherlands), PIC (Spain), RAL (UK) and BNL (USA), the Tier-2 facilities worldwide and large non-WLCG resource providers. Major contributors of computing resources are listed in Ref. [105].

We gratefully acknowledge the support of ANPCyT, Argentina; YerPhI, Armenia; ARC, Australia; BMWFW and FWF, Austria; ANAS, Azerbaijan; CNPq and FAPESP, Brazil; NSERC, NRC and CFI, Canada; CERN; ANID, Chile; CAS, MOST and NSFC, China; Minciencias, Colombia; MEYS CR, Czech Republic; DNRF

and DNSRC, Denmark; IN2P3-CNRS and CEA-DRF/IRFU, France; SRNSFG, Georgia; BMFTR, HGF and MPG, Germany; GSRI, Greece; RGC and Hong Kong SAR, China; ICHEP and Academy of Sciences and Humanities, Israel; INFN, Italy; MEXT and JSPS, Japan; CNRST, Morocco; NWO, Netherlands; RCN, Norway; MNiSW, Poland; FCT, Portugal; MNE/IFA, Romania; MSTDI, Serbia; MSSR, Slovakia; ARIS and MVZI, Slovenia; DSI/NRF, South Africa; MICIU/AEI, Spain; SRC and Wallenberg Foundation, Sweden; SERI, SNSF and Cantons of Bern and Geneva, Switzerland; NSTC, Taipei; TENMAK, Türkiye; STFC/UKRI, United Kingdom; DOE and NSF, United States of America.

Individual groups and members have received support from BCKDF, CANARIE, CRC and DRAC, Canada; CERN-CZ, FORTE and PRIMUS, Czech Republic; COST, ERC, ERDF, Horizon 2020 and Marie Skłodowska-Curie Actions, European Union; Investissements d'Avenir Labex, Investissements d'Avenir Idex and ANR, France; DFG and AvH Foundation, Germany; Herakleitos, Thales and Aristeia programmes co-financed by EU-ESF and the Greek NSRF, Greece; BSF-NSF and MINERVA, Israel; NCN and NAWA, Poland; La Caixa Banking Foundation, CERCA and AGAUR programs from Generalitat de Catalunya and PROMETEO and GenT Programmes Generalitat Valenciana, Spain; Göran Gustafssons Stiftelse, Sweden; The Royal Society and Leverhulme Trust, United Kingdom; Eric and Wendy Schmidt Fund for Strategic Innovation, United States of America.

In addition, individual members wish to acknowledge support from Chile: Agencia Nacional de Investigación y Desarrollo (ANID FONDECYT reg. 1230987, FONDECYT 1230812, FONDECYT 1240864, Fondecyt 3240661, Fondecyt Regular 1240721); China: Chinese Ministry of Science and Technology (MOST-2023YFA1605700, MOST-2023YFA1609300), National Natural Science Foundation of China (NSFC 12275265, NSFC-W2543005); Czech Republic: Czech Science Foundation (GACR - 24-11373S), Ministry of Education Youth and Sports (ERC-CZ-LL2327, FORTE CZ.02.01.01/00/22_008/0004632), PRIMUS Research Programme (PRIMUS/21/SCI/017); EU: H2020 European Research Council (ERC - 101002463); European Union: European Research Council (BARD No. 101116429, ERC - 948254, ERC 101089007), European Regional Development Fund (HE COFUND GA No.101081355, ERDF), Marie Sklodowska-Curie Actions (GAP-101168829); France: Agence Nationale de la Recherche (ANR-21-CE31-0013, ANR-22-EDIR-0002, ANR-24-CE31-0504-01); Germany: Deutsche Forschungsgemeinschaft (DFG - 469666862); China: Research Grants Council (GRF); Italy: Ministero dell'Università e della Ricerca (NextGenEU 153D23001490006 M4C2.1.1, NextGenEU I53D23000820006 M4C2.1.1, NextGenEU I53D23001490006 M4C2.1.1, SOE2024_0000023); Japan: Japan Society for the Promotion of Science (JSPS KAKENHI JP25H0063, JSPS KAKENHI JP22H01227, JSPS KAKENHI JP22H04944, JSPS KAKENHI JP22KK0227, JSPS KAKENHI JP24K23939, JSPS KAKENHI JP24KK0251, JSPS KAKENHI JP25H00650, JSPS KAKENHI JP25H01291, JSPS KAKENHI JP25K01023); Poland: Polish National Science Centre (NCN 2021/42/E/ST2/00350, NCN OPUS 2023/51/B/ST2/02507, NCN OPUS nr 2022/47/B/ST2/03059, NCN UMO-2019/34/E/ST2/00393, UMO-2022/47/O/ST2/00148, UMO-2023/49/B/ST2/04085, UMO-2023/51/B/ST2/00920, UMO-2024/53/N/ST2/00869); Spain: Agència de Gestió d'Ajuts Universitaris i de Recerca. (AGAUR - 2023 BP 00141), Ministry of Science and Innovation (RYC2019-028510-I, RYC2020-030254-I, RYC2021-031273-I, RYC2022-038164-I), Ministerio de Ciencia, Innovación y Universidades/Agencia Estatal de Investigación (PID2022-142604OB-C22); Sweden: Carl Trygger Foundation (Carl Trygger Foundation CTS 22:2312), Swedish Research Council (Swedish Research Council 2023-04654, VR 2021-03651, VR 2022-03845, VR 2022-04683, VR 2023-03403, VR 2024-05451, VR 2025-05940), Knut and Alice Wallenberg Foundation (KAW 2023.0366); Switzerland: Swiss National Science Foundation (SNSF - PCEFP2_194658); United Kingdom: The Binks Trust, Royal Society (NIF-R1-231091); United States of America: U.S. Department of Energy (ECA DE-AC02-76SF00515), John Templeton Foundation (John Templeton Foundation 63206), Neubauer Family Foundation.

Appendix

Figure 12 shows the differential cross sections measured as a function of p_{T}^{ℓ}, $m_{\mathrm{T}}^{\ell\nu\gamma}$ and $\Delta\phi_{\ell\gamma}$. The p_{T}^{ℓ} and $m_{\mathrm{T}}^{\ell\nu\gamma}$ distributions are measured in the baseline region, whereas the $\Delta\phi_{\ell\gamma}$ measurement is performed in the *jet veto* region. Figure 13 presents the double differential cross section as a function of ϕ_f and p_{T}^{γ} in the *baseline* fiducial region. Figure 14 shows the boost asymmetry measured as a function of $|\eta_{\ell}|$. In all cases, the agreement between data and the theoretical predictions is similar to the observables shown in the main body of the paper.

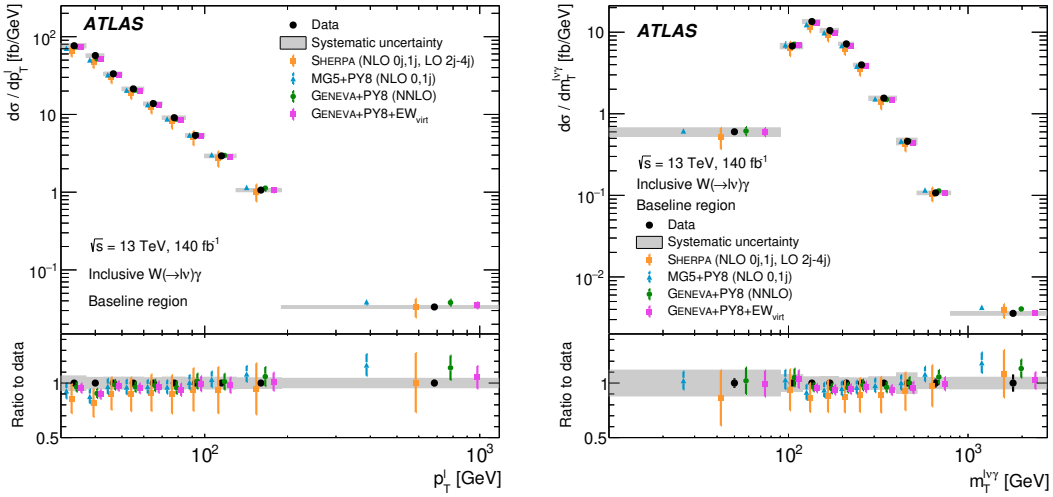

(a) (b)

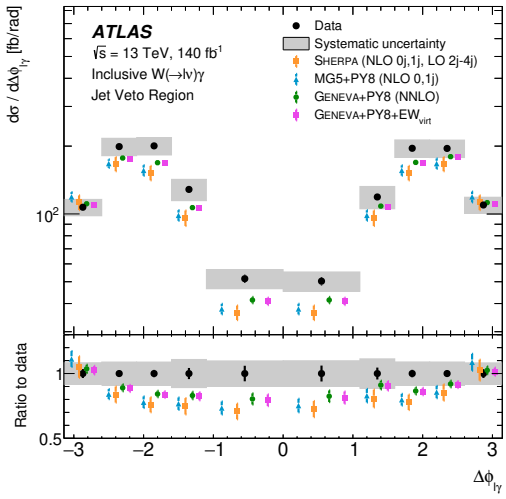

(c)

Figure 12: Unfolded differential cross sections measured as a function of (a) p_{T}^{ℓ}, (b) $m_{\mathrm{T}}^{\ell\nu\gamma}$ and (c) $\Delta\phi_{\ell\gamma}$.The data and theoretical predictions are presented in the same way as for Figure 6.

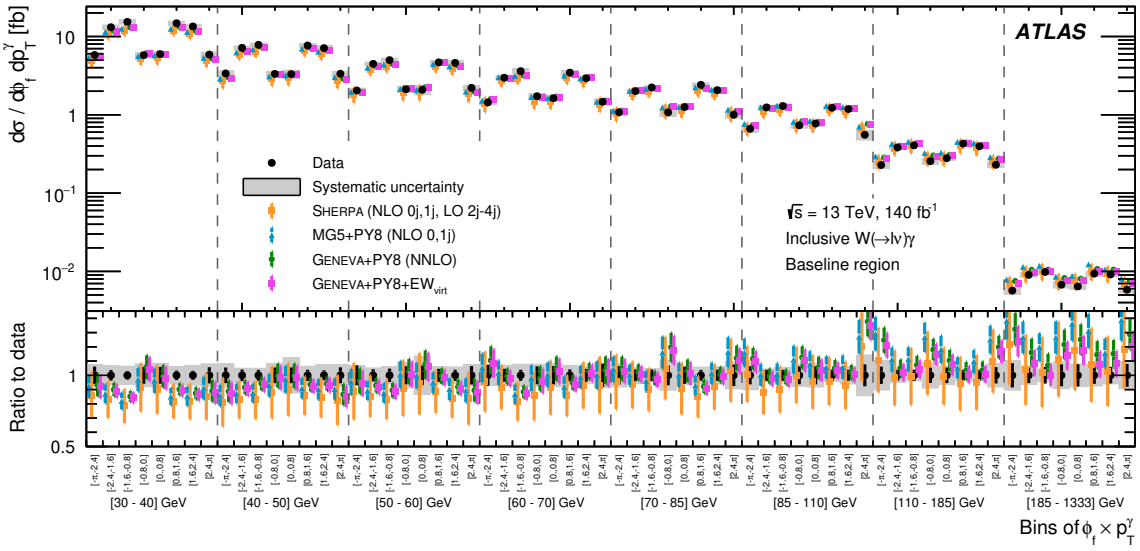

Figure 13: Double differential cross section of inclusive $W\gamma$ production as a function of ϕ_f and p_{T}^{γ} in the baseline fiducial region. The data and theoretical predictions are presented in the same way as for Figure 7.

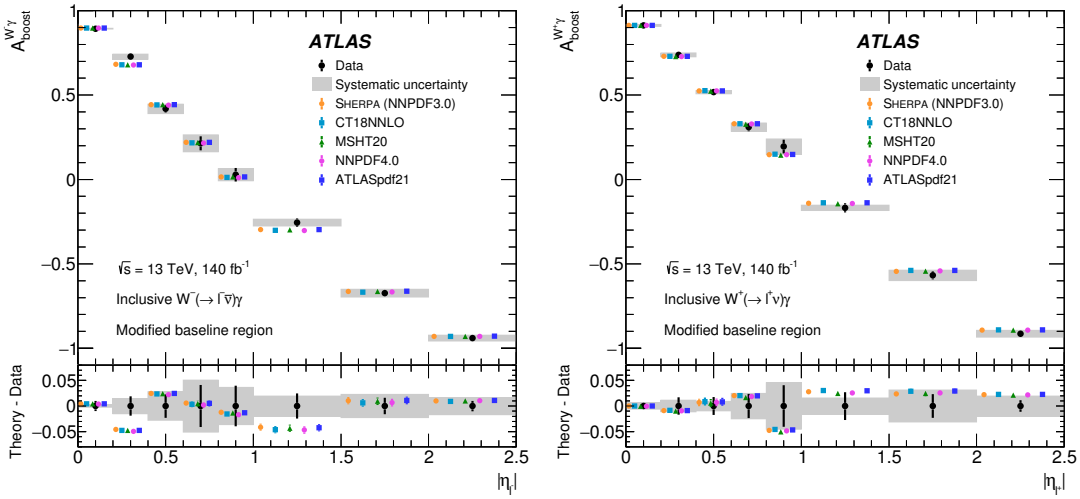

(a) (b)

Figure 14: Boost asymmetry measured as a function of $|\eta_\ell|$ for (a) $W^-\gamma$ production and (b) $W^+\gamma$ production (b). The data and theoretical predictions are presented in the same way as for Figure 9.

References

[1] K. O. Mikaelian, M. A. Samuel and D. Sahdev,
Magnetic Moment of Weak Bosons Produced in pp and $p\bar{p}$ Collisions,
Phys. Rev. Lett. **43** (1979) 746.

[2] C. J. Goebel, F. Halzen and J. P. Leveille, *Angular zeros of Brown, Mikaelian, Sahdev, and Samuel and the factorization of tree amplitudes in gauge theories*, Phys. Rev. D **23** (1981) 2682.

[3] S. J. Brodsky and R. W. Brown, *Zeros in Amplitudes: Gauge Theory and Radiation Interference*, Phys. Rev. Lett. **49** (1982) 966.

[4] R. W. Brown, K. L. Kowalski and S. J. Brodsky,
Classical Radiation Zeros in Gauge Theory Amplitudes,
Phys. Rev. D **28** (1983) 624, [Addendum: Phys.Rev.D 29, 2100–2104 (1984)].

[5] U. Baur, S. Errede and G. Landsberg, *Rapidity correlations in $W\gamma$ production at hadron colliders*, Phys. Rev. D **50** (1994) 1917, arXiv: hep-ph/9402282.

[6] A. Azatov, R. Contino, C. S. Machado and F. Riva,
Helicity selection rules and noninterference for BSM amplitudes, Phys. Rev. D **95** (2017) 065014, arXiv: 1607.05236 [hep-ph].

[7] G. Panico, F. Riva and A. Wulzer, *Diboson interference resurrection*, Phys. Lett. B **776** (2018) 473, arXiv: 1708.07823 [hep-ph].

[8] C. Degrande and J. Touchèque,
A reduced basis for CP violation in SMEFT at colliders and its application to diboson production,
JHEP **04** (2022) 032, arXiv: 2110.02993 [hep-ph].

[9] N. C. Hall et al., *Machine-enhanced CP-asymmetries in the electroweak sector*,
Phys. Rev. D **107** (2023) 016008, arXiv: 2209.05143 [hep-ph].

[10] CMS Collaboration, *Measurement of $W^{\pm}\gamma$ differential cross sections in proton-proton collisions at $\sqrt{s} = 13$ TeV and effective field theory constraints*, Phys. Rev. D **105** (2022) 052003,
arXiv: 2111.13948 [hep-ex].

[11] D. De Florian and A. Signer, *$W\gamma$ and $Z\gamma$ production at hadron colliders*,
Eur. Phys. J. C **16** (2000) 105, arXiv: hep-ph/0002138.

[12] J. M. Campbell, G. De Laurentis, R. K. Ellis and S. Seth,
The $pp \to W(\to l\nu) + \gamma$ process at next-to-next-to-leading order, JHEP **07** (2021) 079,
arXiv: 2105.00954 [hep-ph].

[13] T. Cridge, M. A. Lim and R. Nagar, *$W\gamma$ production at NNLO+PS accuracy in Geneva*,
Phys. Lett. B **826** (2022) 136918, arXiv: 2105.13214 [hep-ph].

[14] S. Yang et al., *Boost asymmetry of the diboson productions in pp collisions*,
Phys. Rev. D **106** (2022) L051301, arXiv: 2207.02072 [hep-ph].

[15] D0 Collaboration, *Measurement of the $p\bar{p} \to W\gamma + X$ cross section at $\sqrt{s} = 1.96$ TeV and $WW\gamma$ anomalous coupling limits*, Phys. Rev. D **71** (2005) 091108, arXiv: hep-ex/0503048.

[16] D0 Collaboration, *First study of the Radiation-Amplitude Zero in $W\gamma$ production and Limits on Anomalous $WW\gamma$ couplings at $\sqrt{s} = 1.96$ TeV*, Phys. Rev. Lett. **100** (2008) 241805,
arXiv: 0803.0030 [hep-ex].

[17] CDF Collaboration, *Measurement of $W\gamma$ and $Z\gamma$ production in $p\bar{p}$ collisions at $\sqrt{s}$ = 1.96 TeV*, Phys. Rev. Lett. **94** (2005) 041803, arXiv: hep-ex/0410008.

[18] ATLAS Collaboration, *Measurements of $W\gamma$ and $Z\gamma$ production in pp collisions at $\sqrt{s}$=7 TeV with the ATLAS detector at the LHC*, Phys. Rev. D **87** (2013) 112003, [Erratum: Phys.Rev.D 91, 119901 (2015)], arXiv: 1302.1283 [hep-ex].

[19] CMS Collaboration, *Measurement of the $W\gamma$ and $Z\gamma$ Inclusive Cross Sections in pp Collisions at $\sqrt{s}$ = 7 TeV and Limits on Anomalous Triple Gauge Boson Couplings*, Phys. Rev. D **89** (2014) 092005, arXiv: 1308.6832 [hep-ex].

[20] CMS Collaboration, *Measurement of the $W\gamma$ Production Cross Section in Proton-Proton Collisions at $\sqrt{s}$=13 TeV and Constraints on Effective Field Theory Coefficients*, Phys. Rev. Lett. **126** (2021) 252002, arXiv: 2102.02283 [hep-ex].

[21] ATLAS Collaboration, *The ATLAS Experiment at the CERN Large Hadron Collider*, JINST **3** (2008) S08003.

[22] ATLAS Collaboration, *ATLAS Insertable B-Layer: Technical Design Report*, ATLAS-TDR-19; CERN-LHCC-2010-013, 2010, URL: https://cds.cern.ch/record/1291633, Addendum: ATLAS-TDR-19-ADD-1; CERN-LHCC-2012-009, 2012, URL: https://cds.cern.ch/record/1451888.

[23] B. Abbott et al., *Production and integration of the ATLAS Insertable B-Layer*, JINST **13** (2018) T05008, arXiv: 1803.00844 [physics.ins-det].

[24] G. Avoni et al., *The new LUCID-2 detector for luminosity measurement and monitoring in ATLAS*, JINST **13** (2018) P07017.

[25] ATLAS Collaboration, *Performance of the ATLAS trigger system in 2015*, Eur. Phys. J. C **77** (2017) 317, arXiv: 1611.09661 [hep-ex].

[26] ATLAS Collaboration, *Operation of the ATLAS trigger system in Run 2*, JINST **15** (2020) P10004, arXiv: 2007.12539 [physics.ins-det].

[27] ATLAS Collaboration, *The ATLAS Collaboration Software and Firmware*, ATL-SOFT-PUB-2021-001, 2021, URL: https://cds.cern.ch/record/2767187.

[28] E. Bothmann et al., *Event generation with Sherpa 2.2*, SciPost Phys. **7** (2019) 034, arXiv: 1905.09127 [hep-ph].

[29] T. Gleisberg and S. Höche, *Comix, a new matrix element generator*, JHEP **12** (2008) 039, arXiv: 0808.3674 [hep-ph].

[30] S. Schumann and F. Krauss, *A parton shower algorithm based on Catani–Seymour dipole factorisation*, JHEP **03** (2008) 038, arXiv: 0709.1027 [hep-ph].

[31] S. Höche, F. Krauss, M. Schönherr and F. Siegert, *A critical appraisal of NLO+PS matching methods*, JHEP **09** (2012) 049, arXiv: 1111.1220 [hep-ph].

[32] S. Höche, F. Krauss, M. Schönherr and F. Siegert, *QCD matrix elements + parton showers. The NLO case*, JHEP **04** (2013) 027, arXiv: 1207.5030 [hep-ph].

[33] S. Catani, F. Krauss, B. R. Webber and R. Kuhn, *QCD Matrix Elements + Parton Showers*, JHEP **11** (2001) 063, arXiv: hep-ph/0109231.

[34] S. Höche, F. Krauss, S. Schumann and F. Siegert, *QCD matrix elements and truncated showers*, JHEP **05** (2009) 053, arXiv: 0903.1219 [hep-ph].

[35] F. Buccioni et al., *OpenLoops 2*, Eur. Phys. J. C **79** (2019) 866, arXiv: 1907.13071 [hep-ph].

[36] F. Cascioli, P. Maierhöfer and S. Pozzorini, *Scattering Amplitudes with Open Loops*, Phys. Rev. Lett. **108** (2012) 111601, arXiv: 1111.5206 [hep-ph].

[37] A. Denner, S. Dittmaier and L. Hofer, *Collier: A fortran-based complex one-loop library in extended regularizations*, Comput. Phys. Commun. **212** (2017) 220, arXiv: 1604.06792 [hep-ph].

[38] NNPDF Collaboration, R. D. Ball et al., *Parton distributions for the LHC run II*, JHEP **04** (2015) 040, arXiv: 1410.8849 [hep-ph].

[39] J. Alwall et al., *The automated computation of tree-level and next-to-leading order differential cross sections, and their matching to parton shower simulations*, JHEP **07** (2014) 079, arXiv: 1405.0301 [hep-ph].

[40] R. Frederix et al., *The automation of next-to-leading order electroweak calculations*, JHEP **07** (2018) 185, arXiv: 1804.10017 [hep-ph], Erratum: JHEP **11** (2021) 085.

[41] R. Frederix et al., JHEP **11** (2021) 085.

[42] R. Frederix and S. Frixione, *Merging meets matching in MC@NLO*, JHEP **12** (2012) 061, arXiv: 1209.6215 [hep-ph].

[43] T. Sjöstrand et al., *An introduction to PYTHIA 8.2*, Comput. Phys. Commun. **191** (2015) 159, arXiv: 1410.3012 [hep-ph].

[44] ATLAS Collaboration, *ATLAS Pythia 8 tunes to 7 TeV data*, ATL-PHYS-PUB-2014-021, 2014, URL: https://cds.cern.ch/record/1966419.

[45] S. Frixione, *Isolated photons in perturbative QCD*, Phys. Lett. B **429** (1998) 369, arXiv: hep-ph/9801442.

[46] ATLAS Collaboration, *Measurements of $Z\gamma$+jets differential cross sections in pp collisions at $\sqrt{s} = 13$ TeV with the ATLAS detector*, JHEP **07** (2023) 072, arXiv: 2212.07184 [hep-ex].

[47] NNPDF Collaboration, R. D. Ball et al., *Parton distributions with LHC data*, Nucl. Phys. B **867** (2013) 244, arXiv: 1207.1303 [hep-ph].

[48] ATLAS Collaboration, *Measurements of inclusive and differential cross-sections of $t\bar{t}\gamma$ production in pp collisions at $\sqrt{s} = 13$ TeV with the ATLAS detector*, JHEP **10** (2024) 191, arXiv: 2403.09452 [hep-ex].

[49] L. Lönnblad, *Correcting the Colour-Dipole Cascade Model with Fixed Order Matrix Elements*, JHEP **05** (2002) 046, arXiv: hep-ph/0112284.

[50] L. Lönnblad and S. Prestel, *Matching tree-level matrix elements with interleaved showers*, JHEP **03** (2012) 019, arXiv: 1109.4829 [hep-ph].

[51] I. Brivio, Y. Jiang and M. Trott, *The SMEFTsim package, theory and tools*, JHEP **12** (2017) 070, arXiv: 1709.06492 [hep-ph].

[52] I. Brivio, *SMEFTsim 3.0 — a practical guide*, JHEP **04** (2021) 073, arXiv: 2012.11343 [hep-ph].

[53] ATLAS Collaboration, *The ATLAS Simulation Infrastructure*, Eur. Phys. J. C **70** (2010) 823, arXiv: 1005.4568 [physics.ins-det].

[54] S. Agostinelli et al., *GEANT4 – a simulation toolkit*, Nucl. Instrum. Meth. A **506** (2003) 250.

[55] ATLAS Collaboration, *The Pythia 8 A3 tune description of ATLAS minimum bias and inelastic measurements incorporating the Donnachie–Landshoff diffractive model*, ATL-PHYS-PUB-2016-017, 2016, URL: https://cds.cern.ch/record/2206965.

[56] ATLAS Collaboration, *Luminosity determination in pp collisions at $\sqrt{s} = 13$ TeV using the ATLAS detector at the LHC*, Eur. Phys. J. C **83** (2023) 982, arXiv: 2212.09379 [hep-ex].

[57] ATLAS Collaboration, *Performance of the ATLAS muon triggers in Run 2*, JINST **15** (2020) P09015, arXiv: 2004.13447 [physics.ins-det].

[58] ATLAS Collaboration, *Performance of electron and photon triggers in ATLAS during LHC Run 2*, Eur. Phys. J. C **80** (2020) 47, arXiv: 1909.00761 [hep-ex].

[59] ATLAS Collaboration, *ATLAS data quality operations and performance for 2015–2018 data-taking*, JINST **15** (2020) P04003, arXiv: 1911.04632 [physics.ins-det].

[60] ATLAS Collaboration, *Vertex Reconstruction Performance of the ATLAS Detector at $\sqrt{s} = 13$ TeV*, (2015).

[61] ATLAS Collaboration, *Muon reconstruction and identification efficiency in ATLAS using the full Run 2 pp collision data set at $\sqrt{s} = 13$ TeV*, Eur. Phys. J. C **81** (2021) 578, arXiv: 2012.00578 [hep-ex].

[62] ATLAS Collaboration, *Electron and photon performance measurements with the ATLAS detector using the 2015–2017 LHC proton–proton collision data*, JINST **14** (2019) P12006, arXiv: 1908.00005 [hep-ex].

[63] ATLAS Collaboration, *Electron and photon efficiencies in LHC Run 2 with the ATLAS experiment*, JHEP **05** (2024) 162, arXiv: 2308.13362 [hep-ex].

[64] M. Cacciari, G. P. Salam and G. Soyez, *The anti-k_t jet clustering algorithm*, JHEP **04** (2008) 063, arXiv: 0802.1189 [hep-ph].

[65] M. Cacciari, G. P. Salam and G. Soyez, *FastJet User Manual*, Eur. Phys. J. C **72** (2012) 1896, arXiv: 1111.6097 [hep-ph].

[66] ATLAS Collaboration, *Jet reconstruction and performance using particle flow with the ATLAS Detector*, Eur. Phys. J. C **77** (2017) 466, arXiv: 1703.10485 [hep-ex].

[67] ATLAS Collaboration, *Jet energy scale and resolution measured in proton–proton collisions at $\sqrt{s} = 13$ TeV with the ATLAS detector*, Eur. Phys. J. C **81** (2021) 689, arXiv: 2007.02645 [hep-ex].

[68] ATLAS Collaboration, *Performance of pile-up mitigation techniques for jets in pp collisions at $\sqrt{s} = 8$ TeV using the ATLAS detector*, Eur. Phys. J. C **76** (2016) 581, arXiv: 1510.03823 [hep-ex].

[69] ATLAS Collaboration, *ATLAS flavour-tagging algorithms for the LHC Run 2 pp collision dataset*, Eur. Phys. J. C **83** (2023) 681, arXiv: 2211.16345 [physics.data-an].

[70] ATLAS Collaboration, *The performance of missing transverse momentum reconstruction and its significance with the ATLAS detector using* $140\,fb^{-1}$ *of* $\sqrt{s} = 13$ *TeV* pp *collisions*, Eur. Phys. J. C **85** (2025) 606, arXiv: 2402.05858 [hep-ex].

[71] I. W. Stewart and F. J. Tackmann, *Theory uncertainties for Higgs mass and other searches using jet bins*, Phys. Rev. D **85** (2012) 034011, arXiv: 1107.2117 [hep-ph].

[72] ATLAS Collaboration, *Measurement of the inclusive isolated prompt photon cross section in* pp *collisions at* $\sqrt{s} = 7$ *TeV with the ATLAS detector*, Phys. Rev. D **83** (2011) 052005, arXiv: 1012.4389 [hep-ex].

[73] ATLAS Collaboration, *Tools for estimating fake/non-prompt lepton backgrounds with the ATLAS detector at the LHC*, JINST **18** (2023) T11004, arXiv: 2211.16178 [hep-ex].

[74] B. Efron, *Bootstrap Methods: Another Look at the Jackknife*, The Annals of Statistics **7** (1979) 1.

[75] ATLAS Collaboration, *Measurement of the photon identification efficiencies with the ATLAS detector using LHC Run 2 data collected in 2015 and 2016*, Eur. Phys. J. C **79** (2019) 205, arXiv: 1810.05087 [hep-ex].

[76] ATLAS Collaboration, *Search for nonpointing photons in the diphoton and* E_T^{miss} *final state in* $\sqrt{s}$*=7 TeV proton-proton collisions using the ATLAS detector*, Phys. Rev. D **88** (2013) 012001, arXiv: 1304.6310 [hep-ex].

[77] ATLAS Collaboration, *Measurement of the* $Z(\to \ell^+\ell^-)\gamma$ *production cross-section in* pp *collisions at* $\sqrt{s} = 13$ *TeV with the ATLAS detector*, JHEP **03** (2020) 054, arXiv: 1911.04813 [hep-ex].

[78] A. Bhardwaj, C. Englert, R. Hankache and A. D. Pilkington, *Machine-enhanced CP-asymmetries in the Higgs sector*, Phys. Lett. B **832** (2022) 137246, arXiv: 2112.05052 [hep-ph].

[79] F. Chollet et al., *Keras*, 2015, URL: https://keras.io.

[80] M. Abadi et al., *TensorFlow: Large-Scale Machine Learning on Heterogeneous Distributed Systems*, (2016), arXiv: 1603.04467 [cs.DC].

[81] G. Hinton, V. Nair and Y. Rachmad, *Rectified Linear Units Improve Restricted Boltzmann Machines Vinod Nair*, **27** (2010) 807.

[82] C. E. Shannon, *A mathematical theory of communication*, Bell Syst. Tech. J. **27** (1948) 623.

[83] D. P. Kingma and J. Ba, 'Adam: A Method for Stochastic Optimization', 2017, arXiv: 1412.6980 [cs.LG].

[84] G. D'Agostini, *A multidimensional unfolding method based on Bayes' theorem*, Nucl. Instrum. Meth. A **362** (1995) 487.

[85] ATLAS Collaboration, *Electron and photon energy calibration with the ATLAS detector using LHC Run 2 data*, JINST **19** (2024) P02009, arXiv: 2309.05471 [hep-ex].

[86] ATLAS Collaboration, *Studies of the muon momentum calibration and performance of the ATLAS detector with* pp *collisions at* $\sqrt{s} = 13$ *TeV*, Eur. Phys. J. C **83** (2023) 686, arXiv: 2212.07338 [hep-ex].

[87] ATLAS Collaboration, *Jet energy scale and resolution measured in proton–proton collisions at $\sqrt{s}$ = 13 TeV with the ATLAS detector*, Eur. Phys. J. C **81** (2021) 689, arXiv: 2007.02645 [hep-ex].

[88] ATLAS Collaboration, *A precise measurement of the jet energy scale derived from single-particle measurements and in situ techniques in proton–proton collisions at $\sqrt{s}$ = 13 TeV with the ATLAS detector*, Eur. Phys. J. C **85** (2025) 927, arXiv: 2407.15627 [hep-ex].

[89] ATLAS Collaboration, *ATLAS b-jet identification performance and efficiency measurement with $t\bar{t}$ events in pp collisions at $\sqrt{s}$ = 13 TeV*, Eur. Phys. J. C **79** (2019) 970, arXiv: 1907.05120 [hep-ex].

[90] S. Alioli et al., *Combining Higher-Order Resummation with Multiple NLO Calculations and Parton Showers in GENEVA*, JHEP **09** (2013) 120, arXiv: 1211.7049 [hep-ph].

[91] S. Alioli et al., *Matching Fully Differential NNLO Calculations and Parton Showers*, JHEP **06** (2014) 089, arXiv: 1311.0286 [hep-ph].

[92] S. Alioli, C. W. Bauer, C. Berggren, F. J. Tackmann and J. R. Walsh, *Drell-Yan production at NNLL'+NNLO matched to parton showers*, Phys. Rev. D **92** (2015) 094020, arXiv: 1508.01475 [hep-ph].

[93] We thank Simone Alioli for providing the HEPMC events used in the GENEVA+PY8 prediction presented in this paper.

[94] CMS Collaboration, *CMS Pythia8 colour reconnection tunes based on underlying-event data*, Eur. Phys. J. C **83** (2023) 587, arXiv: 2205.02905 [hep-ex].

[95] R. Nisius, *BLUE: Combining correlated estimates of physics observables within ROOT using the Best Linear Unbiased Estimate method*, SoftwareX **11** (2020) 100468, arXiv: 2001.10310 [physics.data-an].

[96] T.-J. Hou et al., *New CTEQ global analysis of quantum chromodynamics with high-precision data from the LHC*, Phys. Rev. D **103** (2021) 014013, arXiv: 1912.10053 [hep-ph].

[97] S. Bailey, T. Cridge, L. A. Harland-Lang, A. D. Martin and R. S. Thorne, *Parton distributions from LHC, HERA, Tevatron and fixed target data: MSHT20 PDFs*, Eur. Phys. J. C **81** (2021) 341, arXiv: 2012.04684 [hep-ph].

[98] NNPDF Collaboration, *The path to proton structure at 1% accuracy*, Eur. Phys. J. C **82** (2022) 428, arXiv: 2109.02653 [hep-ph].

[99] ATLAS Collaboration, *Determination of the parton distribution functions of the proton using diverse ATLAS data from pp collisions at $\sqrt{s}$ = 7, 8 and 13 TeV*, Eur. Phys. J. C **82** (2022) 438, arXiv: 2112.11266 [hep-ex].

[100] C. Degrande et al., *Automated one-loop computations in the standard model effective field theory*, Phys. Rev. D **103** (2021) 096024, arXiv: 2008.11743 [hep-ph].

[101] S. S. Wilks, *The Large-Sample Distribution of the Likelihood Ratio for Testing Composite Hypotheses*, The Annals of Mathematical Statistics **9** (1938) 60.

[102] ATLAS Collaboration, *Test of CP-invariance of the Higgs boson in vector-boson fusion production and in its decay into four leptons*, JHEP **05** (2024) 105, arXiv: 2304.09612 [hep-ex].

[103] ATLAS Collaboration,
Combination of measurements of CP properties of Higgs boson interactions to vector bosons using Run 2 proton–proton collisions at $\sqrt{s} = 13$ *TeV with the ATLAS detector*, 2026.

[104] ATLAS Collaboration, *Differential cross-section measurements for the electroweak production of dijets in association with a Z boson in proton–proton collisions at ATLAS*,
Eur. Phys. J. C **81** (2021) 163, arXiv: 2006.15458 [hep-ex].

[105] ATLAS Collaboration, *ATLAS Computing Acknowledgements*, ATL-SOFT-PUB-2026-001, 2026,
URL: https://cds.cern.ch/record/2952666.

The ATLAS Collaboration

G. Aad [102], E. Aakvaag [17], B. Abbott [121], S. Abdelhameed [83b], K. Abeling [54], N.J. Abicht [48], S.H. Abidi [30], M. Aboelela [44], A. Aboulhorma [36e], H. Abramowicz [154], B.S. Acharya [68a,68b,m], A. Ackermann [62a], C. Adam Bourdarios [4], L. Adamczyk [85a], S.V. Addepalli [146], M.J. Addison [101], J. Adelman [117], A. Adiguzel [22c], T. Adye [135], A.A. Affolder [137], Y. Afik [39], M.N. Agaras [13], A. Aggarwal [100], C. Agheorghiesei [28c], A. Ahmad [83a], F. Ahmadov [38,ad], S. Ahuja [95], S. Ahuja [165], X. Ai [113c], G. Aielli [75a,75b], A. Aikot [165], M. Ait Tamlihat [36e], T.P.A. Åkesson [98], D. Akiyama [170], N.N. Akolkar [25], S. Aktas [168], G.L. Alberghi [24b], J. Albert [167], U. Alberti [20], P. Albicocco [52], S. Alderweireldt [51], Z.L. Alegria [122], M. Aleksa [37], I.N. Aleksandrov [38], C. Alexa [28b], T. Alexopoulos [10], F. Alfonsi [24b], M. Algren [55], M. Alhroob [169], B. Ali [133], H.M.J. Ali [91,v], S. Ali [32], S.W. Alibocus [92], M. Aliev [34c], G. Alimonti [70a], C. Allaire [65], B.M.M. Allbrooke [149], D.R. Allen [122], J.S. Allen [101], J.F. Allen [51], C.S. Alley [1], E.R. Almazan [137], A. Aloisio [71a,71b], F. Alonso [90], C. Alpigiani [140], A. Alvarez Fernandez [100], M. Alves Cardoso [55], M.G. Alviggi [71a,71b], M. Aly [101], Y. Amaral Coutinho [81b], C. Amelung [37], M. Amerl [101], T. Amezza [128], B. Amini [53], K. Amirie [158], A. Amirkhanov [38], D. Amperiadou [155], S. An [82], C. Anastopoulos [142], T. Andeen [11], J.K. Anders [92], A.C. Anderson [58], A. Andreazza [70a,70b], S. Angelidakis [9], A. Angerami [41], A.V. Anisenkov [38], A. Annovi [73a], C. Antel [37], E. Antipov [148], M. Antonelli [52], F. Anulli [74a], M. Aoki [82], T. Aoki [156], M.A. Aparo [13], L. Aperio Bella [47], M. Apicella [31], C. Appelt [154], A. Apyan [27], M. Arampatzi [10], S.J. Arbiol Val [86], C. Arcangeletti [52], A.T.H. Arce [50], M. Arcuri [43b,43a], J-F. Arguin [108], S. Argyropoulos [155], J.-H. Arling [47], O. Arnaez [4], H. Arnold [148], G. Artoni [74a,74b], H. Asada [111], S. Asatryan [175], N.A. Asbah [37], R.A. Ashby Pickering [169], A.M. Aslam [95], J. Assahsah [36d], K. Assamagan [30], R. Astalos [29a], K.S.V. Astrand [98], S. Atashi [162], R.J. Atkin [34a], H. Atmani [36f], P.A. Atmasiddha [129], K. Augsten [133], A.D. Auriol [40], V.A. Austrup [101], A.S. Avad [94], G. Avolio [37], A. Azzam [13], D. Babal [29b], H. Bachacou [136], K. Bachas [155,p], A. Bachiu [35], E. Bachmann [49], M.J. Backes [62a], A. Badea [39], T.M. Baer [106], M. Bahmani [19], D. Bahner [53], K. Bai [124], L. Baines [94], O.K. Baker [174], D. Bakshi Gupta [8], L.E. Balabram Filho [81b], V. Balakrishnan [121], R. Balasubramanian [4], P. Balek [85a], E. Ballabene [24b,24a], F. Balli [136], L.M. Baltes [62a], W.K. Balunas [127], I. Bamwidhi [83c], E. Banas [86], M. Bandieramonte [130], A. Bandyopadhyay [25], S. Bansal [25], L. Barak [154], M. Barakat [47], E.L. Barberio [105], D. Barberis [18b], M. Barbero [102], M.Z. Barel [116], T. Barillari [110], M-S. Barisits [37], T. Barklow [146], P. Baron [134], D.A. Baron Moreno [101], A. Baroncelli [61], A.J. Barr [127], J.D. Barr [96], F. Barreiro [99], J. Barreiro Guimarães da Costa [14], M.G. Barros Teixeira [131a], F. Bartels [62a], R. Bartoldus [146], A.E. Barton [91], P. Bartos [29a], M. Baselga [48], S. Bashiri [86], A. Bassalat [65,b], M.J. Basso [159a], S. Bataju [44], R. Bate [166], R.L. Bates [58], S. Batlamous [99], M. Battaglia [137], D. Battulga [19], M. Bauce [74a,74b], L. Bauckhage [47], P. Bauer [25], L.T. Bayer [47], L.T. Bazzano Hurrell [31], T. Beau [128], J.Y. Beaucamp [90], S. Beauceron [128], P.H. Beauchemin [161], P. Bechtle [25], H.P. Beck [20,o], K. Becker [169], A.J. Beddall [80], V.A. Bednyakov [38], C.P. Bee [148], L.J. Beemster [16], M. Begalli [81d], M. Begel [30], J.K. Behr [47], J.F. Beirer [37], F. Beisiegel [25], M. Belfkir [83c], G. Bella [154], L. Bellagamba [24b], A. Bellerive [35], C.D. Bellgraph [67], P. Bellos [21], I. Benaoumeur [21], D. Benchekroun [36a], F. Bendebba [36a], Y. Benhammou [154], K.C. Benkendorfer [167], L. Beresford [47], M. Beretta [52], E. Bergeaas Kuutmann [163], N. Berger [4], B. Bergmann [133], J. Beringer [18a], M. Berkat [136], G. Bernardi [5], C. Bernius [146], F.U. Bernlochner [25], A. Berrocal Guardia [13], T. Berry [95], P. Berta [134], A. Berti [131a],

R. Bertrand[102], S. Bethke[110], A. Betti[74a,74b], T.F. Beumker[173], A.J. Bevan[94], L. Bezio[55], N.K. Bhalla[53], S. Bharthuar[110], S. Bhatta[148], P. Bhattarai[146], Z.M. Bhatti[118], K.D. Bhide[53], V.S. Bhopatkar[122], R.M. Bianchi[130], G. Bianco[24b,24a], O. Biebel[109], M. Biglietti[76a], P. Bijl[53], C.S. Billingsley[44], Y. Bimgdi[36f], M. Bindi[54], A. Bingham[173], A. Bingul[22b], C. Bini[74a,74b], G.A. Bird[33], M. Biros[134], S. Biryukov[149], T. Bisanz[48], E. Bisceglie[24b,24a], J.P. Biswal[135], D. Biswas[144], M. Biyabi[14], I. Bloch[47], A. Blue[58], U. Blumenschein[94], V.S. Bobrovnikov[38], L. Boccardo[56b,56a], M. Boehler[53], B. Boehm[168], D. Bogavac[13], L.S. Boggia[128], V. Boisvert[95], P. Bokan[163], T. Bold[85a], M. Bomben[5], M. Bona[94], M. Boonekamp[136], A.G. Borbély[58], G. Borissov[91], A. Borkar[168], D. Bortoletto[127], M. Borysova[171], D. Boscherini[24b], M. Bosman[13], K. Bouaouda[36a], L. Boudet[136], J. Boudreau[130], E.V. Bouhova-Thacker[91], D. Boumediene[40], R. Bouquet[56b,56a], A. Boveia[120], D. Boye[30], I.R. Boyko[38], L. Bozianu[55], J. Bracinik[21], N. Brahimi[4], G. Brandt[173], O. Brandt[33], B. Brau[103], R. Brener[171], L. Brenner[116], R. Brenner[163], S. Bressler[171], M. Brettell[96], G. Brianti[116], D. Britton[58], D. Britzger[110], I. Brock[25], R. Brock[107], H. Bronson[129], G. Brooijmans[41], A.J. Brooks[67], E.M. Brooks[159b], E. Brost[30], L.M. Brown[167,159a], L.E. Bruce[60], T.L. Bruckler[127], P.A. Bruckman de Renstrom[86], B. Brüers[47], A. Bruni[24b], G. Bruni[24b], D. Brunner[46a,46b], M. Bruschi[24b], N. Bruscino[74a,74b], T. Buanes[17], Q. Buat[140], D. Buchin[110], A.G. Buckley[58], J. Bucko[134], M. Buhring[49], O. Bulekov[80], B.A. Bullard[146], T.O. Buratovich[90], S. Burdin[92], C.D. Burgard[48], A.M. Burger[89], B. Burghgrave[8], O. Burlayenko[53], J. Burleson[164], J.C. Burzynski[121], V. Büscher[100], P.J. Bussey[58], O. But[25], J.M. Butler[26], C.M. Buttar[58], J.M. Butterworth[96], P. Butti[37], W. Buttinger[135], C.J. Buxo Vazquez[107], A.R. Buzykaev[38], S. Cabrera Urbán[165], L. Cadamuro[65], H. Cai[37], Y. Cai[24b,112c,24a], Y. Cai[112a], M.A. Cairo[129], V.M.M. Cairo[37], O. Cakir[3a], N. Calace[37], P. Calafiura[18a], G. Calderini[128], P. Calfayan[35], L. Calic[98], G. Callea[58], L.P. Caloba[81b], D. Calvet[40], S. Calvet[40], R. Camacho Toro[128], S. Camarda[37], D. Camarero Munoz[27], P. Camarri[75a,75b], C. Camincher[37], M. Campanelli[96], A. Camplani[42], V. Canale[71a,71b], A.C. Canbay[3a], E. Canonero[95], J. Cantero[165], F. Capocasa[27], P. Cappelli[27], M. Capua[43b,43a], A. Carbone[70a,70b], R. Cardarelli[75a], J.C.J. Cardenas[8], M.P. Cardiff[27], G. Carducci[43b,43a], T. Carli[37], G. Carlino[71a], J.I. Carlotto[13], B.T. Carlson[130,q], E.M. Carlson[167], L. Carminati[70a,70b], A. Carnelli[4], M. Carnesale[37], S. Caron[115], E. Carquin[138g], I.B. Carr[105], S. Carrá[72a,72b], G. Carratta[24b,24a], C. Carrion Martinez[165], A.M. Carroll[124], N. Cartalade[40], M.P. Casado[13,h], P. Casolaro[71a,71b], M. Caspar[47], F. Cassinese[90], W.R. Castiglioni[39], F.L. Castillo[4], V. Castillo Gimenez[165], N.F. Castro[131a,131e], A. Catinaccio[37], J.R. Catmore[126], T. Cavaliere[4], V. Cavaliere[30], E. Celebi[80], S. Cella[30], V. Cepaitis[55], K. Cerny[123], A.S. Cerqueira[81a], A. Cerri[73a,ap], L. Cerrito[75a,75b], F. Cerutti[18a], B. Cervato[70a,70b], A. Cervelli[24b], G. Cesarini[52], S.A. Cetin[80], V.C. Chabalala[34j], P.M. Chabrillat[128], R. Chakkappai[65], S. Chakraborty[169], A. Chambers[60], J. Chan[18a], J.D. Chapman[33], E. Chapon[136], D.G. Charlton[21], C. Chauhan[132], Y. Che[112a], S. Chekanov[6], G.A. Chelkov[38,a], H. Chen[30], J. Chen[141a], J. Chen[145], M. Chen[59], S. Chen[87], S.J. Chen[112a], X. Chen[141a], X. Chen[15,ai], Z. Chen[61], C.L. Cheng[172], H.C. Cheng[63a], S. Cheong[146], A. Cheplakov[38], E. Cherepanova[116], E. Cheu[7], K. Cheung[64], L. Chevalier[136], G. Chiarelli[73a], G. Chiodini[69a], A.S. Chisholm[21], J.L. Chisholm[166], A. Chitan[28b], M. Chitishvili[165], M.V. Chizhov[38,r], K. Choi[11], Y. Chou[140], E.Y.S. Chow[115], G. Christou[51], K.L. Chu[171], M.C. Chu[63a], Z. Chubinidze[52], J. Chudoba[132], J.J. Chwastowski[86], D. Cieri[110], K.M. Ciesla[85a], V. Cindro[93], A. Ciocio[18a], F. Cirotto[71a,71b], Z.H. Citron[171], M. Citterio[70a], D.A. Ciubotaru[28b], A. Clark[55], P.J. Clark[51], N. Clarke Hall[96], C. Clarry[158], S.E. Clawson[47], C. Clement[46a,46b], L. Clissa[24b,24a], Y. Coadou[102], M. Cobal[68a,68c],

A. Coccaro [56b], M.G. Cochran Branson [140], R.F. Coelho Barrue [131a], R. Coelho Lopes De Sa [103], S. Coelli [70a], M.M. Cohen [129], L.S. Colangeli [158], B. Cole [41], P. Collado Soto [99], J. Collot [59], M.R. Coluccia [69a], I. Combes[65], P. Conde Muiño [131a,131g], L.H.J. Condren [162], M.P. Connell [34c], S.H. Connell [34c], E.I. Conroy [127], M. Contreras Cossio [11], F. Conventi [71a,ak], A.M. Cooper-Sarkar [127], L. Corazzina [74a,74b], F.A. Corchia [24b,24a], A. Cordeiro Oudot Choi [140], L.D. Corpe [40], M. Corradi [74a,74b], F. Corriveau [104,ab], A. Cortes-Gonzalez [156], M.J. Costa [165], F. Costanza [4], D. Costanzo [142], J. Couthures [4], G. Cowan [95], K. Cranmer [172], L. Cremer [48], D. Cremonini [24b,24a], S. Crépé-Renaudin [59], F. Crescioli [128], T. Cresta [72a,72b], M. Cristinziani [144], M. Cristoforetti [77a,77b], T.M. Critchley [55], E. Critelli [96], A. Cueto [99], H. Cui [96], Z. Cui [7], B.M. Cunnett [149], W.R. Cunningham [58], E. Cuppini[110], F. Curcio [165], J.R. Curran [51], M.J. Da Cunha Sargedas De Sousa [56b,56a], J.V. Da Fonseca Pinto [81b], C. Da Via [101], W. Dabrowski [85a], T. Dado [37], S. Dahbi [151], T. Dai [106], D. Dal Santo [20], C. Dallapiccola [103], M. Dam [42], G. D'amen [30], V. D'Amico [109], J.R. Dandoy [35], M. D'Andrea [56b,56a], D. Dannheim [37], G. D'anniballe [73a,73b], M. Danninger [145], V. Dao [148], G. Darbo [56b], F. Dattola [47], S. D'Auria [70a,70b], A. D'Avanzo [71a,71b], T. Davidek [134], J. Davidson [169], I. Dawson [94], K. De [8], C. De Almeida Rossi [158], N. De Biase [47], S. De Castro [24b,24a], N. De Groot [115], P. de Jong [116], H. De la Torre [117], A. De Maria [112a], S. De Miranda Rimes [81d], A. De Salvo [74a], U. De Sanctis [75a,75b], F. De Santis [69a,69b], A. De Santo [149], J.B. De Vivie De Regie [59], K.G. De Vries [116], J. Debevc [93], D.V. Dedovich[38], J. Degens [92], A.M. Deiana [44], J. Del Peso [99], L. Delagrange [27], F. Deliot [136], C.M. Delitzsch [48], M. Della Pietra [71a,71b], D. Della Volpe [55], A. Dell'Acqua [37], L. Dell'Asta [70a,70b], M. Delmastro [4], C.C. Delogu [56b,56a], P.A. Delsart [59], S. Demers [174], M. Demichev [38], H. Denizli [22a,l], M.G. Depala [92], L. D'Eramo [40], D. Derendarz [86], L. Derin [56b,56a], F. Derue [128], P. Dervan [92,*], A.M. Desai [1], K. Desch [25], F.A. Di Bello [73a,73b], A. Di Ciaccio [75a,75b], L. Di Ciaccio [4], D. Di Croce [37], C. Di Donato [71a,71b], A. Di Girolamo [37], G. Di Gregorio [65], A. Di Luca [77a,77b], B. Di Micco [76a,76b], R. Di Nardo [76a,76b], K.F. Di Petrillo [39], M. Diamantopoulou [35], F.A. Dias [116], M.A. Diaz [138a,138b], A.R. Didenko [38], M. Didenko [165], S.D. Diefenbacher [18a], E.B. Diehl [106], S. Díez Cornell [47], C. Diez Pardos [144], C. Dimitriadi [147], A. Dimitrievska [21], A. Dimri [148], Y. Ding[61], J. Dingfelder [25], T. Dingley [127], I-M. Dinu [28b], S.J. Dittmeier [62b], F. Dittus [37], M. Divisek [134], B. Dixit [92], F. Djama [102], T. Djobava [152b], C. Doglioni [101,98], A. Dohnalova [29a], Z. Dolezal [134], K. Domijan [85a], K.M. Dona [39], M. Donadelli [81d], B. Dong [107], J. Donini [40], A. D'Onofrio [71a,71b], M. D'Onofrio [92], J. Dopke [135], A. Doria [71a], N. Dos Santos Fernandes [131a], I.A. Dos Santos Luz [81e], P. Dougan [44], M.T. Dova [90], A.T. Doyle [58], M.P. Drescher [54], E. Dreyer [171], I. Drivas-koulouris [10], M. Drnevich [118], D. Du [61], T. Du[39], T.A. du Pree [116], Z. Duan[112a], M. Dubau [4], F. Dubinin [38], M. Dubovsky [29a], E. Duchovni [171], G. Duckeck [109], P.K. Duckett[96], O.A. Ducu [28b], D. Duda [51], A. Dudarev [37], M.M. Dudek [86], E.R. Duden [27], M. D'uffizi [101], L. Duflot [65], M. Dührssen [37], I. Duminica [28g], A.E. Dumitriu [28b], M. Dunford [62a], T. Duong[4], A. Duperrin [102], A.F. Duque Bran [40], H. Duran Yildiz [3a], A. Durglishvili [152b], G.I. Dyckes [18a], M. Dyndal [85a], B.S. Dziedzic [37], G.H. Eberwein [127], B. Eckerova [29a], J.C. Egan [96], S. Eggebrecht [54], E. Egidio Purcino De Souza [81e], G. Eigen [17], K. Einsweiler [18a], T. Ekelof [163], P.A. Ekman [98], S. El Farkh [36b], Y. El Ghazali [61], H. El Jarrari [104], A. El Moussaouy [36a], I. Elbaz [154], D. Elitez [37], M. Ellert [163], F. Ellinghaus [173], T.A. Elliot [95], J. Elmsheuser [30], M. Elsawy [83b], M. Elsing [37], D. Emeliyanov [135], Y. Enari [82], S. Epari [108], D. Ernani Martins Neto [86], F. Ernst[37], M. Escalier [65], C. Escobar [165], R. Estevam De Paula [81c], E. Etzion [154], G. Evans [131a,131b], H. Evans [67], L.S. Evans [47], S. Ezzarqtouni [36a], F. Fabbri [24b,24a], L. Fabbri [24b,24a], G. Facini [96], V. Fadeyev [137], D. Fakoudis [100], S. Falciano [74a], L.F. Falda Ulhoa Coelho [27], F. Fallavollita [110],

G. Falsetti [43b,43a], J. Faltova [134], C. Fan [164], K.Y. Fan [63b], Y. Fan [14], Y. Fang [14,112c], M. Fanti [70a,70b], M. Faraj [68a,68c], Z. Farazpay [97], A. Farbin [8], A. Farilla [76a], K. Farman [151], J.N. Farr [174], M.S. Farrington [60], S.M. Farrington [135,51], F. Fassi [36e], D. Fassouliotis [9], L. Fayard [65], G. Fazzino [62b], P. Federic [134], P. Federicova [132], M. Feickert [172], L. Feligioni [102], D.E. Fellers [18a], C. Feng [113b], Y. Feng[14], Z. Feng [65], B. Fernandez Barbadillo [91], P. Fernandez Martinez [66], C. Fernandez Ruiz [33], J. Ferrando [91], A. Ferrari [163], P. Ferrari [116,115], R. Ferrari [72a], D. Ferrere [55], C. Ferretti [106], M.P. Fewell [1], D. Fiacco [74a,74b], F. Fiedler [100], P. Fiedler [133], S. Filimonov [38], M.S. Filip [28b,s], A. Filipčič [93], E.K. Filmer [159a], F. Filthaut [115], M.C.N. Fiolhais [131a,131c,c], L. Fiorini [165], W.C. Fisher [107], T. Fitschen [101], I. Fleck [144], P. Fleischmann [106], T. Flick [173], M. Flores [34d,ag], L.R. Flores Castillo [63a], M. Foll [126], F.M. Follega [77a,77b], N. Fomin [33], J.H. Foo [158], A. Formica [136], M. Fornasiero [149], A.C. Forti [101], N. Forti [24b,24a], E. Fortin [102], A.W. Fortman [18a], L. Foster [18a], L. Fountas [9], H. Fox [91], P. Francavilla [73a,73b], S. Francescato [60], S. Franchellucci [20], M. Franchini [24b,24a], S. Franchino [62a], D. Francis[37], L. Franco [47], L. Franconi [47], M. Franklin [60], G. Frattari [37], Y.Y. Frid [154], N. Fritzsche [37], A. Froch [55], D. Froidevaux [37], J.A. Frost [135], Y. Fu [107], S. Fuenzalida Garrido [138g], Y.C. Fujikake [137], M. Fujimoto [148], K.Y. Fung [63a], E. Furtado De Simas Filho [81e], M. Furukawa [156], M. Fuste Costa [47], P. Fuste Martin [13], J. Fuster [165], A. Gaa [54], A. Gabrielli [24b,24a], A. Gabrielli [158], G. Gagliardi [56b,56a], L.G. Gagnon [18a], S. Galantzan [154], J. Gallagher [1], E.J. Gallas [127], A.L. Gallen [163], B.J. Gallop [135], K.K. Gan [120], Y. Gao [51], Z. Gao [112a], A. Garabaglu [140], F.M. Garay Walls [138a,138b], C. García [165], A. Garcia Alonso [116], A.G. Garcia Caffaro [174], J.E. García Navarro [165], M.A. Garcia Ruiz [23b], M. Garcia-Sciveres [18a], G.L. Gardner [129], R.W. Gardner [39], N. Garelli [161], R.B. Garg [146], J.M. Gargan [33], C.A. Garner[158], C.M. Garvey [34a], V.K. Gassmann[161], G. Gaudio [72a], A.J. Gavin [94], J. Gavranovic [93], I.L. Gavrilenko [131a], C. Gay [166], G. Gaycken [124], A. Gekow[120], C. Gemme [56b], M.H. Genest [59], A.D. Gentry [114], S. George [95], T. Geralis [45], A.A. Gerwin [121], P. Gessinger-Befurt [37], M. Ghani [169], K. Ghorbanian [94], A. Ghosal [144], A. Ghosh [162], A. Ghosh [7], B. Giacobbe [24b], S. Giagu [74a,74b], A. Giannini [61], S.M. Gibson [95], D.T. Gil [85b], B.J. Gilbert [41], D. Gillberg [35], G. Gilles [116], D.M. Gingrich [2,aj], M.P. Giordani [68a,68c], P.F. Giraud [136], G. Giugliarelli [68a,68c], D. Giugni [70a], F. Giuli [75a,75b,al], I. Gkialas [9,i], B.C. Gladwyn [127], C. Glasman [99], M. Glazewska [20], R.M. Gleason [162], G. Glemža [47], I. Gnesi [24b,24a,am], Y. Go [30], M. Goblirsch-Kolb [37], B. Gocke [48], D. Godin[108], B. Gokturk [22a], S. Goldfarb [105], T. Golling [55], M.G.D. Gololo [34c], A. Golub [140], J.P. Gombas [107], A. Gomes [131a,131b], G. Gomes Da Silva [144], A.J. Gomez Delegido [37], R. Gonçalo [131a], A. Gongadze [152c], F. Gonnella [21], J.L. Gonski [146], R.Y. González Andana [51], S. González de la Hoz [165], M.V. Gonzalez Rodrigues [47], R. Gonzalez Suarez [163], S. Gonzalez-Sevilla [55], L. Goossens [37], B. Gorini [37], E. Gorini [69a,69b], A. Gorišek [93], T.C. Gosart [129], A.T. Goshaw [50], M.I. Gostkin [38], S. Goswami [122], C.A. Gottardo [37], S.A. Gotz [109], M. Gouighri [36b], A.G. Goussiou [140], N. Govender [34c], R.P. Grabarczyk [127], I. Grabowska-Bold [85a], K. Graham [35], E. Gramstad [126], S. Grancagnolo [69a,69b], C.M. Grant[1], P.M. Gravila [28f], F.G. Gravili [69a,69b], H.M. Gray [18a], M. Greco [110], M.J. Green [1], C. Grefe [25], A.S. Grefsrud [17], I.M. Gregor [47], K.T. Greif [162], P. Grenier [146], S.G. Grewe[110], K. Grimm [32], S. Grinstein [13,x], E. Gross [171], J. Grosse-Knetter [54], L.H. Grossman [18b], L. Guan [106], G. Guerrieri [37], R. Guevara [126], R. Gugel [100], J.A.M. Guhit [106], A. Guida [19], E. Guilloton [169], S. Guindon [37], F. Guo [14,112c], J. Guo [141a], L. Guo [47], L. Guo [112b,u], Y. Guo [106], Y. Guo [41], A. Gupta [48], R. Gupta [130], S. Gupta [27], S. Gurbuz [25], S.S. Gurdasani [47], G. Gustavino [74a,74b], P. Gutierrez [121], L.F. Gutierrez Zagazeta [129], M. Gutsche [49], C. Gutschow [96], W. Guérin [89], C. Gwenlan [127],

C.B. Gwilliam [92], E.S. Haaland [126], A. Haas [118], M. Habedank [58], C. Haber [18a], R.J. Haberle [171], H.K. Hadavand [8], A. Haddad [40], A. Hadef [49], A.I. Hagan [91], J.J. Hahn [144], M. Haleem [168], J. Haley [122], G.D. Hallewell [102], J.A. Hallford [47], K. Hamano [167], H. Hamdaoui [163], M. Hamer [25], S.E.D. Hammoud [65], E.J. Hampshire [95], L. Han [112a], L. Han [61], S. Han [14], K. Hanagaki [82], M. Hance [137], D.A. Hangal [41], H. Hanif [145], M.D. Hank [129], J.B. Hansen [42], P.H. Hansen [42], T. Harenberg [173], S. Harkusha [175], M.L. Harris [103], Y.T. Harris [25], J. Harrison [13], P.F. Harrison[169], M.L.E. Hart [96], N.M. Hartman [110], N.M. Hartmann [109], R.Z. Hasan [95,135], Y. Hasegawa [143], D. Hashimoto [111], F. Haslbeck [37], S. Hassan [126], R. Hauser [107], M. Haviernik [134], C.M. Hawkes [21], R.J. Hawkings [37], Y. Hayashi [156], D. Hayden [107], R.L. Hayes [116], C.P. Hays [127], J.M. Hays [94], H.S. Hayward [92], M. He [14,112c], Y. He [47], Y. He [96], N.B. Heatley [94], V. Hedberg [98], J. Heilman [35], S. Heim [47], T. Heim [18a], J.J. Heinrich [124], L. Heinrich [110], J. Hejbal [132], M. Helbig [49], A. Held [172], S. Hellesund [17], C.M. Helling [166], F.N.E. Henry [58], H. Herde [98], Y. Hernández Jiménez [148], G. Herten [53], R. Hertenberger [109], L. Hervas [37], M.E. Hesping [100], N.P. Hessey [159a], J. Hessler [110], R. Hicks [129], M. Hidaoui [36b], N. Hidic [134], E. Hill [158], T.S. Hillersoy [17], S.J. Hillier [21], J.R. Hinds [107], F. Hinterkeuser [25], M. Hirose [125], S. Hirose [160], D. Hirschbuehl [173], B. Hiti [93], J. Hobbs [148], R. Hobincu [28e], N. Hod [171], A.M. Hodges [164], M.C. Hodgkinson [142], B.H. Hodkinson [127], A. Hoecker [37], D.D. Hofer [106], J. Hofer [165], J. Hofner [100], M. Holzbock [37], L.B.A.H. Hommels [33], V. Homsak [127], J.J. Hong [67], T.M. Hong [130], B.H. Hooberman [164], W.H. Hopkins [6], M.C. Hoppesch [164], Y. Horii [111], M.E. Horstmann [110], M.M. Horzela [54], S. Hou [151], M.R. Housenga [164], J. Howarth [58], J. Hoya [6], M. Hrabovsky [123], T. Hryn'ova [4], P.J. Hsu [64], S.-C. Hsu [140], T. Hsu [65], M. Hu [18a], P. Hu [63b], Q. Hu [61], S. Huang [33], X. Huang [14,112c], Y. Huang [134], Y. Huang [112b], Y. Huang [14], Z. Huang [65], Z. Hubacek [133], F. Huegging [25], T.B. Huffman [127], M. Hufnagel Maranha De Faria [81a], C.A. Hugli [47], M. Huhtinen [37], S.K. Huiberts [17], R. Hulsken [104], C.E. Hultquist [18a], D.L. Humphreys [103], N. Huseynov [12], J. Huston [107], B. Huth [37], J. Huth [60], L. Huth [47], R. Hyneman [7], G. Iacobucci [55], G. Iakovidis [30], L. Iconomidou-Fayard [65], J.P. Iddon [37], P. Iengo [71a,71b], Y. Iiyama [156], T. Iizawa [156], Y. Ikegami [82], D. Iliadis [155], N. Ilic [158], H. Imam [36a], G. Inacio Goncalves [81d], S.A. Infante Cabanas [138c], T. Ingebretsen Carlson [46a,46b], J.M. Inglis [94], G. Introzzi [72a,72b], M. Iodice [76a], V. Ippolito [74a,74b], R.K. Irwin [92], M. Ishino [156], W. Islam [172], C. Issever [19], S. Istin [22a,ar], K. Itabashi [125], H. Ito [170], R. Iuppa [77a,77b], A. Ivina [171], F. Ivone [37], S. Izumiyama [111], V. Izzo [71a], P. Jacka [133], P. Jackson [1], P.R. Jacobson [50], P. Jain [47], K. Jakobs [53], J. Jamieson [58], W. Jang [156], S. Jankovych [116], B.K. Jashal [135], M. Javurkova [103], P. Jawahar [101], L. Jeanty [124], J. Jejelava [152a,ae], P. Jenni [53,f], L. Jerala [93], C.E. Jessiman [35], H. Jia [166], J. Jia [148], X. Jia [110,112c], C. Jiang [51], Q. Jiang [63b], S. Jiggins [47], M. Jimenez Ortega [165], J. Jimenez Pena [13], S. Jin [112a], A. Jinaru [28b], O. Jinnouchi [139], P. Johansson [142], K.A. Johns [7], J.W. Johnson [137], F.A. Jolly [47], D.M. Jones [149], E. Jones [47], K.S. Jones[8], P. Jones [33], R.W.L. Jones [91], T.J. Jones [92], H.L. Joos [37], R. Joshi [120], J. Jovicevic [16], X. Ju [18a], J.J. Junggeburth [37], T. Junkermann [62a], A. Juste Rozas [13,x], M.K. Juzek [86], S. Kabana [138f], A. Kaczmarska [86], S.A. Kadir[146], M. Kado [110], H. Kagan [120], M. Kagan [146], A. Kahn [129], C. Kahra [100], T. Kaji [156], E. Kajomovitz [153], N. Kakati [171], N. Kakoty [13], S. Kandel [8], E. Kanellaki[45], N. Kanellos [10], D. Kar [34j,*], E. Karentzos [25], K. Karki [8], O. Karkout [116], S.N. Karpov [38], Z.M. Karpova [38], V. Kartvelishvili [91,152b], E. Kasimi [155], J. Katzy [47], S. Kaur [35], R. Kavak [164], K. Kawade [143], M.P. Kawale [121], C. Kawamoto [87], E.F. Kay [37], S. Kazakos [107], K. Kazakova [102], J.M. Keaveney [34a], R. Keeler [167], G.V. Kehris [60], J.S. Keller [35], J.M. Kelly [167], J.J. Kempster [149], O. Kepka [132],

J. Kerr [159b], B.P. Kerridge [135], B.P. Kerševan [93], L. Keszeghova [29a], R.A. Khan [130], A. Khanov [122], M. Kholodenko [131a], T.J. Khoo [19], G. Khoriauli [168], Y. Khoulaki [36a], Y.A.R. Khwaira [128], D. Kim [6], D.W. Kim [18b], Y.K. Kim [39], N. Kimura [96], M.K. Kingston [54], F. Kirfel [25], J. Kirk [135], A.E. Kiryunin [110], S. Kita [160], O. Kivernyk [25], M. Klassen [161], C. Klein [35], L. Klein [168], M.H. Klein [44], S.B. Klein [55], U. Klein [92], A. Klimentov [30], P. Kluit [116], S. Kluth [110], E. Kneringer [78], T.M. Knight [158], A. Knue [48], M. Kobel [49], D. Kobylianskii [171], S.F. Koch [37], M. Kocian [146], P. Kodyš [134], D.M. Koeck [124], T. Koffas [35], K. Kojima [82], O. Kolay [49], I. Koletsou [4], T. Komarek [86], S. Kondo [156], K. Köneke [54], A.X.Y. Kong [1], T. Kono [119], N. Konstantinidis [96], P. Kontaxakis [55], B. Konya [98], R. Kopeliansky [41], S. Koperny [85a], R. Koppenhofer [53], K. Korcyl [86], K. Kordas [155,d], A. Korn [96], S. Korn [54], I. Korolkov [13], B. Kortman [116], O. Kortner [110], S. Kortner [110], W.H. Kostecka [117], M. Kostov [29a], V.V. Kostyukhin [144], A. Kotsokechagia [37], A. Kotwal [50], A. Koulouris [37], A. Kourkoumeli-Charalampidi [72a,72b], O. Kovanda [124], R. Kowalewski [167], W. Kozanecki [124], G. Kramberger [93], P. Kramer [25], A. Krasznahorkay [103], A.C. Kraus [117], J.W. Kraus [173], J.A. Kremer [47], N.B. Krengel [144], T. Kresse [158], L. Kretschmann [173], J. Kretzschmar [92], P. Krieger [158], K. Krizka [21], K. Kroeninger [48], H. Kroha [110], J. Kroll [132], J. Kroll [129], K.S. Krowpman [107], U. Kruchonak [38], H. Krüger [25], N. Krumnack [79], J. Krupa [146], M.C. Kruse [50], O. Kuchinskaia [38], S. Kuday [3a], S. Kuehn [37], R. Kuesters [53], T. Kuhl [47], V. Kukhtin [38], Y. Kulchitsky [38], S. Kuleshov [138d,138b], J. Kull [1], E.V. Kumar [109], M. Kumar [34j], N. Kumari [47], P. Kumari [159b], A. Kupco [132], O. Kuprash [53], H. Kurashige [84], L.L. Kurchaninov [159a], O. Kurdysh [4], M. Kuze [139], A.K. Kvam [103], J. Kvita [123], N.G. Kyriacou [140], M. Laassiri [30], C. Lacasta [165], H. Lacker [19], D. Lacour [128], E. Ladygin [38], A. Lafarge [40], B. Laforge [128], T. Lagouri [174], F.Z. Lahbabi [36a], S. Lai [54], W.S. Lai [96], I.K. Lakomiec [54], J.E. Lambert [167], S. Lammers [67], W. Lampl [7], C. Lampoudis [155], G. Lamprinoudis [168], A.N. Lancaster [117], U. Landgraf [53], M.P.J. Landon [94], V.S. Lang [53], A.J. Lankford [162], F. Lanni [37], C.S. Lantz [164], K. Lantzsch [25], A. Lanza [72a], M. Lanzac Berrocal [165], T. Lari [70a], D. Larsen [17], L. Larson [11], F. Lasagni Manghi [24b], M. Lassnig [37], H.C. Lau [167], S.D. Lawlor [142], R. Lazaridou [162], M. Lazzaroni [70a,70b], E.T.T. Le [162], H.D.M. Le [107], E.M. Le Boulicaut [174], D.O. Le Guennec [136], L.T. Le Pottier [18a], B. Leban [24b,24a], F. Ledroit-Guillon [59], T.F. Lee [159b], L.L. Leeuw [34h], M. Lefebvre [167], C. Leggett [18a], L.M. Lehmann [116], G. Lehmann Miotto [37], M. Leigh [55], W.A. Leight [103], W. Leinonen [115], A. Leisos [155,t], M.A.L. Leite [81c], C.E. Leitgeb [19], R. Leitner [134], K.J.C. Leney [44], T. Lenz [25], S. Leone [73a], C. Leonidopoulos [51], A. Leopold [147], J. LePage-Bourbonnais [35], R. Les [107], C.G. Lester [33], J. Levêque [4], L.J. Levinson [171], G. Levrini [24b,24a], M.P. Lewicki [86], C. Lewis [140], D.J. Lewis [4], L. Lewitt [142], A. Li [30], B. Li [113b], C. Li [106], C-Q. Li [110], H. Li [113b], H. Li [101], H. Li [15], H. Li [61], H. Li [113b], J. Li [141a], L. Li [141a], R. Li [174], S. Li [141b,141a], T. Li [5], Y. Li [14], Z. Li [14,112c], Z. Li [61], S. Liang [14,112c], Z. Liang [14], M. Liberatore [136], B. Liberti [75a], G.B. Libotte [81d], K. Lie [63c], J. Lieber Marin [81e], H. Lien [67], H. Lin [106], S.F. Lin [148], L. Linden [109], R.E. Lindley [7], J.H. Lindon [37], J. Ling [60], E. Lipeles [129], A. Lipniacka [17], A. Lister [166], J.D. Little [67], B. Liu [113a], B.X. Liu [112b], D. Liu [153], D. Liu [137], E.H.L. Liu [21], H. Liu [112b], J.K.K. Liu [118], K. Liu [141b], K. Liu [141b], M. Liu [61], M.Y. Liu [61], P. Liu [113b], Q. Liu [146], S. Liu [148], X. Liu [113b], Y. Liu [112b,112c], Y. Liu [164], Y.L. Liu [113b], Y.W. Liu [61], Z. Liu [65,j], S.L. Lloyd [94], E.M. Lobodzinska [47], P. Loch [7], E. Lodhi [158], K. Lohwasser [142], E. Loiacono [122], J.D. Lomas [21], I. Longarini [162], R. Longo [24b,24a,am], A. Lopez Solis [13], N.A. Lopez-canelas [7], N. Lorenzo Martinez [4], A.M. Lory [109], M. Losada [83b], G. Löschcke Centeno [4], X. Lou [14,112c], P.A. Love [91], M. Lu [65], S. Lu [129], Y.J. Lu [151], H.J. Lubatti [140], C. Luci [74a,74b], F.L. Lucio Alves [112a], F. Luehring [67], B.S. Lunday [129],

O. Lundberg[147], J. Lunde[37], N.A. Luongo[6], M.S. Lutz[158], A.B. Lux[26], D. Lynn[30], R. Lysak[132], V. Lysenko[133], E. Lytken[98], V. Lyubushkin[38], T. Lyubushkina[38], M.M. Lyukova[148], H. Ma[30], K. Ma[61], L.L. Ma[113b], W. Ma[61], Y. Ma[113b], J.C. MacDonald[100], P.C. Machado De Abreu Farias[81e], D. Macina[37], R. Madar[40], T. Madula[96], J. Maeda[84], T. Maeno[30], P.T. Mafa[34f], H. Maguire[142], M. Maheshwari[33], V. Maiboroda[65], G. Maineri[70a,70b], A. Maio[131a,131b,131d], K. Maj[85a], O. Majersky[47], S. Majewski[124], A. Makita[156], N. Makovec[65], V. Maksimovic[16], B. Malaescu[128], J. Malamant[126], Pa. Malecki[86], F. Malek[59,n], M. Mali[93], D. Malito[95], A. Maloizel[5], A. Malvezzi Lopes[81d], S. Malyukov[38], J. Mamuzic[93], G. Mancini[52], M.N. Mancini[27], G. Manco[72a,72b], S.S. Mandarry[149], I. Mandić[93], L. Manhaes de Andrade Filho[81a], I.M. Maniatis[171], J. Manjarres Ramos[89], D.C. Mankad[171], A. Mann[109], T. Manoussos[37], M.N. Mantinan[39], S. Manzoni[37], L. Mao[141a], X. Mapekula[34c], A. Marantis[155], R.R. Marcelo Gregorio[1], G. Marchiori[5], C. Marcon[70a], E. Maricic[16], M. Marinescu[47], S. Marium[47], M. Marjanovic[121], A. Markhoos[53], M. Markovitch[65], M.K. Maroun[103], M.C. Marr[145], T.L. Marsault[136], G.T. Marsden[101], Z. Marshall[18a], S. Marti-Garcia[165], J. Martin[96], T.A. Martin[135], V.J. Martin[51], B. Martin dit Latour[17], L. Martinelli[74a,74b], V.I. Martinez Outschoorn[103], P. Martinez Suarez[37], S. Martin-Haugh[135], G. Martinovicova[134], V.S. Martoiu[28b], A. Martone[89], A.C. Martyniuk[96], A. Marzin[37], D. Mascione[77a,77b], L. Masetti[100], J. Masik[101], A.L. Maslennikov[38], S.L. Mason[41], P. Massarotti[71a,71b], P. Mastrandrea[73a,73b], A. Mastroberardino[43b,43a], R. Mastrofrancesco[72a,72b], T. Masubuchi[125], T.T. Mathew[124], J. Matousek[134], D.M. Mattern[48], K. Mauer[47], J. Maurer[28b], T. Maurin[58], A.J. Maury[65], B. Maček[93], C. Mavungu Tsava[102], A.E. May[101], E. Mayer[40], R. Mazini[34j], S.M. Mazza[137], E. Mazzeo[37], J.P. Mc Gowan[167], S.P. Mc Kee[106], C.C. McCracken[166], E.F. McDonald[105], L.F. Mcelhinney[91], J.A. Mcfayden[149], R.P. McGovern[129], R.P. Mckenzie[34j], D.J. Mclaughlin[96], S.J. McMahon[135], C.M. Mcpartland[92], R.A. McPherson[167,ab], S. Mehlhase[109], A. Mehta[92], D. Melini[165], B.R. Mellado Garcia[14,ah], A.H. Melo[54], F. Meloni[47], A.M. Mendes Jacques Da Costa[101], L. Meng[91], S. Menke[110], M. Mentink[37], E. Meoni[43b,43a], G. Mercado[117], S. Merianos[155], C. Merlassino[68a,68c], C. Meroni[70a,70b], J. Metcalfe[6], A.S. Mete[6], E. Meuser[100], C. Meyer[67], J-P. Meyer[136], Y. Miao[112a], R.P. Middleton[135], M. Mihovilovic[65], L. Mijović[51], G. Mikenberg[171], M. Mikestikova[132], M. Mikuž[93], H. Mildner[100], A. Milic[37], D.W. Miller[39], E.H. Miller[146], A. Milov[171], D.A. Milstead[46a,46b], T. Min[112a], I.A. Minashvili[152b], A.I. Mincer[118], B. Mindur[85a], M. Mineev[38], Y. Mino[87], L.M. Mir[13], M. Miralles Lopez[58], M. Mironova[18a], M. Missio[40], A. Mitra[169], V.A. Mitsou[165], Y. Mitsumori[111], P.S. Miyagawa[94], R. Mizuhiki[84], T. Mkrtchyan[37], M. Mlinarevic[96], T. Mlinarevic[96], M. Mlynarikova[134], L. Mlynarska[85a], C. Mo[141a], H. Mobius[47], S. Mobius[20], M.H. Mohamed Farook[114], S. Mohapatra[41], M.F. Mohd Soberi[51], S. Mohiuddin[122], G. Mokgatitswane[34j], R. Mole[21], L. Moleri[171], U. Molinatti[127], L.G. Mollier[20], L. Monaco[37,58], B. Mondal[132], S. Mondal[134], K. Mönig[47], E. Monnier[102], L. Monsonis Romero[165], A. Montella[46a,46b], M. Montella[120], F. Montereali[76a,76b], F. Monticelli[90], S. Monzani[68a,68c], M.E.E. Moors[25], A. Morancho Tarda[42], N. Morange[65], M. Moreno Llácer[165], C. Moreno Martinez[55], J.M. Moreno Perez[23b], P. Morettini[56b], S. Morgenstern[62a], M. Morii[60], M. Morinaga[156], F. Morodei[74a,74b], P. Moschovakos[37], B. Moser[53], M. Mosidze[152b], T. Moskalets[44], P. Moskvitina[115], C.J. Mosomane[34b], J. Moss[32], T. Motta Quirino[81d], A. Moussa[36d], Y. Moyal[171,k], H. Moyano Gomez[13], E.J.W. Moyse[103], T.G. Mroz[86], S. Muanza[102], M. Mucha[25], J. Mueller[130], D. Muller[144], G.A. Mullier[163], A.J. Mullin[33], J.J. Mullin[50], A.C. Mullins[44], A.E. Mulski[60], D.P. Mungo[158], D. Munoz Perez[122], F.J. Munoz Sanchez[101],

W.J. Murray [169,135], E. Musajan [61], M. Muškinja [93], C. Mwewa [47], A.J. Myers [8], G. Myers [106], M. Myska [133], B.P. Nachman [146], K. Nagai [127], K. Nagano [82], R. Nagasaka[156], J.L. Nagle [30,ao], E. Nagy [102], A.M. Nairz [37], T. Nakagawa [87], Y. Nakahama [82], K. Nakamura [82], K. Nakkalil [5], A. Nandi [62b], H. Nanjo [125], E.A. Narayanan [44], Y. Narukawa [156], L. Nasella [70a,70b], S. Nasri [83c], C. Nass [25], G. Navarro [23a], A. Nayaz [19], S. Nechaeva [24b,24a], F. Nechansky [132], L. Nedic [127], A. Negri [72a,72b], M. Negrini [24b], C. Nellist [116], C. Nelson [104], K. Nelson [106], S. Nemecek [132], M. Nessi [37,g], M.S. Neubauer [164], J. Newell [92], P.R. Newman [21], Y.W.Y. Ng [164], B. Ngair [83b], H.D.N. Nguyen [108], J.D. Nichols [121], R. Nicolaidou [136], J. Nielsen [137], M. Niemeyer [54], J. Niermann [37], N. Nikiforou [37], I. Nikolic-Audit [128], P. Nilsson [30], G. Ninio [154], A. Nisati [74a], R. Nisius [110], N. Nitika [171], E.K. Nkadimeng [34b], T. Nobe [156], D. Noll [146], T. Nommensen [150], M.B. Norfolk [142], B.J. Norman [35], L.C. Nosler[18a], M. Noury [36a], J. Novak [93], T. Novak [93], P. Novotny [171], R. Novotny [133], L. Nozka [123], K. Ntekas [37], D. Ntounis [146], N.M.J. Nunes De Moura Junior [81b], J. Ocariz [128], I. Ochoa [131a], A. Odella Rodriguez [13], S. Oerdek [47], J.T. Offermann [39], A. Ogrodnik [86], A. Oh [101], C.C. Ohm [147], H. Oide [82], M.L. Ojeda [37], Y. Okumura [156], L.F. Oleiro Seabra [131a], I. Oleksiyuk [55], G. Oliveira Correa [13], D. Oliveira Damazio [30], J.L. Oliver [1], R. Omar [67], A.P. O'Neill [20], Y. Onoda[139], A. Onofre [131a,131e,e], P.U.E. Onyisi [11], M.J. Oreglia [39], D. Orestano [76a,76b], R. Orlandini [76a,76b], R.S. Orr [158], L.M. Osojnak [41], Y. Osumi [111], G. Otero y Garzón [31], H. Otono [88], M. Ouchrif [36d], F. Ould-Saada [126], T. Ovsiannikova [140], M. Owen [58], R.E. Owen [135], S.A. Oyeniran [114], V.E. Ozcan [22a], F. Ozturk [86], N. Ozturk [8], S. Ozturk [80], H.A. Pacey [127], K. Pachal [159a], A. Pacheco Pages [13], C. Padilla Aranda [13], G. Padovano [74a,74b], S. Pagan Griso [18a], L. Pagani [75a,75b], J. Pampel [25], D.K. Panchal [11], C.E. Pandini [59], J.G. Panduro Vazquez [135], H.D. Pandya [1], H. Pang [136], P. Pani [47], G. Panizzo [68a,68c], L. Panwar [128,w], L. Paolozzi [21], S. Parajuli [164], A. Paramonov [6], C. Paraskevopoulos [52], D. Paredes Hernandez [63b], S.R. Paredes Saenz [51], A. Pareti [72a,72b], K.R. Park [41], T.H. Park [110], F. Parodi [56b,56a], J.A. Parsons [41], U. Parzefall [53], B.A. Paschen [18a], B. Pascual Dias [40], L. Pascual Dominguez [99], E. Pasqualucci [74a], S. Passaggio [56b], F. Pastore [95], P. Patel [86], U.M. Patel [50], J.R. Pater [101], T. Pauly [37], A. Paunovic [16], F. Pauwels [134], C.I. Pazos [161], M. Pedersen [126], R. Pedro [131a], O. Penc [132], C.C. Penelaud [128], S. Peng [15], G.D. Penn [174], B.S. Peralva [81d], A.P. Pereira Peixoto [140], L. Pereira Sanchez [146], D.V. Perepelitsa [30,ao], G. Perera [103], E. Perez Codina [37], M. Perganti [10], H. Pernegger [37], S. Perrella [74a,74b], K. Peters [47], R.F.Y. Peters [101], B.A. Petersen [37], T.C. Petersen [42], E. Petit [102], V. Petousis [133], A.R. Petri [70a,70b], T. Petru [134], M. Pettee [18a], A. Petukhov [80], K. Petukhova [37], R. Pezoa [138g], L. Pezzotti [24b,24a], G. Pezzullo [174], L. Pfaffenbichler [37], A.J. Pfleger [78], T.M. Pham [172], T. Pham [105], P.W. Phillips [135], G. Piacquadio [148], E. Pianori [18a], F. Piazza [124], R. Piegaia [31], D. Pietreanu [28b], A.D. Pilkington [101], T. Pilusa [34j], M. Pinamonti [68a,68c], J.L. Pinfold [2], G. Pinheiro Matos [41], B.C. Pinheiro Pereira [131a], J. Pinol Bel [13], A.E. Pinto Pinoargote [128], L. Pintucci [68a,68c], K.M. Piper [149], A. Pirttikoski [55], D.A. Pizzi [35], L. Pizzimento [63b], A. Plebani [33], M.-A. Pleier [30], V. Pleskot [134], E. Plotnikova[38], G. Poddar [94], R. Poettgen [98], L. Poggioli [128], S. Polacek [134], G. Polesello [72a], A. Poley [145], A. Polini [24b], C.S. Pollard [169], Z.B. Pollock [120], E. Pompa Pacchi [121], N.I. Pond [96], D. Ponomarenko [67], L. Pontecorvo [37], S. Popa [28a], G.A. Popeneciu [28d], A. Poreba [37], D.M. Portillo Quintero [159a], S. Pospisil [133], M.A. Postill [142], P. Postolache [28c], K. Potamianos [169], P.A. Potepa [85a], I.N. Potrap [38], C.J. Potter [33], H. Potti [150], J. Poveda [165], M.E. Pozo Astigarraga [37], R. Pozzi [37], A. Prades Ibanez [75a,75b], S.R. Pradhan [142], J. Pretel [167], D. Price [101], M. Primavera [69a], L. Primomo [68a,68c], M.A. Principe Martin [99], R. Privara [123], T. Procter [85b], M.L. Proffitt [140], N. Proklova [129], K. Prokofiev [63c], G. Proto [110], J. Proudfoot [6], M. Przybycien [85a],

W.W. Przygoda [85b], A. Psallidas [45], D. Pudzha [52], P. Puhl [57], H.I. Purnell [1], D. Pyatiizbyantseva [115], J. Qian [106], R. Qian [107], D. Qichen [127], Y. Qin [13], T. Qiu [51], A. Quadt [54], M. Queitsch-Maitland [101], G. Quetant [55], R.P. Quinn [166], D. Rafanoharana [110], J.L. Rainbolt [39], S. Rajagopalan [30], E. Ramakoti [38], L. Rambelli [56b,56a], I.A. Ramirez-Berend [35], K. Ran [106,112c], S.D. Randles [92], D.S. Rankin [129], N.P. Rapheeha [34j], H. Rasheed [28b], A. Rastogi [18a], S. Rave [100], S. Ravera [56b,56a], B. Ravina [37], I. Ravinovich [171], M. Raymond [37], A.L. Read [126], N.P. Readioff [142], D.M. Rebuzzi [72a,72b], A.S. Reed [58], K. Reeves [27], D. Reikher [37], A. Rej [48], C. Rembser [37], H. Ren [61], M. Renda [28b], F. Renner [47], A.G. Rennie [58], M. Repik [55], A.L. Rescia [56b,56a], S. Resconi [70a], M. Ressegotti [56b], S. Rettie [116], W.F. Rettie [35], M.M. Revering [33], O.L. Rezanova [38], P. Reznicek [134], H. Riani [36d], N. Ribaric [50], B. Ricci [68a,68c], E. Ricci [77a,77b], R. Richter [110], E. Richter-Was [85b], M. Ridel [128], S. Ridouani [36d], P. Riedler [37], E.M. Riefel [46a,46b], J.O. Rieger [116], M. Rimoldi [34c], L. Rinaldi [24b,24a], P. Rincke [163,54], G. Ripellino [163], I. Riu [13], J.C. Rivera Vergara [167], F. Rizatdinova [122], E. Rizvi [94], B.R. Roberts [39], S.S. Roberts [137], D. Robinson [33], A. Robson [58], A. Rocchi [75a,75b], C. Roda [73a,73b], F.A. Rodriguez [117], S. Rodriguez Bosca [37], Y. Rodriguez Garcia [23a], A.M. Rodríguez Vera [117], S. Roe[37], J.T. Roemer [37], O. Røhne [126], R.A. Rojas [37], Z. Rokavec[93], C.P.A. Roland [128], A. Romaniouk [78], E. Romano [72a,72b], M. Romano [24b], N. Rompotis [92], L. Roos [128], S. Rosati [74a], L. Roscher [47], B.J. Rosser [39], E. Rossi [127], E. Rossi [71a,71b], L.P. Rossi [60], L. Rossini [53], R. Rosten [120], M. Rotaru [28b], R. Roth [37], D. Rousseau [65], D. Rousso [47], S. Roy-Garand [55], A. Rozanov [102], Z.M.A. Rozario [58], Y. Rozen [153], A. Rubio Jimenez [165], V.H. Ruelas Rivera [19], T.A. Ruggeri [1], A. Ruggiero [127], A. Ruiz-Martinez [165], A. Rummler [37], G.B. Rupnik Boero [37], N.A. Rusakovich [38], S. Ruscelli [48], H.L. Russell [167], G. Russo [137], J.P. Rutherfoord [7], S. Rutherford Colmenares [118], M. Rybar [134], P. Rybczynski [85a], A. Ryzhov [44], F. Safai Tehrani [74a], S. Saha [1], B. Sahoo [171], B.T. Saifuddin [121], M. Saimpert [136], I. Sainz Saenz Diez [62a], G.T. Saito [81c], M. Saito [156], T. Saito [156], A. Sala [70a,70b], O.T. Salin [65], A. Salnikov [146], J. Salt [165], A. Salvador Salas [154], F. Salvatore [149], A. Salzburger [37], D. Sammel [53], E. Sampson [91], D. Sampsonidis [155,d], D. Sampsonidou [124], M.A.A. Samy [58], J. Sánchez [165], V. Sanchez Sebastian [165], H. Sandaker [126], C.O. Sander [47], J.A. Sandesara [172], M. Sandhoff [173], C. Sandoval [23b], L. Sanfilippo [62a], D.P.C. Sankey [135], T. Sano [87], A. Sansar [22c], A. Sansoni [52], M. Santana Queiroz [18b], L. Santi [37], C. Santoni [40], H. Santos [131a,131b], L. Santos Pereira Trigo [47], E. Sanzani [24b,24a], K.A. Saoucha [83d], J.G. Saraiva [131a,131d], J. Sardain [7], S. Sarkar [50], O. Sasaki [82], K. Sato [160], C. Sauer[37], E. Sauvan [4], P. Savard [158,aj], R. Sawada [156], C. Sawyer [135], L. Sawyer [97], A.M. Sayed [27], C. Sbarra [24b], A. Sbrizzi [24b,24a], R. Scaglioni [72a,72b], T. Scanlon [96], J. Schaarschmidt [140], U. Schäfer [100], A.C. Schaffer [65,44], D. Schaile [109], R.D. Schamberger [148], C. Scharf [19], M.M. Schefer [20], D. Scheirich [134], M. Schernau [138f], C. Scheulen [55], C. Schiavi [56b,56a], M. Schioppa [43b,43a], S. Schlenker [37], T. Schlomer [54], J. Schmeing [173], C.R. Schmidt [49], E. Schmidt [110], M.A. Schmidt [173], K. Schmieden [25], C. Schmitt [100], N. Schmitt [100], S. Schmitt [47], N.A. Schneider [109], L. Schoeffel [136], A. Schoening [62b], P.G. Scholer [35], E. Schopf [144], M. Schott [25], S. Schramm [55], T. Schroer [55], H-C. Schultz-Coulon [62a], M. Schumacher [53], B.A. Schumm [137], Ph. Schune [136], H.R. Schwartz [7], A. Schwartzman [146], T.A. Schwarz [106], Ph. Schwemling [136], R. Schwienhorst [107], F.G. Sciacca [20], A. Sciandra [30], G. Sciolla [27], S.A. Scoville [130], F. Scuri [73a], C.D. Sebastiani [37], K. Sedlaczek [117], A. Sehrawat [138b], S.C. Seidel [114], B.D. Seidlitz [41], C. Seitz [47], J.M. Seixas [81b], G. Sekhniaidze [71a], L. Selem [128], N. Semprini-Cesari [24b,24a], A. Semushin [175], V. Senthilkumar [116], L. Serin [65], M. Sessa [71a,71b], H. Severini [121], F. Sforza [56b,56a], A. Sfyrla [55], Q. Sha [14], H. Shaddix [117], A.H. Shah [33],

R. Shaheen[147], J.D. Shahinian[129], M. Shamim[37], L.Y. Shan[14], M. Shapiro[18a], A. Sharma[37], A.S. Sharma[166], P. Sharma[30], K. Shaw[149], S.M. Shaw[101], D. Shemyakin[171], Q. Shen[14], D.J. Sheppard[145], P. Sherwood[96], L. Shi[112b], X. Shi[14], S. Shimizu[82], S. Shirabe[88], M. Shiyakova[38,z], M.J. Shochet[39], D.R. Shope[126], B. Shrestha[121], S. Shrestha[120,aq], I. Shreyber[38], M.J. Shroff[104], P. Sicho[132], A.M. Sickles[164], E. Sideras Haddad[34j], A.C. Sidley[116], A. Sidoti[24b], F. Siegert[49], Dj. Sijacki[16], F. Sili[61], J.M. Silva[51], I. Silva Ferreira[81b], M.V. Silva Oliveira[30], S.B. Silverstein[46a], S. Simion[65], R. Simoniello[37], E.L. Simpson[101], H. Simpson[149], L.R. Simpson[6], S. Simsek[80], S. Sindhu[54], S.N. Singh[27], S. Singh[30], S. Sinha[47], S. Sinha[101], M. Sioli[24b,24a], K. Sioulas[9], I. Siral[37], E. Sitnikova[47], J. Sjölin[46a,46b], A. Skaf[54], E. Skorda[21], P. Skubic[121], M. Slawinska[86], I. Slazyk[17], I. Sliusar[126], V. Smakhtin[171], B.H. Smart[135], S.Yu. Smirnov[138b], Y. Smirnov[34c], O. Smirnova[98], J.L. Smith[101], M.B. Smith[35], R. Smith[146], H. Smitmanns[100], M. Smizanska[91], K. Smolek[133], P. Smolyanskiy[133], A.A. Snesarev[38], H.L. Snoek[116], R.M. Snyder[50], S. Snyder[30], R. Sobie[167,ab], A. Soffer[154], C.A. Solans Sanchez[37], E.Yu. Soldatov[38], U. Soldevila[165], A.A. Solodkov[34j], S. Solomon[27], A. Soloshenko[38], O.V. Solovyanov[40], P. Sommer[49], A. Sopczak[133], A.L. Sopio[51], F. Sopkova[29b], J.D. Sorenson[114], I.R. Sotarriva Alvarez[139], V. Sothilingam[62a], O.J. Soto Sandoval[138c,138b], S. Sottocornola[67], R. Soualah[83a], D. South[47], N. Soybelman[171], S. Spagnolo[69a,69b], A.S. Spellman[124], D. Sperlich[53], B. Spisso[71a,71b], L. Splendori[102], M. Spousta[134], E.J. Staats[35], R. Stamen[62a], E. Stanecka[86], W. Stanek-Maslouska[47], M.V. Stange[49], B. Stanislaus[18a], M.M. Stanitzki[47], G.H. Stark[137], J. Stark[89], P. Staroba[132], P. Starovoitov[83d], R. Staszewski[86], C. Stauch[109], G. Stavropoulos[45], A. Stefl[37], A. Stein[100], P. Steinberg[30], B. Stelzer[145,159a], H.J. Stelzer[130], O. Stelzer[159a], H. Stenzel[57], T.J. Stevenson[149], G.A. Stewart[47], G. Stoicea[28b], M. Stolarski[131a], S. Stonjek[110], A. Straessner[49], J. Strandberg[147], S. Strandberg[46a,46b], M. Stratmann[173], M. Strauss[121], T. Strebler[102], P. Strizenec[29b], R. Ströhmer[168], D.M. Strom[124], R. Stroynowski[44], A. Strubig[46a,46b], S.A. Stucci[30], B. Stugu[17], J. Stupak[121], N.A. Styles[47], D. Su[146], S. Su[61], X. Su[61], D. Suchy[29a], A.D. Sudhakar Ponnu[54], L. Sudit[171], Y. Sue[82], K. Sugizaki[129], D.M.S. Sultan[127], L. Sultanaliyeva[25], S. Sultansoy[3b], S. Sun[172], W. Sun[14], S. Sundar Raman[166], N. Sur[98], J.P. Surdutovich[120], N. Suri Jr[174], M.R. Sutton[149], M. Svatos[132], P.N. Swallow[33], S.N. Swatman[37], M. Swiatlowski[159a], A. Swoboda[37], I. Sykora[29a], M. Sykora[134], T. Sykora[134], D. Ta[100], K. Tackmann[47,y], A. Taffard[162], R. Tafirout[159a], Y. Takubo[82], M. Talby[102], N.M. Tamir[154], A. Tanaka[156], J. Tanaka[156], R. Tanaka[65], M. Tanasini[148], Z. Tao[166], S. Tapia Araya[138g], S. Tapprogge[100], A. Tarek Abouelfadl Mohamed[37], S. Tarem[153], K. Tariq[14], G. Tarna[37], G.F. Tartarelli[70a], M.J. Tartarin[141b], P. Tas[134], M. Tasevsky[132], E. Tassi[43b,43a], A.C. Tate[164], Y. Tayalati[36e,aa], G.N. Taylor[105], W. Taylor[159b], R.J. Taylor Vara[165], A.S. Tegetmeier[89], P. Teixeira-Dias[95], J.J. Teoh[158], K. Terashi[156], J. Terron[99], S. Terzo[13], M. Testa[52], R.J. Teuscher[158,ab], A. Thaler[78], T. Theveneaux-Pelzer[102], J.P. Thomas[21], E.A. Thompson[18a], P.D. Thompson[21], E. Thomson[129], R.E. Thornberry[30], T.M. Thory-Rao[21], C.N. Thotamuna Wijewardhana[148], C. Tian[61], Y. Tian[55], V. Tikhomirov[80], Yu.A. Tikhonov[38], D. Timoshyn[134], E.X.L. Ting[1], P. Tipton[174], A. Tishelman-Charny[30], K. Todome[139], S. Todorova-Nova[134], L. Toffolin[68a,68c], M. Togawa[82], J. Tojo[88], S. Tokár[29a], O. Toldaiev[67], G. Tolkachev[102], M. Tomoto[82], L. Tompkins[146], E. Torrence[124], H. Torres[89], D.I. Torres Arza[138g], E. Torres Reoyo[165], E. Torró Pastor[165], M. Toscani[31], C. Tosciri[39], M. Tost[11], D.R. Tovey[142], T. Trefzger[168], P.M. Tricarico[13], A. Tricoli[30], I.M. Trigger[159a], S. Trincaz-Duvoid[128], D.A. Trischuk[167], A. Tropina[38], D. Truncali[75a,75b], L. Truong[34c], M. Trzebinski[86], A. Trzupek[86], F. Tsai[148], A. Tsiamis[155], P.V. Tsiareshka[38], S. Tsigaridas[159a], A. Tsirigotis[155,t], V. Tsiskaridze[152a],

E.G. Tskhadadze [152a], H.F. Tsoi [129], Y. Tsujikawa [87], V. Tsulaia [18a], K. Tsuri [119], D. Tsybychev [148], Y. Tu [63b], A. Tudorache [28b], V. Tudorache [28b], S.B. Tuncay [127], S. Turchikhin [56b,56a], I. Turk Cakir [3a], R. Turra [70a], T. Turtuvshin [38,ac], P.M. Tuts [41], Y. Uematsu [82], F. Ukegawa [160], P.A. Ulloa Poblete [138c,138b], G. Unal [37], A. Undrus [30], J. Urban [29b], P. Urrejola [138e], G. Usai [8], R. Ushioda [157], M. Usman [108], F. Ustuner [51], Z. Uysal [80], V. Vacek [133], B. Vachon [104], T. Vafeiadis [37], A. Vaitkus [96], C. Valderanis [109], E. Valdes Santurio [46a,46b], M. Valente [37], S. Valentinetti [24b,24a], A. Valero [165], E. Valiente Moreno [165], A. Vallier [89], J.A. Valls Ferrer [165], D.R. Van Arneman [116], R. Van Den Broucke [128], A. Van Der Graaf [48], H.Z. Van Der Schyf [34j], P. Van Gemmeren [6], M. Van Rijnbach [37], S. Van Stroud [96], I. Van Vulpen [116], P. Vana [134], M. Vanadia [75a,75b], U.M. Vande Voorde [147], W. Vandelli [37], E.R. Vandewall [146], D. Vannicola [154], R. Vari [74a], M. Varma [174], E.W. Varnes [7], C. Varni [85a], D. Varouchas [65], L. Varriale [165], K.E. Varvell [150], M.E. Vasile [28b], A. Vasileiadou[9], L. Vaslin[82], M.D. Vassilev [146], A. Vasyukov [38], L.M. Vaughan [122], R. Vavricka[134], T. Vazquez Schroeder [13], J. Veatch [32], V. Vecchio [101], M.J. Veen [103], I. Veliscek [30], I. Velkovska [93], L.M. Veloce [158], F. Veloso [131a,131c], A.G. Veltman [51], S.H. Venetianer [161], S. Veneziano [74a], A. Ventura [69a,69b], A. Verbytskyi [110], M. Verducci [73a,73b], C. Vergis [94], M. Verissimo De Araujo [81b], W. Verkerke [116], J.C. Vermeulen [116], C. Vernieri [146], M. Vessella [162], M.C. Vetterli [145,aj], A. Vgenopoulos [100], N. Viaux Maira [138g,af], L. Vicenik [133], T. Vickey [142], O.E. Vickey Boeriu [142], G.H.A. Viehhauser [127], L. Vigani [62b], M. Vigl [110], M. Villa [24b,24a], M. Villaplana Perez [165], E.M. Villhauer[39], E. Vilucchi [52], M. Vincent [165], M.G. Vincter [35], A. Visibile [116], A. Visive [116], C. Vittori [161], I. Vivarelli [24b,24a], M.I. Vivas Albornoz [47], E. Voevodina [110], F. Vogel [109], J.C. Voigt [49], P. Vokac [133], Yu. Volkotrub [85b], L. Vomberg [25], E. Von Toerne [25], B. Vormwald [37], K. Vorobev [50], M. Vos [165], K. Voss [144], M. Vozak [37], L. Vozdecky [121], N. Vranjes [16], M. Vranjes Milosavljevic [16], M. Vreeswijk [116], N.K. Vu [112a], R. Vuillermet [37], O. Vujinovic [100], I. Vukotic [39], I.K. Vyas [35], J.F. Wack [33], A. Wada [111], S. Wada [160], C. Wagner[146], J.M. Wagner [18a], W. Wagner [173], S. Wahdan [173], H. Wahlberg [90], C.H. Waits [121], J. Walder [135], R. Walker [109], K. Walkingshaw Pass [58], W. Walkowiak [144], A. Wall [129], E.J. Wallin [98], T. Wamorkar [146], K. Wandall-Christensen [165], A. Wang [61], A.Z. Wang [137], C. Wang [47], C. Wang [11], H. Wang [18a], J. Wang [63c], P. Wang [101], P. Wang [96], R. Wang [60], R. Wang [106], R. Wang [6], S.M. Wang [151], S. Wang [14,an], T. Wang [115], T. Wang [61], W.T. Wang [127], W. Wang[113c], X. Wang [164], X. Wang [141a], X. Wang [47], Y. Wang [148], Y. Wang [114], Z. Wang [106], Z. Wang [14], Z. Wang[63b], C. Wanotayaroj [82], A. Warburton [104], A.L. Warnerbring [144], S. Waterhouse [96], A.T. Watson [21], H. Watson [51], M.F. Watson [21], E. Watton [37], G. Watts [140], B.M. Waugh [96], J.M. Webb [53], C. Weber [30], M.S. Weber [20], C. Wei [61], Y. Wei [53], A.R. Weidberg [127], E.J. Weik [118], J. Weingarten [48], C. Weiser [53], C.J. Wells [47], T. Wenaus [30], T. Wengler [37], N.S. Wenke[110], N. Wermes [25], D. Werner [47], M. Wessels [62a], A.M. Wharton [91], A.S. White [37], A. White [8], M.J. White [1], D. Whiteson [162], L. Wickremasinghe [125], W. Wiedenmann [172], M. Wielers [135], R. Wierda [147], C. Wiglesworth [42], H.G. Wilkens [37], J.J.H. Wilkinson [33], S. Williams [33], S. Willocq [103], D.J. Wilson [101], P.J. Windischhofer [39], F.I. Winkel [31], F. Winklmeier [124], B.T. Winter [53], M. Wittgen[146], M. Wobisch [97], T. Wojtkowski[59], Z. Wolffs [116], J. Wollrath[37], M.W. Wolter [86], H. Wolters [131a,131c], M.C. Wong[137], E.L. Woodward [41], S.D. Worm [47], B.K. Wosiek [86], K.A. Wozniak [55], K.W. Woźniak [86], S. Wozniewski [54], K. Wraight [58], C. Wu [158], C. Wu [21], J. Wu [156], M. Wu [112b], M. Wu [115], S.L. Wu [172], S. Wu [14,an], X. Wu [61], Y.Q. Wu [158], Y. Wu [61], Z. Wu [102], Z. Wu [112a], J. Wuerzinger [110], T.R. Wyatt [101], B.M. Wynne [51], S. Xella [42], L. Xia [112a], M. Xie [61], A. Xiong [124], I. Xiotidis [37], D. Xu [14], H. Xu [61], L. Xu [61], R. Xu [129],

T. Xu [106], W. Xu[112a], Y. Xu [140], Z. Xu [51], R. Xue [130], B. Yabsley [150], S. Yacoob [11], Y. Yamaguchi [82], E. Yamashita [156], H. Yamauchi [160], T. Yamazaki [18a], Y. Yamazaki [84], S. Yan [58], Z. Yan [103], C. Yang [18a], H.J. Yang [141a], H.T. Yang [61], S. Yang [61], X. Yang [37], X. Yang [14], Y. Yang [156], Y. Yang[61], W-M. Yao [18a], C.L. Yardley [149], J. Ye [14], S. Ye [30], X. Ye [61], I. Yeletskikh [38], B. Yeo [18b], M.R. Yexley [96], T.P. Yildirim [127], K. Yorita [170], C.J.S. Young [37], C. Young [146], I.N.L. Young [58], N.D. Young[124], Y. Yu [61], J. Yuan [14,112c,an], M. Yuan [106], R. Yuan [141b], L. Yue [96], M. Zaazoua [61], B. Zabinski [86], I. Zahir [36a], Q.U.A. Zahoor [51], A. Zaio[56b,56a], Z.K. Zak [86], T. Zakareishvili [165], S. Zambito [55], J. Zang [156], R. Zanzottera [70a,70b], O. Zaplatilek [133], E. Zaya [147], C. Zeitnitz [173], H. Zeng [14], D.T. Zenger Jr [27], T. Ženiš [29a], S. Zenz [94], D. Zerwas [65], W. Zhan [61], B. Zhang [169], D.F. Zhang [142], G. Zhang [14,an], J. Zhang [113b], J. Zhang [6], L. Zhang [61], L. Zhang [112a], P. Zhang [14,112c], R. Zhang [112a], S. Zhang [36e], Y. Zhang [140], Y. Zhang [96], Y. Zhang [61], Y. Zhang [112a], Z. Zhang [101], Z. Zhang [18a], Z. Zhang [113b], Z. Zhang [65], H. Zhao [140], T. Zhao [113b], Y. Zhao [35], Z. Zhao [61], Z. Zhao [61], A. Zhemchugov [38], J. Zheng [112a], K. Zheng [164], L. Zheng [113b], X. Zheng [61], Z. Zheng [146], D. Zhong [164], B. Zhou [106], B. Zhou [141b,141a], N. Zhou [141a], Y. Zhou [15], Y. Zhou [112a], Y. Zhou[7], Z. Zhou [61], J. Zhu [106], X. Zhu[141b], Y. Zhu [141a], X. Zhuang [14], K. Zhukov [67], P. Ziakas [4], N.I. Zimine [38], J. Zinsser [62b], M. Ziolkowski [144], L. Živković [16], A. Zoccoli [24b,24a], K. Zoch [37], A. Zografos [37], T.G. Zorbas [142], L. Zwalinski [37].

[1]Department of Physics, University of Adelaide, Adelaide; Australia.
[2]Department of Physics, University of Alberta, Edmonton AB; Canada.
[3(a)]Department of Physics, Ankara University, Ankara;[(b)]Division of Physics, TOBB University of Economics and Technology, Ankara; Türkiye.
[4]LAPP, Université Savoie Mont Blanc, CNRS/IN2P3, Annecy; France.
[5]APC, Université Paris Cité, CNRS/IN2P3, Paris; France.
[6]High Energy Physics Division, Argonne National Laboratory, Argonne IL; United States of America.
[7]Department of Physics, University of Arizona, Tucson AZ; United States of America.
[8]Department of Physics, University of Texas at Arlington, Arlington TX; United States of America.
[9]Physics Department, National and Kapodistrian University of Athens, Athens; Greece.
[10]Physics Department, National Technical University of Athens, Zografou; Greece.
[11]Department of Physics, University of Texas at Austin, Austin TX; United States of America.
[12]Institute of Physics, Azerbaijan Academy of Sciences, Baku; Azerbaijan.
[13]Institut de Física d'Altes Energies (IFAE), Barcelona Institute of Science and Technology, Barcelona; Spain.
[14]Institute of High Energy Physics, Chinese Academy of Sciences, Beijing; China.
[15]Physics Department, Tsinghua University, Beijing; China.
[16]Institute of Physics, University of Belgrade, Belgrade; Serbia.
[17]Department for Physics and Technology, University of Bergen, Bergen; Norway.
[18(a)]Physics Division, Lawrence Berkeley National Laboratory, Berkeley CA;[(b)]University of California, Berkeley CA; United States of America.
[19]Institut für Physik, Humboldt Universität zu Berlin, Berlin; Germany.
[20]Albert Einstein Center for Fundamental Physics and Laboratory for High Energy Physics, University of Bern, Bern; Switzerland.
[21]School of Physics and Astronomy, University of Birmingham, Birmingham; United Kingdom.
[22(a)]Department of Physics, Bogazici University, Istanbul;[(b)]Department of Physics Engineering, Gaziantep University, Gaziantep;[(c)]Department of Physics, Istanbul University, Istanbul; Türkiye.

[23](a)Facultad de Ciencias y Centro de Investigaciónes, Universidad Antonio Nariño, Bogotá;(b)Departamento de Física, Universidad Nacional de Colombia, Bogotá; Colombia.
[24](a)Dipartimento di Fisica e Astronomia A. Righi, Università di Bologna, Bologna;(b)INFN Sezione di Bologna; Italy.
[25]Physikalisches Institut, Universität Bonn, Bonn; Germany.
[26]Department of Physics, Boston University, Boston MA; United States of America.
[27]Department of Physics, Brandeis University, Waltham MA; United States of America.
[28](a)Transilvania University of Brasov, Brasov;(b)Horia Hulubei National Institute of Physics and Nuclear Engineering, Bucharest;(c)Department of Physics, Alexandru Ioan Cuza University of Iasi, Iasi;(d)National Institute for Research and Development of Isotopic and Molecular Technologies, Physics Department, Cluj-Napoca;(e)National University of Science and Technology Politechnica, Bucharest;(f)West University in Timisoara, Timisoara;(g)Faculty of Physics, University of Bucharest, Bucharest; Romania.
[29](a)Faculty of Mathematics, Physics and Informatics, Comenius University, Bratislava;(b)Department of Subnuclear Physics, Institute of Experimental Physics of the Slovak Academy of Sciences, Kosice; Slovak Republic.
[30]Physics Department, Brookhaven National Laboratory, Upton NY; United States of America.
[31]Universidad de Buenos Aires, Facultad de Ciencias Exactas y Naturales, Departamento de Física, y CONICET, Instituto de Física de Buenos Aires (IFIBA), Buenos Aires; Argentina.
[32]California State University, CA; United States of America.
[33]Cavendish Laboratory, University of Cambridge, Cambridge; United Kingdom.
[34](a)Department of Physics, University of Cape Town, Cape Town;(b)iThemba Labs, Western Cape;(c)Department of Mechanical Engineering Science, University of Johannesburg, Johannesburg;(d)National Institute of Physics, University of the Philippines Diliman (Philippines);(e)Department of Physics, Stellenbosch University, Matieland;(f)University of KwaZulu-Natal, School of Agriculture and Science, Mathematics, Westville;(g)University of South Africa, Department of Physics, Pretoria;(h)University of Pretoria, Department of Mechanical and Aeronautical Engineering, Pretoria;(i)University of Zululand, KwaDlangezwa;(j)School of Physics, University of the Witwatersrand, Johannesburg; South Africa.
[35]Department of Physics, Carleton University, Ottawa ON; Canada.
[36](a)Faculté des Sciences Ain Chock, Université Hassan II de Casablanca;(b)Faculté des Sciences, Université Ibn-Tofail, Kénitra;(c)Faculté des Sciences Semlalia, Université Cadi Ayyad, LPHEA-Marrakech;(d)LPMR, Faculté des Sciences, Université Mohamed Premier, Oujda;(e)Faculté des sciences, Université Mohammed V, Rabat;(f)Institute of Applied Physics, Mohammed VI Polytechnic University, Ben Guerir; Morocco.
[37]CERN, Geneva; Switzerland.
[38]Affiliated with an international laboratory covered by a cooperation agreement with CERN.
[39]Enrico Fermi Institute, University of Chicago, Chicago IL; United States of America.
[40]LPC, Université Clermont Auvergne, CNRS/IN2P3, Clermont-Ferrand; France.
[41]Nevis Laboratory, Columbia University, Irvington NY; United States of America.
[42]Niels Bohr Institute, University of Copenhagen, Copenhagen; Denmark.
[43](a)Dipartimento di Fisica, Università della Calabria, Rende;(b)INFN Gruppo Collegato di Cosenza, Laboratori Nazionali di Frascati; Italy.
[44]Physics Department, Southern Methodist University, Dallas TX; United States of America.
[45]National Centre for Scientific Research "Demokritos", Agia Paraskevi; Greece.
[46](a)Department of Physics, Stockholm University;(b)Oskar Klein Centre, Stockholm; Sweden.
[47]Deutsches Elektronen-Synchrotron DESY, Hamburg and Zeuthen; Germany.
[48]Fakultät Physik, Technische Universität Dortmund, Dortmund; Germany.

[49]Institut für Kern- und Teilchenphysik, Technische Universität Dresden, Dresden; Germany.
[50]Department of Physics, Duke University, Durham NC; United States of America.
[51]SUPA - School of Physics and Astronomy, University of Edinburgh, Edinburgh; United Kingdom.
[52]INFN e Laboratori Nazionali di Frascati, Frascati; Italy.
[53]Physikalisches Institut, Albert-Ludwigs-Universität Freiburg, Freiburg; Germany.
[54]II. Physikalisches Institut, Georg-August-Universität Göttingen, Göttingen; Germany.
[55]Département de Physique Nucléaire et Corpusculaire, Université de Genève, Genève; Switzerland.
[56(a)]Dipartimento di Fisica, Università di Genova, Genova;[(b)]INFN Sezione di Genova; Italy.
[57]II. Physikalisches Institut, Justus-Liebig-Universität Giessen, Giessen; Germany.
[58]SUPA - School of Physics and Astronomy, University of Glasgow, Glasgow; United Kingdom.
[59]LPSC, Université Grenoble Alpes, CNRS/IN2P3, Grenoble INP, Grenoble; France.
[60]Laboratory for Particle Physics and Cosmology, Harvard University, Cambridge MA; United States of America.
[61]Department of Modern Physics and State Key Laboratory of Particle Detection and Electronics, University of Science and Technology of China, Hefei; China.
[62(a)]Kirchhoff-Institut für Physik, Ruprecht-Karls-Universität Heidelberg, Heidelberg;[(b)]Physikalisches Institut, Ruprecht-Karls-Universität Heidelberg, Heidelberg; Germany.
[63(a)]Department of Physics, Chinese University of Hong Kong, Shatin, N.T., Hong Kong;[(b)]Department of Physics, University of Hong Kong, Hong Kong;[(c)]Department of Physics and Institute for Advanced Study, Hong Kong University of Science and Technology, Clear Water Bay, Kowloon, Hong Kong; China.
[64]Department of Physics, National Tsing Hua University, Hsinchu; Taiwan.
[65]IJCLab, Université Paris-Saclay, CNRS/IN2P3, 91405, Orsay; France.
[66]Centro Nacional de Microelectrónica (IMB-CNM-CSIC), Barcelona; Spain.
[67]Department of Physics, Indiana University, Bloomington IN; United States of America.
[68(a)]INFN Gruppo Collegato di Udine, Sezione di Trieste, Udine;[(b)]ICTP, Trieste;[(c)]Dipartimento Politecnico di Ingegneria e Architettura, Università di Udine, Udine; Italy.
[69(a)]INFN Sezione di Lecce;[(b)]Dipartimento di Matematica e Fisica, Università del Salento, Lecce; Italy.
[70(a)]INFN Sezione di Milano;[(b)]Dipartimento di Fisica, Università di Milano, Milano; Italy.
[71(a)]INFN Sezione di Napoli;[(b)]Dipartimento di Fisica, Università di Napoli, Napoli; Italy.
[72(a)]INFN Sezione di Pavia;[(b)]Dipartimento di Fisica, Università di Pavia, Pavia; Italy.
[73(a)]INFN Sezione di Pisa;[(b)]Dipartimento di Fisica E. Fermi, Università di Pisa, Pisa; Italy.
[74(a)]INFN Sezione di Roma;[(b)]Dipartimento di Fisica, Sapienza Università di Roma, Roma; Italy.
[75(a)]INFN Sezione di Roma Tor Vergata;[(b)]Dipartimento di Fisica, Università di Roma Tor Vergata, Roma; Italy.
[76(a)]INFN Sezione di Roma Tre;[(b)]Dipartimento di Matematica e Fisica, Università Roma Tre, Roma; Italy.
[77(a)]INFN-TIFPA;[(b)]Università degli Studi di Trento, Trento; Italy.
[78]Universität Innsbruck, Department of Astro and Particle Physics, Innsbruck; Austria.
[79]Department of Physics and Astronomy, Iowa State University, Ames IA; United States of America.
[80]Istinye University, Sariyer, Istanbul; Türkiye.
[81(a)]Departamento de Engenharia Elétrica, Universidade Federal de Juiz de Fora (UFJF), Juiz de Fora;[(b)]Universidade Federal do Rio De Janeiro COPPE/EE/IF, Rio de Janeiro;[(c)]Instituto de Física, Universidade de São Paulo, São Paulo;[(d)]Rio de Janeiro State University, Rio de Janeiro;[(e)]Federal University of Bahia, Bahia; Brazil.
[82]KEK, High Energy Accelerator Research Organization, Tsukuba; Japan.
[83(a)]Khalifa University of Science and Technology, Abu Dhabi;[(b)]New York University Abu Dhabi, Abu Dhabi;[(c)]United Arab Emirates University, Al Ain;[(d)]University of Sharjah, Sharjah; United Arab

Emirates.
[84]Graduate School of Science, Kobe University, Kobe; Japan.
[85(a)]AGH University of Krakow, Faculty of Physics and Applied Computer Science, Krakow;[(b)]Marian Smoluchowski Institute of Physics, Jagiellonian University, Krakow; Poland.
[86]Institute of Nuclear Physics Polish Academy of Sciences, Krakow; Poland.
[87]Faculty of Science, Kyoto University, Kyoto; Japan.
[88]Research Center for Advanced Particle Physics and Department of Physics, Kyushu University, Fukuoka ; Japan.
[89]L2IT, Université de Toulouse, CNRS/IN2P3, UPS, Toulouse; France.
[90]Instituto de Física La Plata, Universidad Nacional de La Plata and CONICET, La Plata; Argentina.
[91]Physics Department, Lancaster University, Lancaster; United Kingdom.
[92]Oliver Lodge Laboratory, University of Liverpool, Liverpool; United Kingdom.
[93]Department of Experimental Particle Physics, Jožef Stefan Institute and Department of Physics, University of Ljubljana, Ljubljana; Slovenia.
[94]Department of Physics and Astronomy, Queen Mary University of London, London; United Kingdom.
[95]Department of Physics, Royal Holloway University of London, Egham; United Kingdom.
[96]Department of Physics and Astronomy, University College London, London; United Kingdom.
[97]Louisiana Tech University, Ruston LA; United States of America.
[98]Fysiska institutionen, Lunds universitet, Lund; Sweden.
[99]Departamento de Física Teorica C-15 and CIAFF, Universidad Autónoma de Madrid, Madrid; Spain.
[100]Institut für Physik, Universität Mainz, Mainz; Germany.
[101]School of Physics and Astronomy, University of Manchester, Manchester; United Kingdom.
[102]CPPM, Aix-Marseille Université, CNRS/IN2P3, Marseille; France.
[103]Department of Physics, University of Massachusetts, Amherst MA; United States of America.
[104]Department of Physics, McGill University, Montreal QC; Canada.
[105]School of Physics, University of Melbourne, Victoria; Australia.
[106]Department of Physics, University of Michigan, Ann Arbor MI; United States of America.
[107]Department of Physics and Astronomy, Michigan State University, East Lansing MI; United States of America.
[108]Group of Particle Physics, University of Montreal, Montreal QC; Canada.
[109]Fakultät für Physik, Ludwig-Maximilians-Universität München, München; Germany.
[110]Max-Planck-Institut für Physik (Werner-Heisenberg-Institut), München; Germany.
[111]Graduate School of Science and Kobayashi-Maskawa Institute, Nagoya University, Nagoya; Japan.
[112(a)]Department of Physics, Nanjing University, Nanjing;[(b)]School of Science, Shenzhen Campus of Sun Yat-sen University;[(c)]University of Chinese Academy of Science (UCAS), Beijing; China.
[113(a)]School of Physics, Nankai University, Tianjin;[(b)]Institute of Frontier and Interdisciplinary Science and Key Laboratory of Particle Physics and Particle Irradiation (MOE), Shandong University, Qingdao;[(c)]School of Physics, Zhengzhou University; China.
[114]Department of Physics and Astronomy, University of New Mexico, Albuquerque NM; United States of America.
[115]Institute for Mathematics, Astrophysics and Particle Physics, Radboud University/Nikhef, Nijmegen; Netherlands.
[116]Nikhef National Institute for Subatomic Physics and University of Amsterdam, Amsterdam; Netherlands.
[117]Department of Physics, Northern Illinois University, DeKalb IL; United States of America.
[118]Department of Physics, New York University, New York NY; United States of America.
[119]Ochanomizu University, Otsuka, Bunkyo-ku, Tokyo; Japan.

[120]Ohio State University, Columbus OH; United States of America.
[121]Homer L. Dodge Department of Physics and Astronomy, University of Oklahoma, Norman OK; United States of America.
[122]Department of Physics, Oklahoma State University, Stillwater OK; United States of America.
[123]Palacký University, Joint Laboratory of Optics, Olomouc; Czech Republic.
[124]Institute for Fundamental Science, University of Oregon, Eugene, OR; United States of America.
[125]Graduate School of Science, University of Osaka, Osaka; Japan.
[126]Department of Physics, University of Oslo, Oslo; Norway.
[127]Department of Physics, Oxford University, Oxford; United Kingdom.
[128]LPNHE, Sorbonne Université, Université Paris Cité, CNRS/IN2P3, Paris; France.
[129]Department of Physics, University of Pennsylvania, Philadelphia PA; United States of America.
[130]Department of Physics and Astronomy, University of Pittsburgh, Pittsburgh PA; United States of America.
[131(a)]Laboratório de Instrumentação e Física Experimental de Partículas - LIP, Lisboa;[(b)]Departamento de Física, Faculdade de Ciências, Universidade de Lisboa, Lisboa;[(c)]Departamento de Física, Universidade de Coimbra, Coimbra;[(d)]Centro de Física Nuclear da Universidade de Lisboa, Lisboa;[(e)]Departamento de Física, Escola de Ciências, Universidade do Minho, Braga;[(f)]Departamento de Física Teórica y del Cosmos, Universidad de Granada, Granada (Spain);[(g)]Departamento de Física, Instituto Superior Técnico, Universidade de Lisboa, Lisboa; Portugal.
[132]Institute of Physics of the Czech Academy of Sciences, Prague; Czech Republic.
[133]Czech Technical University in Prague, Prague; Czech Republic.
[134]Charles University, Faculty of Mathematics and Physics, Prague; Czech Republic.
[135]Particle Physics Department, Rutherford Appleton Laboratory, Didcot; United Kingdom.
[136]IRFU, CEA, Université Paris-Saclay, Gif-sur-Yvette; France.
[137]Santa Cruz Institute for Particle Physics, University of California Santa Cruz, Santa Cruz CA; United States of America.
[138(a)]Departamento de Física, Pontificia Universidad Católica de Chile, Santiago;[(b)]Millennium Institute for Subatomic physics at high energy frontier (SAPHIR), Santiago;[(c)]Instituto de Investigación Multidisciplinario en Ciencia y Tecnología, y Departamento de Física, Universidad de La Serena;[(d)]Universidad Andres Bello, Department of Physics, Santiago;[(e)]Universidad San Sebastian, Recoleta;[(f)]Instituto de Alta Investigación, Universidad de Tarapacá, Arica;[(g)]Departamento de Física, Universidad Técnica Federico Santa María, Valparaíso; Chile.
[139]Department of Physics, Institute of Science, Tokyo; Japan.
[140]Department of Physics, University of Washington, Seattle WA; United States of America.
[141(a)]State Key Laboratory of Dark Matter Physics, School of Physics and Astronomy, Shanghai Jiao Tong University, Key Laboratory for Particle Astrophysics and Cosmology (MOE), SKLPPC, Shanghai;[(b)]State Key Laboratory of Dark Matter Physics, Tsung-Dao Lee Institute, Shanghai Jiao Tong University, Shanghai; China.
[142]Department of Physics and Astronomy, University of Sheffield, Sheffield; United Kingdom.
[143]Department of Physics, Shinshu University, Nagano; Japan.
[144]Department Physik, Universität Siegen, Siegen; Germany.
[145]Department of Physics, Simon Fraser University, Burnaby BC; Canada.
[146]SLAC National Accelerator Laboratory, Stanford CA; United States of America.
[147]Department of Physics, Royal Institute of Technology, Stockholm; Sweden.
[148]Departments of Physics and Astronomy, Stony Brook University, Stony Brook NY; United States of America.
[149]Department of Physics and Astronomy, University of Sussex, Brighton; United Kingdom.

[150]School of Physics, University of Sydney, Sydney; Australia.
[151]Institute of Physics, Academia Sinica, Taipei; Taiwan.
[152](a)E. Andronikashvili Institute of Physics, Iv. Javakhishvili Tbilisi State University, Tbilisi;(b)High Energy Physics Institute, Tbilisi State University, Tbilisi;(c)University of Georgia, Tbilisi; Georgia.
[153]Department of Physics, Technion, Israel Institute of Technology, Haifa; Israel.
[154]Raymond and Beverly Sackler School of Physics and Astronomy, Tel Aviv University, Tel Aviv; Israel.
[155]Department of Physics, Aristotle University of Thessaloniki, Thessaloniki; Greece.
[156]International Center for Elementary Particle Physics and Department of Physics, University of Tokyo, Tokyo; Japan.
[157]Graduate School of Science and Technology, Tokyo Metropolitan University, Tokyo; Japan.
[158]Department of Physics, University of Toronto, Toronto ON; Canada.
[159](a)TRIUMF, Vancouver BC;(b)Department of Physics and Astronomy, York University, Toronto ON; Canada.
[160]Division of Physics and Tomonaga Center for the History of the Universe, Faculty of Pure and Applied Sciences, University of Tsukuba, Tsukuba; Japan.
[161]Department of Physics and Astronomy, Tufts University, Medford MA; United States of America.
[162]Department of Physics and Astronomy, University of California Irvine, Irvine CA; United States of America.
[163]Department of Physics and Astronomy, University of Uppsala, Uppsala; Sweden.
[164]Department of Physics, University of Illinois, Urbana IL; United States of America.
[165]Instituto de Física Corpuscular (IFIC), Centro Mixto Universidad de Valencia - CSIC, Valencia; Spain.
[166]Department of Physics, University of British Columbia, Vancouver BC; Canada.
[167]Department of Physics and Astronomy, University of Victoria, Victoria BC; Canada.
[168]Fakultät für Physik und Astronomie, Julius-Maximilians-Universität Würzburg, Würzburg; Germany.
[169]Department of Physics, University of Warwick, Coventry; United Kingdom.
[170]Waseda University, Tokyo; Japan.
[171]Department of Particle Physics and Astrophysics, Weizmann Institute of Science, Rehovot; Israel.
[172]Department of Physics, University of Wisconsin, Madison WI; United States of America.
[173]Fakultät für Mathematik und Naturwissenschaften, Fachgruppe Physik, Bergische Universität Wuppertal, Wuppertal; Germany.
[174]Department of Physics, Yale University, New Haven CT; United States of America.
[175]Yerevan Physics Institute, Yerevan; Armenia.
[a] Also at Affiliated with an institute formerly covered by a cooperation agreement with CERN.
[b] Also at An-Najah National University, Nablus; Palestine.
[c] Also at Borough of Manhattan Community College, City University of New York, New York NY; United States of America.
[d] Also at Center for Interdisciplinary Research and Innovation (CIRI-AUTH), Thessaloniki; Greece.
[e] Also at Centre of Physics of the Universities of Minho and Porto (CF-UM-UP); Portugal.
[f] Also at CERN, Geneva; Switzerland.
[g] Also at Département de Physique Nucléaire et Corpusculaire, Université de Genève, Genève; Switzerland.
[h] Also at Departament de Fisica de la Universitat Autonoma de Barcelona, Barcelona; Spain.
[i] Also at Department of Financial and Management Engineering, University of the Aegean, Chios; Greece.
[j] Also at Department of Modern Physics and State Key Laboratory of Particle Detection and Electronics, University of Science and Technology of China, Hefei; China.
[k] Also at Department of Physics, Ben Gurion University of the Negev, Beer Sheva; Israel.
[l] Also at Department of Physics, Bolu Abant Izzet Baysal University, Bolu; Türkiye.

[m] Also at Department of Physics, King's College London, London; United Kingdom.
[n] Also at Department of Physics, Stellenbosch University; South Africa.
[o] Also at Department of Physics, University of Fribourg, Fribourg; Switzerland.
[p] Also at Department of Physics, University of Thessaly; Greece.
[q] Also at Department of Physics, Westmont College, Santa Barbara; United States of America.
[r] Also at Faculty of Physics, Sofia University, 'St. Kliment Ohridski', Sofia; Bulgaria.
[s] Also at Faculty of Physics, University of Bucharest; Romania.
[t] Also at Hellenic Open University, Patras; Greece.
[u] Also at Henan University; China.
[v] Also at Imam Mohammad Ibn Saud Islamic University; Saudi Arabia.
[w] Also at Indian Institute of Technology (IIT), Jodhpur; India.
[x] Also at Institucio Catalana de Recerca i Estudis Avancats, ICREA, Barcelona; Spain.
[y] Also at Institut für Experimentalphysik, Universität Hamburg, Hamburg; Germany.
[z] Also at Institute for Nuclear Research and Nuclear Energy (INRNE) of the Bulgarian Academy of Sciences, Sofia; Bulgaria.
[aa] Also at Institute of Applied Physics, Mohammed VI Polytechnic University, Ben Guerir; Morocco.
[ab] Also at Institute of Particle Physics (IPP); Canada.
[ac] Also at Institute of Physics and Technology, Mongolian Academy of Sciences, Ulaanbaatar; Mongolia.
[ad] Also at Institute of Physics, Azerbaijan Academy of Sciences, Baku; Azerbaijan.
[ae] Also at Institute of Theoretical Physics, Ilia State University, Tbilisi; Georgia.
[af] Also at Millennium Institute for Subatomic physics at high energy frontier (SAPHIR), Santiago; Chile.
[ag] Also at National Institute of Physics, University of the Philippines Diliman (Philippines); Philippines.
[ah] Also at School of Physics, University of the Witwatersrand, Johannesburg; South Africa.
[ai] Also at The Collaborative Innovation Center of Quantum Matter (CICQM), Beijing; China.
[aj] Also at TRIUMF, Vancouver BC; Canada.
[ak] Also at Università di Napoli Parthenope, Napoli; Italy.
[al] Also at Universita degli Studi Link; Italy.
[am] Also at University and INFN Torino, Torino; Italy.
[an] Also at University of Chinese Academy of Sciences (UCAS), Beijing; China.
[ao] Also at University of Colorado Boulder, Department of Physics, Colorado; United States of America.
[ap] Also at University of Siena; Italy.
[aq] Also at Washington College, Chestertown, MD; United States of America.
[ar] Also at Yeditepe University, Physics Department, Istanbul; Türkiye.
[*] Deceased